An Examination of the Effect of Plant Density on Low Reynolds Number Flow in a Wetland

A Thesis in
Water Resources and Environmental Engineering
By
Erin Burke

Submitted to:
Villanova University
Department of Civil and Environmental Engineering
in Partial Fulfillment of the Requirements
for the degree of Master of Science
August 2007

An Examination of the Effect of Plant Density on Low Reynolds Number Flow in a Wetland

By Erin Burke
August 2007

Bridget M. Wadzuk, Ph.D
Assistant Professor of Civil and Environmental Engineering

Robert G. Traver, Ph.D, P.E.
Associate Professor of Civil and Environmental Engineering

Ronald A. Chadderton, Ph.D., PE.
Chairman, Department of Civil and Environmental Engineering

Gary Gabriele, Ph.D
Dean of the College of Engineering

Abstract

A field experiment was conducted at a constructed stormwater wetland (CSW) on Villanova University's campus in the summer of 2006 to measure the effect of plant density on diffusion under low flow conditions. Numerical analysis and computer modeling using the Mike 21 software, a 2D unsteady flow model, was also conducted. The field study results were compared to two laboratory flume experiments, Nepf et al., 1997 and Serra et al., 2004, to determine the effects of field conditions. The field results were also used to examine the validity of a model proposed by Nepf (1999) which predicts diffusion based on plant density. Results show that field measured diffusion is one to two orders of magnitude higher than laboratory results and that the total diffusion model proposed by Nepf (1999) is a better estimate of diffusion in the Villanova CSW. A sensitivity analysis of the dead zone term proposed by Pendersen et al. (1977) shows that field conditions can produce a range of values for a given channel with respect to changing time and location and that a range of diffusion coefficients should be considered in design. The Mike 21 model was used to quantify the effects of individual field parameters and it was observed that nonuniform velocities were the most important factor, however discrepancies between the model and the field experiment prevent definitive conclusions from being drawn.

Acknowledgements

I would like to thank Dr. Bridget Wadzuk for her guidance and support in this report, Dr. Robert Traver and William Heasom for their insight and George Pappas and the Villanova graduate students for their assistance in the field procedure. I would also like to acknowledge the Danish Hydraulic Institute for providing the Model software and Technical Support. This project was partially funded by the Villanova Summer Grant Program and the Civil and Environmental Engineering Department. I would also like to thank my parents and family for their support.

Table of Contents

_Toc174451022

Chapter 1: Introduction 1
1.1 Research Objectives 1
1.2 Stormwater Problem 2
1.3 Best Management Practices 4
1.4 Constructed Stormwater Wetlands 5
1.5 Site Description 8

Chapter 2: Literature Review 17
2.1 Dispersion, Flow Regimes and Their Importance 18
2.2 Dispersion in Traditional Open Channel Conditions 22
2.3 The Effect of Emergent Vegetation on the Hydrodynamic Conditions of Natural Wetlands 26
2.4 Diffusion in Stormwater Wetlands 28
2.5 Model 33

Chapter 3: Methods 37
3.1 Field Experiment 37
3.1.1 Site Selection 37
3.1.2 Site Preparation 40
3.1.3 Dye Preparation and Instrument Calibration 42
3.1.4 Daily Experimental Procedure 43
3.2 Numerical Analysis 44
3.2.1 Simple Diffusivity Calculations 44
3.2.2 Diffusivity Calculations using Localized Velocity 45
3.2.3 Reynolds Number Analysis 46
3.2.4 Diffusion model 46
3.2.5 Addition and Sensitivity Analysis of Dead Zone Term 47
3.3 Model Procedure 49
3.3.1 Model Creation 49
3.3.2 Stability Calculations 51
3.3.3 Model Calibration 52
3.3.4 Model Analysis 53

Chapter 4: Results and Discussion **56**
4.1 Results of Field Experiment 56
4.1.1 Plant Diameter and Density 56
4.1.2 Example of Daily Results 58
4.2 Numerical Modeling Results 65
4.2.1 Diffusion Calculation Results 65
4.2.2 Reynolds Number Analysis 67
4.2.3 Diffusion Model Analysis 69
4.2.4 Dead Zone Sensitivity Analysis 70
4.3 Model Results and Analysis 76
4.3.1 Hydrodynamic verification 77
4.3.2 Resistance Calibration and Verification 79
4.3.3 Effect of Simulated Field Conditions on Diffusion in the Mike 21 83
4.3.4 Variations between the Mike 21 Model and Field Experiments 87

Works Cited **93**

Appendix **96**

List of Figures

Figure 1.1: Diagram of a shallow/extended detention CSW. 6
Figure 1.2: Diagram of a pocket wetland..... 7
Figure 1.3: Diagram of Wet Pond/Wetland System. 7
Figure 1.4: Location of Stormwater Wetland 9
Figure 1.5: Original Detention Basin..... 9
Figure 1.6: Drainage Area of Villanova CSW. 10
Figure 1.7: Diagram of Villanova CSW. 13
Figure 1.8: Picture of the Villanova CSW. 14
Figure 1.9: Sediment Forebay. 15
Figure 1.10: Wooden Weir located next to outlet structure of wetland. 15
Figure 1.11: Outlet Structure. 16
Figure 2.1: Advection and Diffusion Diagram. 19
Figure 2.2: Existing Diffusion Data..... 30
Figure 2.3: Effect of Reynolds number on Diffusion Coefficient. 33
Figure 3.1: Potential Research Sites 39
Figure 3.2: Site Preparation Diagram. 41
Figure 3.3: Diagram of Test Setup..... 42
Figure 3.4: Diagram of Cross Section Locations. 46
Figure 3.5: Bathymetry Input File 50
Figure 3.6: Example of Resistance Cell. 55
Figure 4.1: Coordinate Diagram 59
Figure 4.2: Depth on 7/17/06 across the cross section..... 61
Figure 4.3: Longitudinal Velocity Results on 7/17 across cross section 61
Figure 4.4: Lateral Velocity Results on 7/17 across the cross section..... 62
Figure 4.5: Concentration Results..... 63
Figure 4.6: Non-dimensional Longitudinal Velocity and Concentration 64
Figure 4.7: Diffusion Coefficient Results. 66
Figure 4.8: Reynolds Number Analysis..... 69
Figure 4.9: Effect of $\in$ on Diffusion Coefficient 74
Figure 4.10: Effect of T^{-1} on Diffusion Coefficient. 74
Figure 4.11: Effect of $\frac{dC_{dz}}{dt}$ on Diffusion Coefficient. 75
Figure 4.12: Dye Results of Model Hydrodynamic Calibration. 77
Figure 4.13: Velocity Results of Hydrodynamic Calibration 78
Figure 4.14: Dye Concentrations at different simulated densities. 80
Figure 4.15: Velocity Distribution at different plant densities 80
Figure 4.16: Model Results Plotted with Nepf's 1999 model. 83
Figure 4.17: Effect of Simulated Field Conditions on the 3.5% plant density. 84
Figure 4.18: Effect of Simulated Field Conditions of the 5.5% plant density. 85
Figure 4.19: Effect of Simulated Field Conditions on the 10% plant density. 85
Figure 4.20: Effect of Simulated Field Conditions on Velocity at the 3.5% Plant Density. 86

Figure 4.21: Dye Distribution Profiles with a defined diffusion coefficient of 0.5, IUDC. 89
Figure A.4.22: Plant Box. 100
Figure A.4.23: Peristalic Pump. 101
Figure A.4.24: Velcomimeter, SonTrek FlowTracker. 101
Figure A.4.25: Probe that entered the water for SonTek FlowTracker. 102
Figure A.4.26: Hand held control device for SonTek FlowTracker. 102
Figure A.4.27: Flourometer, YSI 600 OMS optical monitoring system. 103

List of Tables

Table 3.1: Dead Zone parameter Estimation…… 48
Table 3.2: Nonuniform Velocity Boundary Condition 55
Table 4.1: Stem Stalk Statistical Information 57
Table 4.2: Example Calculation of Plant Density 58
Table 4.3: Example of Table Velocities 59
Table 4.4: Sample Velocity Results 62
Table 4.5: Dye Results 63
Table 4.6: Reynolds Number Results 68
Table 4.7: Average Velocity and Standard Deviation at Different Plant Densities 81

Chapter 1: Introduction

This chapter is designed to introduce the present study, stormwater issues, their causes, consequences, and technology used to solve them, specifically constructed stormwater wetlands, and how knowledge gained in the present study can contribute to the constructed stormwater wetland (CSW) design. The research objectives are described in §1.1, §1.2 discusses the stormwater problem, §1.3 reviews best management practices while §1.4 focuses on the technology used in CSWs and §1.5 describes the research site.

1.1 Research Objectives

During low flow or baseflow conditions in a CSW the majority of the groundwater recharge, evaporation and water treatment occur because the detention time is the longest. There are several factors that play into the detention time, and one is the mixing that occurs; the diffusion coefficient can be thought of as an indicator of the mixing processes occurring through the CSW. Two laboratory studies were conducted by Nepf et al. (1997), herein referred to as Nepf (1997), and Serra et al. (2004), herein referred to as Serra, to examine the effect of plant density on diffusion in laminar flow wetlands. Nepf (1999) proposed a model to predict diffusion (D) in stormwater wetlands based upon plant density for both laminar and turbulent conditions

$$\frac{D}{ud} = \alpha_n \left[C_d \left(\frac{4P}{\pi} \right) \right]^{\frac{1}{3}} + \left(\frac{\beta^2 n}{2} \right) \left(\frac{4P}{\pi} \right) \qquad \text{(eq 2.16)}$$

where α_n and β are constants, P is the percent plant density, C_d is the drag coefficient and $\frac{D}{ud}$ is the dimensionless diffusion coefficient (see §2.4 for further discussion). There is a gap in plant densities examined in Nepf's (1997) and Serra's data, as well as an order of magnitude difference between their diffusion coefficients (Figure 2.2). Using a β=2, α_n=0.9 and C_d=3, Nepf's (1999) mechanical model is a good fit for Nepf's data with a Reynolds number (using the stem diameter as the characteristic length (See §2.1)) less than 114, but an order of magnitude lower than Serra's data, which discussed in more detail in §2.4.

A field experiment was conducted at Villanova University to examine the discrepancies in the laboratory results and examine the effect of field conditions. Plant densities between 3 and 10% were studied to fill in the gap between Nepf's (1997) and Serra's data. The goal of the present study is to examine how plant density and field conditions affect the diffusion in laminar stormwater wetlands and to see if Nepf's (1999) diffusion model is valid for field conditions. The results of this work can be incorporated into a larger scale hydrodynamic model of a stormwater wetland, which can be applied in designing more effective and efficient water treatment structures and ecosystems.

1.2 Stormwater Problem

Urbanization has been the demographic trend over the last half century (Ichimura, 2003). The developed land in the United States has increased from 72.9 to 108 million acres between 1982 and 2003, a 48% increase (NRCS, 2003). In the 1990s cities in Pennsylvania lost 23.3% of their population while second class townships increased their population by 48% subsequently increasing the amount of developed acres by 53.6% (PA

DCEP, 2005; Carlson, 2004). The country is experiencing urban sprawl; as communities develop, pervious areas, such as forests and farmlands, are converted to impervious areas due to buildings, pavement and compacted soils. These new surfaces cannot infiltrate water into the ground as well as their historic counterparts and there is increased volume and intensity of runoff during storm events (Carlson, 2004).

These increases cause both structural and environmental concerns. Structural concerns are due to increased erosion and flooding from the higher volume and intensity of runoff associated with large storm events, for example stream bank erosion. As the volume of water entering streams increases, the stream velocity will increase, which causes bank destabilization and morphological changes to the surface water system. Although this is a natural process, stream channel erosion was traditionally the result of major flood events. In many watersheds around PA with changed hydrology, stream channel erosion occurs as the result of small and medium sized rainfall events. Increased stream channel erosion is detrimental to the wildlife habitat and property value. (DEP, 2006)

Environmental concerns associated with storm events arise from nutrients such as nitrogen (Groffman et al, 2004), heavy metals such as lead (Laxen and Harrison, 1977) and hydrocarbons (Whipple and Hunter, 1979), that are incorporated into the runoff and carried to surface water systems degrading the water quality. There are also environmental concerns in ultra urban areas with combined sewer overflows in older cities, such as Philadelphia and New York (Adams and Papa, 2000). Traditional stormwater structures, such as detention basins, only reduce peak flow from large storm events, however the majority of the environmental pollution is due to small storm events.

Only recently have engineers addressed these environmental problems by detaining smaller storms and the first portion of larger storms; this is called capturing the first flush. The first flush is the first portion of a rainstorm that captures and carries the majority of the pollutants from the watershed. By detaining the first flush, water can be treated or infiltrated back into the ground, thus protecting the surface waters (DEP, 2006). This concept is practiced at the Villanova Urban Stormwater Park where Best Management Practices (BMPs), such as a bioinfiltration traffic island and a pervious concrete research sites, are designed to capture and infiltrate the first flush. The storm water wetland BMP slows down the flow and provides treatment but does not have significant infiltration (VUSP, 2005).

1.3 Best Management Practices

Stormwater is a large problem, specifically in urbanized areas. The Pennsylvania Department of Environmental Protection (PA DEP) has indicated urban stormwater runoff as the third most important cause of stream impairment in the state (DEP, 2006). The PA DEP has developed a stormwater Management Program to address the issue. The three main stormwater issues that the PA DEP is perusing are reducing volume, improving water quality and recharging the ground water system (DEP, 2006).

To accomplish the stormwater goals, the PA DEP is regulating stormwater discharge from recent land development through National Pollutant Discharge Elimination System Permits and educating engineering professionals with the PA BMP Manual found at <http://www.dep.state.pa.us/dep/deputate/watermgt/wc/subjects/stormwatermanagement/BMP%20Manual/BMP%20Manual.htm>. Stormwater regulation authority is shared

between the state and local governments with jurisdiction over 376 stormwater management watersheds in PA. Each stormwater management watershed authority has the ability to change specific requirements of the stormwater BMPs used within it (DEP, 2006).

Throughout the state of Pennsylvania, BMPs are added to land development projects to control and treat stormwater effluent from a site. A stormwater BMP is designed to uphold the following principles: using stormwater as a resource, preserving natural features of the ecosystem, managing stormwater close to the source, sustaining the hydrologic balance, spreading out discharges, slowing down runoff and preventing water quality problems (DEP, 2006). Stormwater BMPs should be integrated into the design of any land development project to help protect the health of the watershed (LID, 2007).

1.4 Constructed Stormwater Wetlands

One popular BMP is a CSW. A CSW serves three main purposes: to reduce peak flow, recharge groundwater, and treat water quality (Serra, 2000). CSWs function like traditional detention basins with controlled outflow and storage space to reduce the peak flow, however there is an additional water quality benefit. A variety of plant life and hydrologic structures, such as meandering streams and internal weirs, are part of a CSW's design to allow more contact time with plants and soil; this increases the amount of groundwater recharge, evapotranspiration and water treatment possible (DEP, 2006).

There are four main types of CSWs. A shallow wetland has a large surface area and water treatment is performed by displacement of a permanent pool (Figure 1.1). An extended detention stormwater wetland is the same as a shallow wetland except there is

an extended detention time to aid in water treatment and peak flow reduction (Figure 1.1). A pocket wetland may be implemented for small drainage areas (5 to 10 acres), and it is constructed close to the ground water table (Figure 1.2). A Pond/Wetland CSW is a combination of a wet pond where settlement and infiltration occurs and one of the previous CSW designs (Figure 1.3). (DEP, 2006).

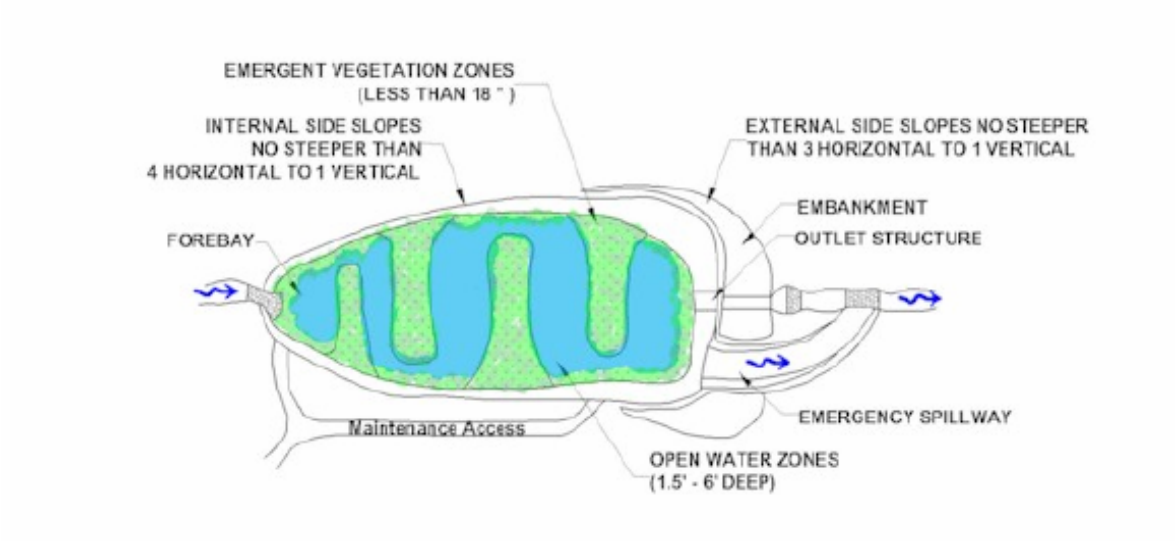

Figure 1.1: Diagram of a shallow/extended detention CSW.
Water travels through each wetland where water treatment occurs (DEP, 2006).

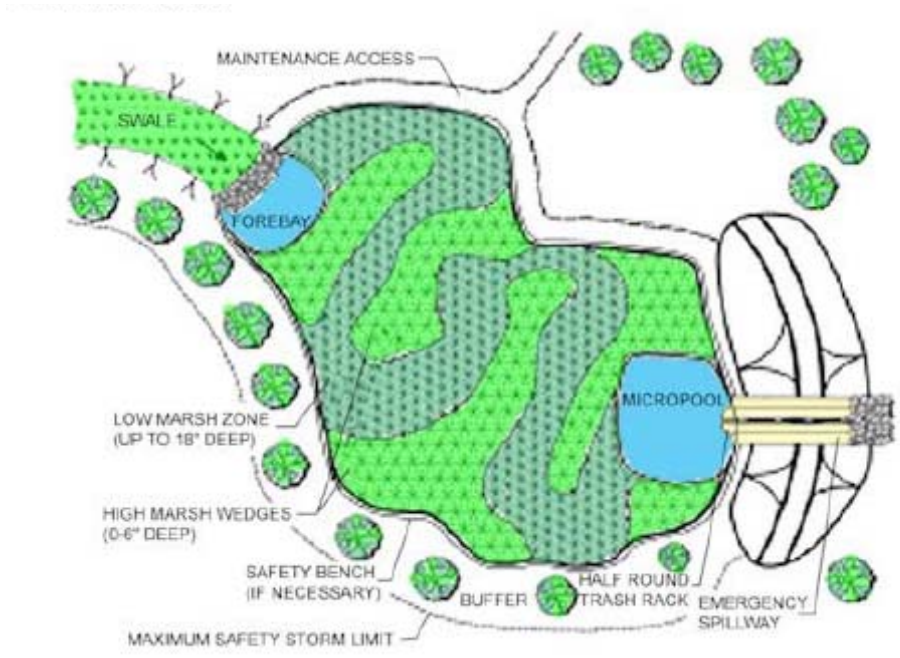

Figure 1.2: Diagram of a pocket wetland.
Pocket wetland is a similar design as the shallow wetland but is smaller and designed for watersheds 5-10 acres (DEP, 2006).

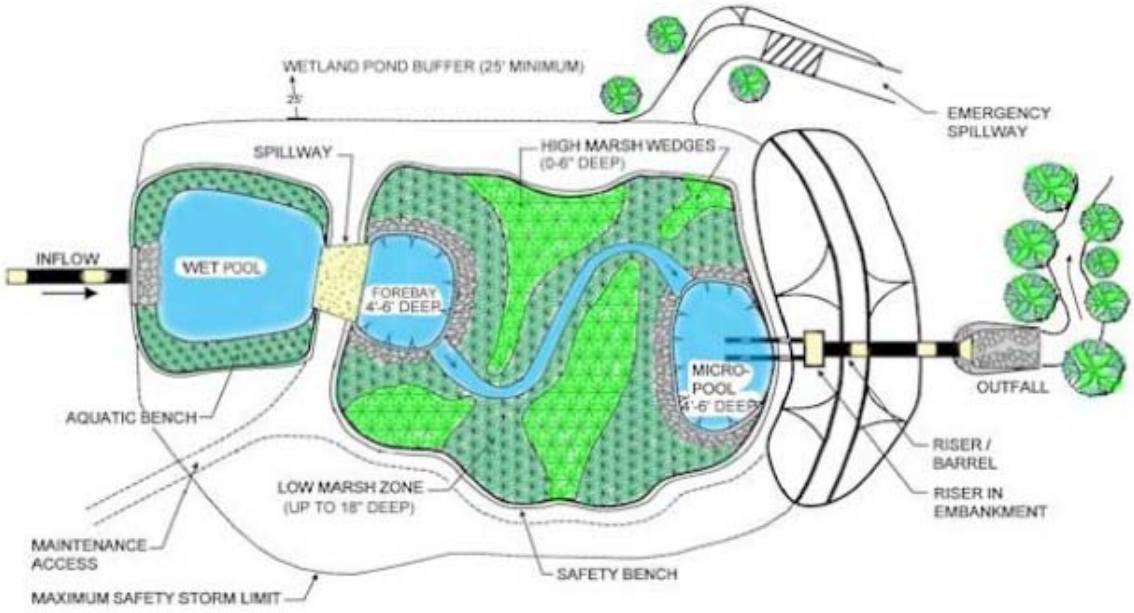

Figure 1.3: Diagram of Wet Pond/Wetland System.
Water first enters a pool where sediment is deposited. The water then travels through a meandering stream where water treatment occurs (DEP, 2006).

There are several considerations which must be accounted for when designing a CSW. The wetland surface area should be 3 to 5% of the drainage area (DEP, 2006). There should always be a minimum water level in the CSW, except during the most extreme dry conditions, to maintain a permanent pool and a viable wildlife habitat. Type C and D soils, as defined by the PA BMP manual, are preferred because they have lower infiltration rates preventing drying during periods of no rainfall. The soil should be organic to maximize pollutant absorption and provide a good medium for plant growth. (DEP, 2006)

Forebays, along with a weir, are often located close to the inlet to capture debris and heavy sediment before the water reaches the main section of the wetland. Hydraulic structures, such as meandering streams, are used to increase the detention time which will allow for more water treatment. Water depths should vary in order to increase plant diversity. Flow at the outlet is controlled to reduce the peak flows leaving the drainage area during storm events.

1.5 Site Description

The Villanova CSW is located on Villanova University's campus, on the border of Montgomery and Delaware County in PA (Figure 1.4). An existing detention basin was retrofitted into an extended detention stormwater wetland in 1999 (Figure 1.5). The two main purposes of this CSW are to treat non point pollutants while preserving the original function of the detention basin (i.e. peak flow reduction) and to provide a permanent research site for stormwater BMPs (Chadderton, 2000).

Figure 1.4: Location of Stormwater Wetland
Wetland is located where the star is (Mapquest, 2007).

Figure 1.5: Original Detention Basin

The stormwater wetland is shown in blue and the drainage area is enclosed by the green lines.The drainage area is approximately 41 acres, 16 of which are impervious (Figure 1.6). The drainage area is categorized as a suburban area with parking, dormitories, office buildings and railroads. The stormwater wetland drains into Mill Creek, which is a tributary of the Schuylkill River. The wetland itself is a medium priority habitat, however it is upstream of a high priority habitat, the Delaware estuary. The original detention basin had plant life consisting of *Phragmites australis* (Phragmites) and *Carduus personata* (thistles). After the wetland was constructed a variety of plant life was planted (Chadderton, 2000), however, the Phragmites have returned and dominate the plant life in the stormwater wetland. Phragmites are an aggressive invasive species (Saltonstall, 2001) that thrive in the high chloride environment that is found in the Villanova CSW.

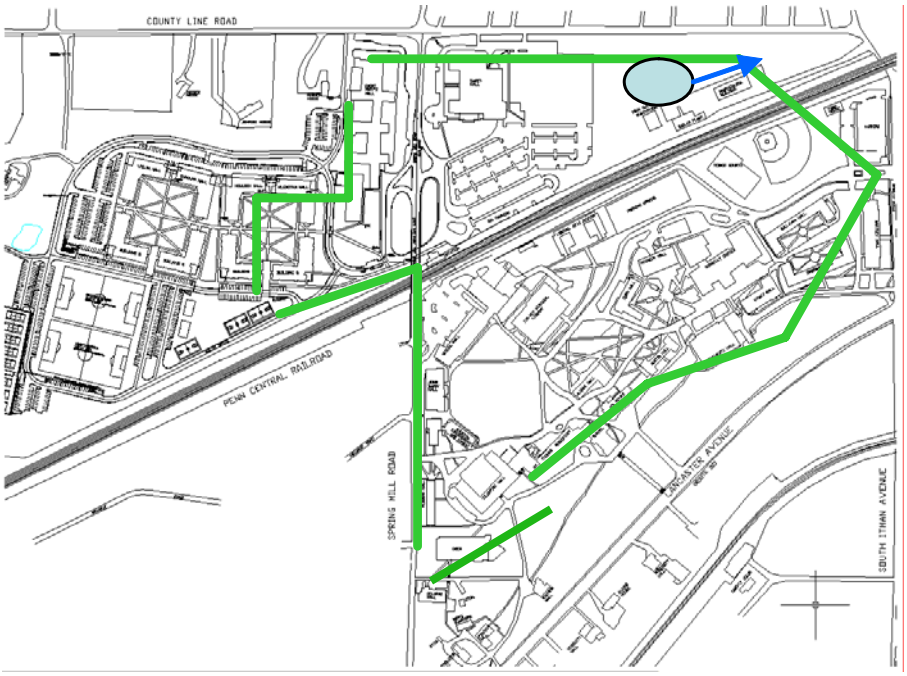

Figure 1.6: Drainage Area of Villanova CSW.

The constructed stormwater wetland is divided into four main design components: the inlet, sediment forebay, meandering stream and outlet structure. Figure 1.7 and 1.8 show autocad, graphical illustrations, and pictures of the wetland. The inlet consists of two monitored inlet pipes and one ungauged pipe that brings stormflow from a nearby law school; these three pipes all enter the CSW at the headwall. The two monitored pipes carry stormwater from the west and main campuses of Villanova, approximately 80% of the flow. In addition to the three pipes, there is sheet flow draining into the stormwater wetland from the adjacent area which includes a grassy area, a maintenance facility and a parking lot. Flow entering the wetland is designed to spread over a flat floodplain area and move towards the sediment forebay, however, especially during low flow conditions, the flow path is a direct channel to the sediment forebay, thus the available volume of this part of the CSW is not completely used. The sediment forebay is 40ft by 40ft concrete pad with flow retained by a gabion weir (Figure 1.9). As water enters the deep sediment forebay the flow is slowed, sediments are allowed to settle and outflow is controlled by the weir (Chadderton, 2000). The outflow moves into the extended detention meandering stream, which is created by earthen berms. The flow path between the sediment forebay and the outlet is extended allowing more contact time with plant life and the channel bottom to improve water quality. After the meandering stream, the flow reaches the outlet, where there is a small wooden weir to slow down the outflow and create a final pool for settlement (Figure 1.10). Directly upstream of the weir is where the field experiment was conducted as described in §3.1. Water moves from this small pool through an outlet structure in place to control the outflow (Figure 1.11). There are three openings to accommodate baseflow and small, medium and large storm events. The path

just described is the path taken by the water during low flow conditions, during extreme storm event water will bypass the sediment forebay and meandering stream system creating a direct path to the outlet. (Chadderton, 2000)

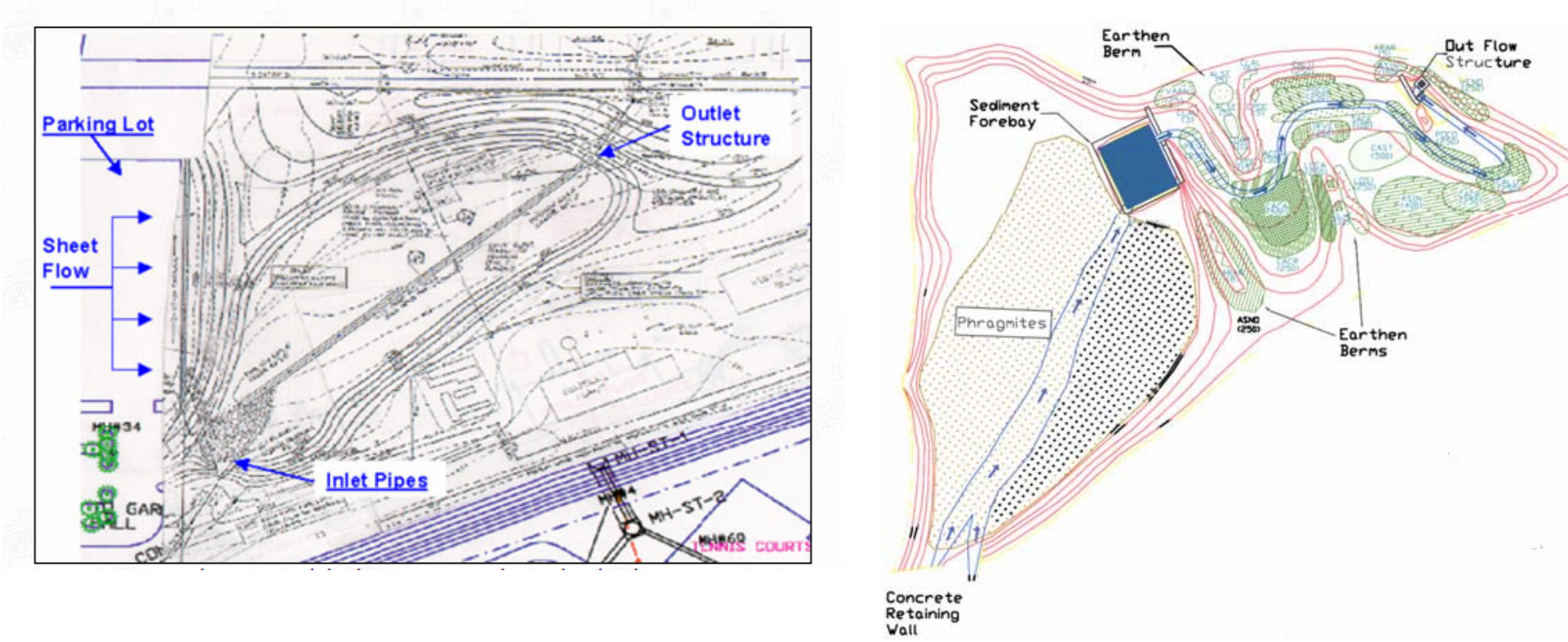

Figure 1.7: Diagram of Villanova CSW.
Water travels through the sediment forebay and meandering streams. It then exists the wetland through the outlet structure.

Figure 1.8: Picture of the Villanova CSW.

Figure 1.9: Sediment Forebay.
The gabian weir is located on the left and controls the flow leaving the Sediment Forebay.

Figure 1.10: Wooden Weir located next to outlet structure of wetland.

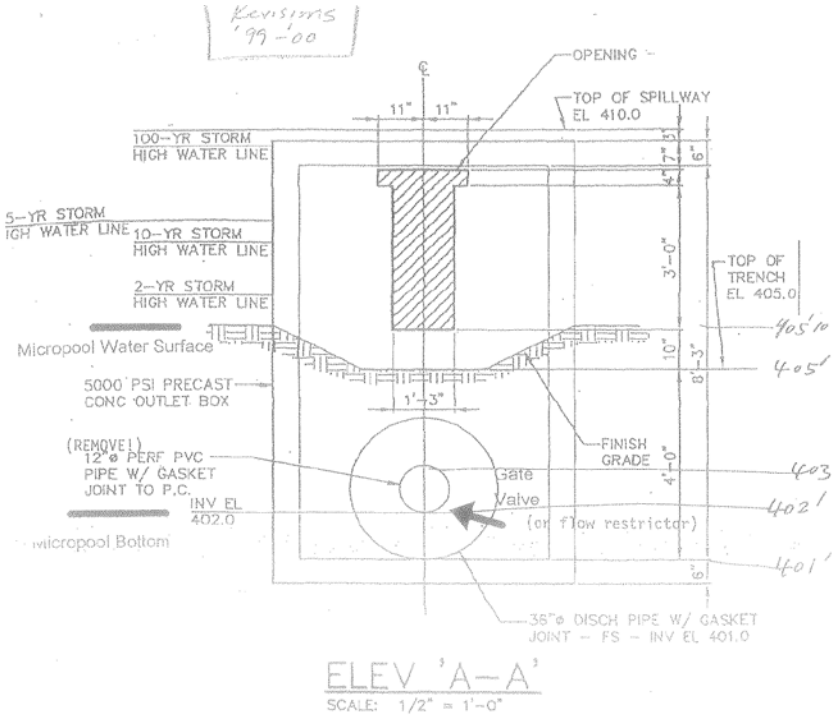

Figure 1.11: Outlet Structure.

A small orifice at the bottom of the structures allows stormwater from smaller storms to exit the wetland. The T shaped orifice allows storm from medium to large flow to exit the wetland. There is an open orifice on top of the outlet structure to allow for extremely high flows and maintenance.

Chapter 2: Literature Review

The present study conducted at Villanova University during the summer of 2006 encompasses many different areas of hydraulic engineering. This literature review is intended to give the reader a comprehensive understanding of the many factors and ideas that have influenced this thesis.

Diffusion is an important factor in many environmental engineering applications because it determines how contaminants and nutrients will be distributed throughout a system; this is of particular concern for flow through a CSW (Nepf, 1999), it can also be applied to air pollution (Nunnari, 2003). The terms diffusion and dispersion have been used interchangeably in literature. Studies focusing on longitudinal mixing in streams have used dispersion (e.g. Fischer, 1967 and Seo et al., 1998) while studies examining lateral mixing in CSWs have used diffusion. Dispersion will be used to describe the fundamental equations and reference stream channel studies, while diffusion will be used to discuss lateral diffusion in a CSW.

The first topic that will be covered is dispersion itself. The effect dispersion has on different aspects of ecology and engineering is examined. In §2.2 research predicting the dispersion coefficients in stream channels is reviewed. There is a large body of work concerning this subject in natural channels for the turbulent flow regime. §2.3 examines how emergent vegetation affects the hydrodynamic flow conditions in natural wetlands. §2.4 of this literature review isolates and examines the effect of emergent vegetation on diffusion in laminar flow stormwater wetlands. §2.5 of this literature review examines the Danish Hydraulic Institute's (DHI) Model software used to validate the results of the

field experiment and demonstrate where and how the software has been used in the past to solve similar problems.

2.1 Dispersion, Flow Regimes and Their Importance

Particles spread out through water and air through the processes of advection and dispersion. Advection is when particles spread out and are carried by the movement of the fluid; an example of this is when sand is carried downstream in a river by the current. Dispersion is when the particles spread out through the fluid independent of the current; an example of this is when perfume spreads out through a room. A diagram of how particles spread through advection and dispersion can be seen in Figure 2.1. If only advection were to take place the particles would travel exclusively in the downstream direction. If the dispersion process were to take process exclusively, as it would in a static fluid, the particles would spread out evenly in the upstream, downstream and lateral directions. When advection and dispersion happen at the same time particles will travel in both the upstream and downstream direction as shown in Figure 2.1 (Traver, 2007).

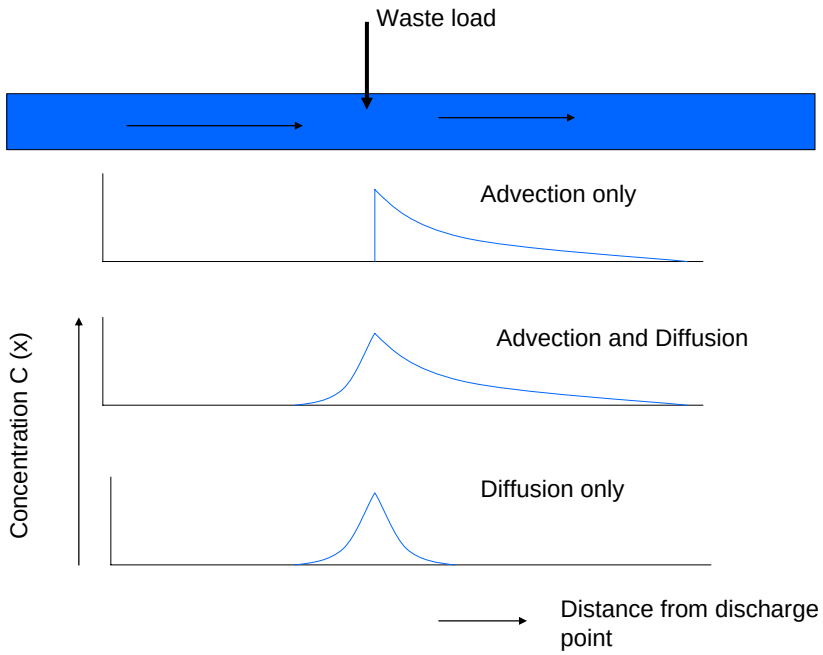

Figure 2.1: Advection and Diffusion Diagram.
An example stream is shown where a pollutant load is traced under advection, advection and diffusion and diffusion only conditions.

The present study focuses on the dispersion aspect of particle travel. Dispersion can be described and calculated using Fick's law, which is based on the premise that particles will travel from a high to low concentration. Dispersive transport is assumed proportional to the concentration gradient (Traver, 2007). The dispersion coefficient is a measure of the ability of a particle to spread; the greater the dispersion number the greater the ability of the particles to spread out. Fick's law is given

$$J_{a,x} = -D_{a,b} \frac{\partial c_A}{\partial x} \qquad \text{(eq 2.1)}$$

where $D_{a,b}$ is the dispersion coefficient of particle a in fluid b, x is the distance traveled, c is the average cross section concentration and $J_{a,x}$ is the flux (Streeter et al., 1998). In

1954 Taylor produced a one dimensional Fickian advection-dispersion equation taking the asymptotic limit as the discrete time step and spatial step approach zero

$$\frac{\partial c}{\partial t} + u\frac{\partial c}{\partial x} = D\frac{\partial^2}{\partial x^2} \qquad \text{(eq 2.2)}$$

where u is the cross-sectional mean velocity and t is time.

Fundamental to dispersive behavior in laminar and turbulent flow is the distinction between the two regimes. The laminar flow regime is described as flow where the relationship between velocity and shear stress is linear. In turbulent flow conditions the flow is variable and the relationship between shear stress and velocity is unpredictable. The Reynolds number (Re) (eq 2.3), the relationship between inertial forces and viscous forces, determines the flow regime

$$\mathrm{Re} = \frac{ud}{\nu} \qquad \text{(eq 2.3)}$$

where d is the characteristic length and ν is the kinematic viscosity of the fluid (Fox, 2004). Inertial forces cause particles to stay in place or keep moving while viscous forces are formed by shear stress and cause the fluid to deform. The Re characteristic length in stormwater wetlands is commonly the diameter of the emergent vegetation stem stalks

$$\mathrm{Re}_d = \frac{ud_{stem}}{\nu}. \qquad \text{(eq 2.4)}$$

The bed resistance is assumed to have a negligible effect (Serra, 2004; Nepf, 1997 and 1999). The boundary between laminar and turbulent flow for Re_d in stormwater wetlands is approximately 200 (Serra, 2004). The channel depth has also been used as a characteristic length to account for turbulence created by bed shear stress where

$$\mathrm{Re}_h = \frac{ud_{depth}}{\nu} \qquad \text{(eq 2.5)}$$

The boundary between laminar and turbulent flow is not clearly defined for Re_h, but a transitional zone between 600 and 12,500 separates the laminar and turbulent flow regimes (Leonard and Luther, 1995).

In the laminar flow regime, diffusion is due solely to Brownian motion or molecular diffusion. In molecular diffusion particles travel randomly and collide, eventually evenly spreading out from high to low concentration (Nepf, 1999). Turbulent diffusion occurs when wakes and eddies develop behind the stem stalks in turbulent flow conditions, creating additional circulation and mixing of the water and particles which increases the diffusion (Nepf, 1997).

Nepf (1999) proposes that mechanical and turbulent diffusion are independent of each other (eq 2.16; a detailed explanation of this model is in §2.4); the diffusion resulting from each type must be combined to produce the total diffusion. Diffusion is an important part of pollutant transport science, for example longitudinal dispersion (the process by which a solute dilutes as it travels downstream) in rivers which has traditionally dominated dispersion literature because it plays an important role in predicting pollutant behavior within an aquatic system (Fischer, 1967).

Wetlands are a transition zone between aquatic and tertiary systems and have flow and diffusion in longitudinal and lateral directions increasing retention time and treatment capacity (Serra, 2004). Nutrients and metals travel through wetlands and are absorbed by the sediments and plants (Nepf, 1999). Diffusion is the key mechanism affecting these particles, as well as seeds and larvae that travel through the wetland system (Nepf, 1997). The hydrodynamics of a wetland must be understood in order to predict the diffusion (Kadlec and Knight, 1996). The presence of emergent vegetation can significantly affect

the hydrodynamic conditions in a wetland (see §2.3). Nepf (1999) proposes the production of turbulence in vegetated flows is due primarily to emergent vegetation in cases where it is present rather than bed shear stress as it is in traditional open channel flows. The water will slow down as the result of turbulence and the advection and diffusion processes will be altered (Nepf, 1997). These effects are the main focus of the present study and will be studied in detail in Chapter 4.

2.2 Dispersion in Traditional Open Channel Conditions

There has been significant research concerning the dispersion coefficient in rivers and streams to aid in modeling and predicting pollution distribution. Taylor proposed that dispersion in pipes was the result of velocity differences in the radial direction (Fischer, 1967); this can be extrapolated to say that dispersion in stream flow is the result of differences in lateral velocities (Fischer, 1967). There are differences between theoretical and observed dispersion due to the non-prismatic qualities of natural stream channels (Beltaos, 1980). Predicting dispersion in natural stream channels is a difficult task because dispersion characteristics vary from stream to stream and can be difficult to measure (Fischer, 1967).

In longitudinal dispersion the mixing period is the time it takes for a constituent to become uniform across a cross section. The dispersive period occurs after the mixing period and is when Fickian behavior can be expected (Fisher, 1967). Fickian behavior is not always observed due to abnormalities in the field (Carleton, 2006), including dead zones (Purnama, 1988) and nonuniform velocities (Baek and Seo, 2004). Fischer (1967) attempted to link channel characteristics, specifically width, depth and velocity

distribution to the dispersion coefficient. A series of flume experiments were conducted and during the initial mixing period there was a sharp skew towards downstream, while in the dispersive regime, particles spread out approaching a Gaussian distribution in the longitudinal direction. The laboratory experiments indicated that

$$\frac{D}{ud_{depth}} \propto \frac{w^2}{d_{depth}} \qquad \text{(eq 2.6)}$$

where $\frac{D}{ud_{depth}}$ is the dimensionless dispersion coefficient, w is the channel width and d_{depth} is the channel depth. These experiments were performed in a laboratory setting with careful consideration given to matching the velocity distributions, however, error must be expected when applying these assumptions to field conditions. (Fischer, 1967)

Beltaos (1980) proposed a model to describe the non-Fickian behavior of longitudinal dispersion in natural streams.

$$\frac{D}{ud_{depth}} = \beta_1 Lu \qquad \text{(eq 2.7)}$$

where β_1 and L are parameters calculated based upon characteristics of the channel. Natural channel nonuniformities cause the mixing period, length and dispersion to increase. When the model (eq 2.7) was compared to natural channels, field and theoretical results are within one order of magnitude, an improvement over past literature (Beltaos, 1980).

Seo et al. (1998) examined dispersion in field conditions compared to previously developed empirical equations. The field study included 59 data sets from 26 streams in the United States. Seo et al. (1998) found that the empirical equations tended to underestimate the measured field dispersion coefficients. The effect fluid properties,

hydraulic characteristics and geometric configurations had on the dispersion coefficient was examined. The Re had an insignificant affect on the dimensionless dispersion coefficient and the dispersion coefficient increases as the width (w) to depth (h) ratio increases and as the friction (u/u^*; where u^* is the shear velocity) increases. The field observations were used to derive an empirical equation to predict dispersion coefficients.

Geometric conditions were also examined by Kashefipour and Falconer (2001); 81 measured data sets from 30 rivers were used to examine the affect of hydraulic and geometric parameters on the dispersion coefficient. The equation they proposed was

$$D = 10.612hu\left(\frac{u}{u^*}\right)_1 \qquad \text{(eq 2.8)}$$

The combination of the work predicting dispersion based on channel characteristics provides potential insight, but does not come to a consensus or conclusion, most likely to due varying hydrodynamic conditions.

Dead zones, areas with relatively still water and no downstream velocity, produce high lateral diffusivity and long tails of low concentrations in the longitudinal direction because dye is detained in the still water and slowly released over time (Purnama, 1988). Purnama (1998) did a mathematical and theoretical analysis using the method of moments to predict the effect of dead zones on the dispersion coefficient. A parameter $\in$ was established representing the percentage of the cross sectional area that was occupied by dead zones. The shear dispersion coefficients will increase by 0.01 to 0.02 as $\in$ increases from 0 to 20% showing the dead zones and daily hydrodynamic conditions play an important role in dispersion, as discussed in §4.2 (Purnama, 1988).

Pendersen et al. (1977) examined the effect of dead zones and proposed adding an additional term to the traditional Fickian equation to account for the temporary storage of particles and the resulting skewness

$$\frac{\partial C}{\partial t} + U\frac{\partial c}{\partial x} - D\frac{\partial^2 c}{\partial x^2} = \in T^{-1}(c_{dz} - c) \qquad \text{(eq 2.9)}$$

The model assumes that the change in concentration in a dead zone is proportional to the difference in concentration inside the dead zone and in the main stream channel

$$\frac{\partial c_{dz}}{\partial t} = T^{-1}\left(c_{dz} - c\right) \qquad \text{(eq 2.10)}$$

where c_{dz} is the concentration within the dead zone and c is the concentration within the main stream channel, T^{-1} is a constant of proportionality and $\in$ is the percentage of the cross sectional area occupied by dead zones (Pendersen, 1977). (Eq 2.9) allows for a range of dispersion coefficients based upon varying field conditions.

Nonuniform velocities affect the distribution of particles and the dispersion coefficient; Basha (1997) attempted to work with the nonuniform velocities in order to examine dispersion in both the longitudinal and lateral directions. The original two dimensional advection dispersion equation was given by French in 1985

$$\frac{\partial c}{\partial t} + \frac{\partial (uc)}{\partial x} = \frac{\partial}{\partial x}(D_x\frac{\partial c}{\partial x}) + \frac{\partial}{\partial y}\left(D_y\frac{\partial c}{\partial y}\right) + f \qquad \text{(eq 2.11)}$$

where f is the source function (M/L^3). To adapt this equation to field conditions, the shape and skewness of the velocity profile are adjusted over time. Numerical analysis shows that symmetric velocity profiles reach stable dispersion values faster than non-symmetric ones and the dispersion coefficient rate of increase is influenced by the location of the source relative to the area of maximum velocity. This information can be

used to predict dispersion when the transverse velocity profile is known (Basha, 1997). Seo and Baek (2004) proposed a model where the velocity distribution is based upon the beta probability density function

$$\frac{D}{ud_h} = \gamma_1 \frac{u^2 w^2}{hu^*} \qquad \text{(eq 2.12)}$$

where γ_1 is obtained through the processing geometric parameters through a complex numerical analysis. The discrepancy ratio (eq 2.13) is between -0.6 and 0.3 indicating a slight tendency to overestimate the dispersion coefficient where

$$Discrepancy\ ratio = \log \frac{\frac{D}{ud}_{pre}}{\frac{D}{ud}_{obs}} \qquad \text{(eq 2.13)}$$

Where *pre* is the predicted dispersion and *obs* is the observed dispersion. Overall this study showed that the beta function can be an appropriate way to predict the dispersion in a complex natural stream system (Baek and Seo, 2004).

2.3 The Effect of Emergent Vegetation on the Hydrodynamic Conditions of Natural Wetlands.

Wetlands are excellent water treatment systems; in fact they have been called kidneys for their remarkable cleaning ability. The biota and sediment present in the wetlands are the primary water treatment devices (Kadlec and Knight, 1996). The plants in the wetland can affect the flow speed, turbulent intensity, and shape of the vertical velocity profile (Leonard and Luther, 1995). The water conditions (i.e. velocity and turbulence) determine the type of biota present and affect soil nutrients (Kadlec and Knight, 1996).

For this reason it is important for scientists and engineers to understand the effects of emergent vegetation on the hydrodynamic conditions of a wetland.

Significant research has been conducted in order to better understand the effect of emergent vegetation on the hydrodynamics of flows in natural wetlands systems. One study was produced by Leonard and Luther (1995). Field experiments were conducted in Florida and Louisiana to measure flow conditions in different densities of marsh grasses. Leonard and Luther determined that energy is lost when flow enters a tidal marsh system by approximately one order of magnitude and this reduction in energy causes sediment deposition. The mean flow speed and turbulence intensity are inversely proportional to the stem density and distance from the creek bed; thus, there is a greater energy loss in dense wetland than sparsely populated wetlands. The energy reduction can reduce mixing and diffusion in marine macrophyte canopies (Ackerman and Okubo, 1993). Ackerman and Okubu examined mixing within eel grass, *Zostera Marina*, in Woods Hole, Massachusetts. As flow moved through the eel grass, turbulent eddies were produced and the plants began to oscillate. The observed mixing effects were compared to the theoretical values of eddy viscosity and mixing length (calculated using law of resistance and turbulent transport theory). As predicted by Leonard and Luther (1995) the velocity of the flow was dampened; the eddy velocities and mixing length were also reduced, showing that too much vegetation can decrease the mixing capacity under certain hydrodynamic conditons (Ackerman and Okubo, 1993).

There have been several studies on the effect of seagrass and other emergent vegetation on the hydrodynamics in laboratory flumes; however, the results are inconsistent (Leonard and Luther, 1995; Ackerman and Okubo, 1993). The variation in

diffusion between field and laboratory data within CSWs reflects past literature where field conditions significantly affect the diffusion coefficients in longitudinal streams (Beltaos, 1980). This trend is shown in the present study where variations in field conditions cause significant differences between field and laboratory conditions.

2.4 Diffusion in Stormwater Wetlands

Emergent aquatic vegetation affects the flow and diffusion within a waterbody by providing an additional source of drag and altering the hydrodynamic conditions (Serra, 2004). In vegetated stormwater wetlands, turbulence is created mainly by emergent vegetation, rather than bed shear stress as in traditional open channel flow. The additional drag is produced by the plant stems (Nepf, 1997), decreases the velocity and increases the residence time (Nepf, 1999).

The boundary between laminar and turbulent flow is when Re_d is approximately 200 in vegetated stormwater wetlands (Serra, 2004), although the transition varies (Leonard and Luther, 1995). Re_h has a transitional zone of 600 to 12,500 (Leonard and Luther, 1995). Depending on the flow regime, there are different diffusion mechanisms; Nepf (1997) defines two diffusion mechanisms as mechanical diffusion and turbulent diffusion. Mechanical diffusion is the result of Brownian motion, particles of water physically moving around each plant stem in a random walk fashion. Turbulent diffusion is the result of wakes and eddies where particles become trapped in the wake oscillations and are dispersed (Nepf, 1997).

Two laboratory experiments will be examined closely in this literature review, one conducted by Nepf (1997) and one conducted by Serra. In Nepf's experiment a 20 m

long, 0.3 m wide flume represented a channel in a wetland. Vegetation was modeled using rigid plexiglass rods of 0.6 and 1.2 cm diameter; the rod length was greater than the water depth to mimic the emergent state. Dye was injected through a 0.15 cm stainless steel tube at the in situ velocity. Flourescing dye was measured using an argon laser and velocities were measured using laser Doppler velocimetry. The plant densities examined were 0 to 5.3% and the Re_d ranged from 66 to 1800. To calculate diffusion of the dye through the vegetated flume, Nepf used (eq 3.3; discussed more in §3.2) based on Fick's law

$$\frac{\bar{c}_y}{c_{\max}} = \exp\left(-\frac{y^2 u}{4D_y x}\right) \qquad \text{(eq 3.3)}$$

where c_{max} is the maximum dye concentration, y is the distance along the cross section, D_y is the diffusion (L/t^2).

In Serra's experiment the setup was designed to quantify the lateral diffusion of passive substances in the shallow zones of a stormwater wetland. A flume 12m long, 0.41 meters wide with variable depths and vegetation modeled as rigid plexiglass rods (of 1 cm diameter) represented a wetland. Plant densities fell between 10% and 35% and the Re_d ranged from 10 to 90. Serra also calculated the diffusion coefficient from a form of Fick's Law, in the form

$$c_{(x,y)} = c_0 e^{U(r-x)/2D} \qquad \text{(eq 2.14)}$$

c_o is the concentration at y = 0 (which tends to be c_{max}), $c_{(x,y)}$ is the concentration at (x,y) and r is $(x^2 + y^2)^{1/2}$ (Serra, 2004). This form is essentially the same as Nepf (1997) as it accounts for lateral diffusion using the average channel velocity.

The results of Nepf's and Serra's experiments are shown in Figure 2.2. The differences in the two studies were 1) a gap in plant densities, 2) an order of magnitude difference in the calculated diffusion coefficients, and 3) Serra had an uncertainty of 30%, while Nepf had an uncertainty of 10% (Nepf, 1997; Serra, 2004). The purpose of the present experiment at Villanova University is to bridge the gap between the data and explore the effects of field conditions on the diffusion coefficient.

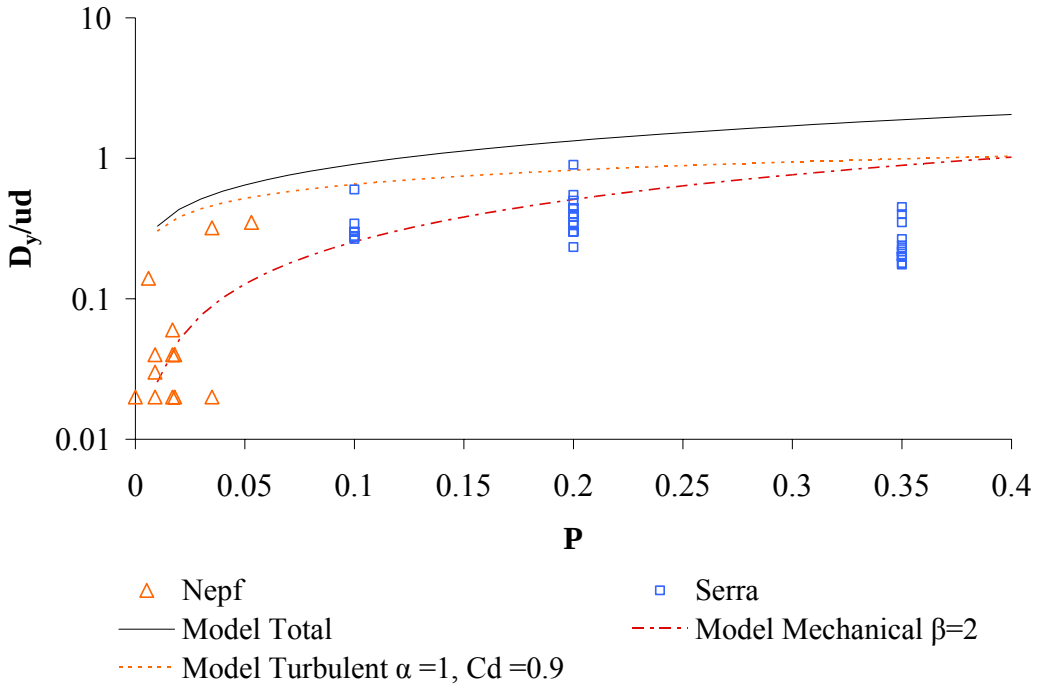

Figure 2.2: Existing Diffusion Data
Laboratory diffusion coefficients of Nepf (triangle) and Serra (squares) for plant densities between 0 and 35%. The mechanical model is shown with the dot dash line, the turbulent model is shown with the dotted line and the total diffusion model is shown with the solid line, where β=2, α_n=0.9 and C_d=3, as suggested by Nepf (1999). The non-dimensional lateral diffusion coefficient in the lateral direction (D_y/ud) is shown versus the percent plant density.

Analytical models have been applied to previous calculated diffusion coefficients to determine how the experimental parameters (such as stem diameter, density, wave size) can be explained. Nepf (1997) proposed a model based upon the probability that a particle would reside in the wake fraction of particular stem, such that

$$\frac{D}{ud} = \frac{1}{2}\frac{d\sigma^2}{dt} = (1-WF)\left[\frac{1}{2}\frac{(\Delta y)^2}{\Delta t}\right] + (WF)\left[\frac{1}{2}\frac{(\Delta y_w)^2}{\Delta t}\right] \qquad \text{(eq 2.15)}$$

where WF is the wake fraction, σ is the variance of the particle distribution, and y_w is the change in position of the wake. The WF is difficult to determine due to interactions between multiple plant wakes (Serra, 2004), so Nepf (1999) revisited the diffusion coefficient and defined a total diffusion model in

$$\frac{D}{ud} = \alpha_n\left[C_d\left(\frac{4P}{\pi}\right)\right]^{\frac{1}{3}} + \left(\frac{\beta^2 n}{2}\right)\left(\frac{4P}{\pi}\right) \qquad \text{(eq 2.16)}$$

The first term on the right-hand side is turbulent diffusion and the second term is mechanical diffusion. During laminar flow conditions, mechanical diffusion is the sole contributor to the total diffusion (Nepf , 1999).

The mechanical model (eq 2.16) is fit over both data sets (Figure 2.2). Nepf proposes a β value of 1; in the present study it is proposed that a β value of 2 is a better representation of the field data. The total diffusion model including turbulent diffusion is a better fit for Nepf's data points with Re_d of 192, the three data points with the highest diffusion coefficients (Figure 2.2). These points may lie in the transitional zone and may experience pockets of turbulence. Serra's data is one to two orders of magnitude higher than the mechanical model and is not a good fit.

Fischer, List and Kohl (1979) also examined lateral diffusion and produced a model that would account for local velocities (eq 3.6), which can more accurately reflect the field conditions present in a wetland. It is assumed that the flow is parallel to the channel, however the velocity is not uniform. The velocity fluctuation is the deviation from the mean velocity. This is the primary equation used in the numerical modeling sections, 3.3 and 4.3.

Nepf (1997) and Serra examined the relationship between Re_d and the diffusion coefficient; the results are inconclusive. A plot of the dimensionless diffusion coefficients versus stem Re_d is shown in Figure 2.3, with data from Nepf (1997) and Serra. Nepf's data are an order of magnitude less than Serra's data but there is no correlation to the Reynolds number (Serra, 2004); Seo et al. (1998) did not find a correlation either.

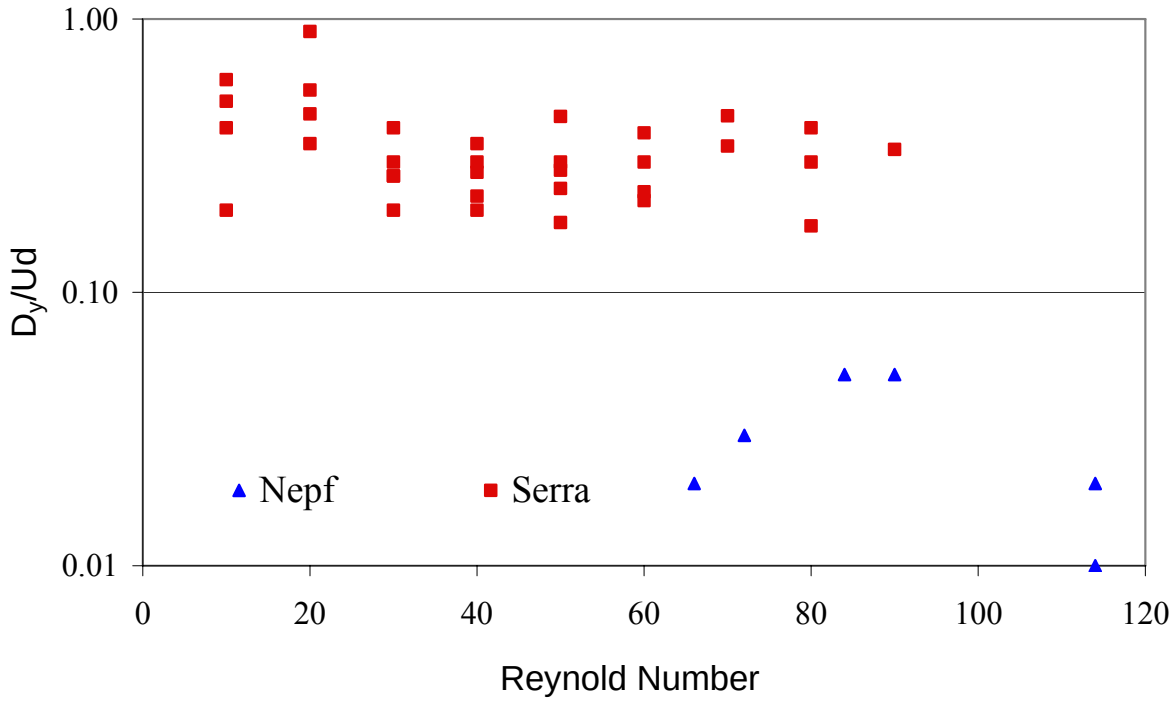

Figure 2.3: Effect of Reynolds number on Diffusion Coefficient.
The diffusion coefficient is plotted against Re_d; Nepf's data is represented by triangles and Serra's data is represented by squares.

2.5 Model

Mike 21 (herein referred to as the Model) is a professional engineering software package, which simulates flows, waves, sediments and ecology in rivers, lakes estuaries, bays, coastal areas and seas. The software has an advanced graphic user interface and has been widely used in engineering applications. It has a modular framework with the hydrodynamic module being the basis for all other calculations. The advection diffusion module will also be used in present study to predict diffusion coefficients under different conditions; this has been done successfully in the past (DHI, 2007).

The hydrodynamic module is based upon the conservation of mass and momentum and simulates two-dimensional (2-D) unsteady flow; the equations can be

seen in the Appendix A. The alternating direction implicit technique (ADIT) is used to integrate the equations over the vertical axis. The governing equations are solved over a grid when provided with bathymetry, bed resistance, coefficients, wind field and hydrographic boundary conditions. The hydrodynamic module also takes into account sources and sinks. It can be applied to model a wide variety of applications, including flow through a wetland (DHI, 2006).

Chezy's number (C) determines the bed resistance. It is calculated from Manning's number (M) as defined by DHI (2006)

$$C = M \times h^{\frac{1}{6}} \qquad \text{(eq 2.17)}$$

The M is the reciprocal of what is used in many text books (e.g. 'n' in Robertson et al, 1998). The normal range for M is 20 – 40 (which corresponds to n = 0.05 – 0.025); if no other information is given a M value of 32 (n = 0.031) should be used (DHI, 2006). The resistance value M = 5 represents stem stalks in the hydrodynamic model created in the present study.

The advection diffusion (AD) module simulates the transport, diffusion and decay of dissolved and suspended substances (e.g. typical uses include water recirculation and tracer simulation). Substances of any type can be modeled including non-conservative and decaying ones. The AD model is based on Fickian dispersion

$$\frac{\partial}{\partial t}(hc) + \frac{\partial}{\partial x}(uhc) + \frac{\partial}{\partial x}(vhc) = \frac{\partial}{\partial x}(h \times D_x \times \frac{\partial c}{\partial x}) + \frac{\partial}{\partial y}(h \times D_y \frac{\partial c}{\partial y}) - F \times h \times c + Q_s(c_s - c) \qquad \text{(eq 2.18)}$$

where D_x and D_y are the diffusion coefficients (L/m^2), the present study is focusing on D_y, F is the linear decay coefficient, Q_s us the source or sink discharge and c_s is the concentration of the compound in the source or sink.

The stability of the hydrodynamic and advection diffusion module must be checked by three separate tasks. The first two are the Courant number based on wave celerity, noted as Cr_c, and current speed, U_{max}, noted as Cr_U

$$Cr_c = \frac{\sqrt{gh}}{\left(\frac{\Delta x}{\Delta t}\right)} \quad \text{(eq 2.19)}$$

$$Cr_U = \frac{U_{max}}{\left(\frac{\Delta x}{\Delta t}\right)} \quad \text{(eq 2.20)}$$

In both cases the Courant number should be less than one. The third stability check is the diffusion coefficient must be in the proper range in relationship to the time step. If D_y and D_x are the same and Δx and Δy are the same then

$$D_y < \frac{\Delta x^2}{\Delta t}. \quad \text{(eq 21)}$$

All three of these conditions must be met in order for the hydrodynamic and AD modules to run properly. Even when these conditions are met oscillations in the solution may occur (DHI, 2006).

The Model AD module has been used to predict diffusion in the past. Nicolini et al. (1999) used the Model to predict the diffusion of the suspended sediment concentrations at the mouth of the Arno River in Tuscan Italy. The Arno River runs through several industrialized cities and the effect different pollutant loads would have on the water quality is very important information to the lucrative tourism industry. Landsat Thematic Mapper, an earth observation system, images were taken to give the actual suspended sediment concentrations. This information was used to calculate the diffusion coefficients in the Model for given flows, wind velocities and bathymetry. Although a

model was successfully produced, the variability in the sediment concentrations, flows, wind velocities and bathymetry produce a model that is not an exact replication of the Arno River (Nicolini et al., 1999). Additional error results when emergent vegetation is modeled. Tennerman et al. (2005) modeled stems stalks with increased resistance in a similar model, Delft3D. Increasing the resistance will alter the flow path, but will not physically block current or create wakes, thereby decreasing the realistic effect model emergent vegetation has on diffusion in the model (see §4.3.4 for more information).

Chapter 3: Methods

The methods chapter of this thesis gives a comprehensive outline of the steps taken to more fully examine the effects of plant density on diffusion in laminar flow stormwater wetlands. §3.1 gives a detailed description of the setup and procedure of the field experiment in the summer of 2006. §3.2 explains the equations and methods used to conduct the numerical modeling. §3.3 gives an overview of the steps and calculations of the modeling process.

3.1 Field Experiment

§3.1 describes the field experiment conducted at the CSW located on Villanova University's campus during the summer of 2006. The equipment used is explained in Appendix B. The site selection and preparation processes will be described in §3.1.1 and §3.1.2. Dye preparation and instrument calibration is explained in §3.1.3 and the daily experimental procedure is described in §3.1.4. The procedure was based on Nepf's (1999) field experiment.

3.1.1 Site Selection

The first step in the field experiment was selecting a site. The criteria for site selection were: the plant density should be between 10% and 20% to reflect the laboratory experiments, the Re_d should be less than 200, it should be accessible and close to a power source. To calculate the plant densities and Re_d, several steps were taken. The plants per unit area were counted using the plant box and the number of plants contained within the plant box was counted three times for each area. Forty-seven

Phragmites were sampled from the wetland. The water depth was marked with duct tape and the surface perpendicular to flow was marked with a Sharpie pen. The diameter was measured using a yard stick and recorded (see §4.1.1 for results). Preliminary velocities were measured using a fishing bopper and a stop watch. The stem diameter and the number of plants per area were used to calculate the plant density. The average velocity, average plant stem diameter and the kinematic viscosity of water were used to calculate Re_d using eq 2.4.

Three potential sites were selected (Figure 3.1) within the Villanova wetland (power supplies are shown by red triangles). The first site is directly downstream of the Sediment Forebay; the depth was 0.78 feet and plant density was approximately 5.7%. Plants were clumped together with lots of open spaces in between; this did not resemble the randomly distributed plants of Nepf's and Serra's experiments. The current flowed in all directions and there did not appear to be a defined channel. The low plant density, poor spacing of Phragmites and undefined flow direction were the reasons site number one was not selected.

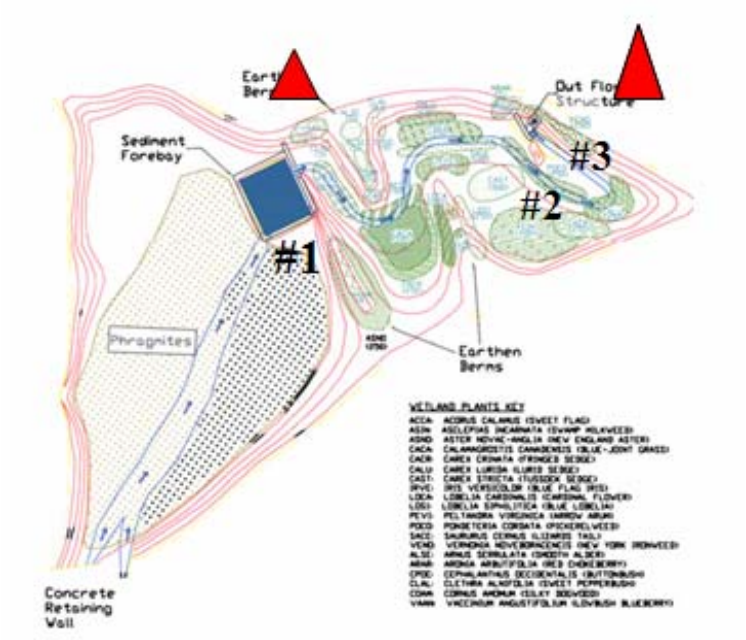

Figure 3.1: Potential Research Sites

Site number two was along the meandering stream of the wetland. The depth was very shallow in this section, between 6 and 10 cm. There was channel flow here, however the low depth of the water interfered with taking the velocity measurements and would most likely interfere with taking the Rhodamine WT reading. The plant density was measured as 3.2%; this site had too low of a plant density and depth to be a viable test site.

The final site was directly upstream of the weir and outlet structure. The depth was 0.40 feet. The flow appeared to travel in a traditional linear channel. The plant density was determined to be 10.24%. The velocities were between 1 and 3 cm/sec which would correspond to Re_d less than 200. The site was also very close to the power supply. The third site was chosen for the experimental setup because it had channel flow, the correct plant density, correct Re_d and was close to a power source.

3.1.2 Site Preparation

A 1.8m x 1.8m section of the CSW was closely examined to study the effect of plant density on the diffusion coefficient (Figure 3.2 and Figure 3.3). The first step in the test setup was to install two wooden rods to support the measuring rope which was then tied between the two boards and marked every 10 cm to be used in measurements of the dye concentration. The area directly below the rope had to be weeded to allow the flourometer and the velocimeter to be used without interference from stems. A working area with a table was also created and shown in yellow in Figure 3.3. The area was weeded and a table placed before the specified test site in order to allow for a clear and mobile testing environment. The actual 1.8m x 1.8m Phragmites bed being studied was weeded in between experiments to achieve the different plant densities to be analyzed.

Figure 3.2: Site Preparation Diagram.
Table is highlighted in yellow. Cross section where dye is measured is highlighted in red and plywood holding up the rope is shown in blue.

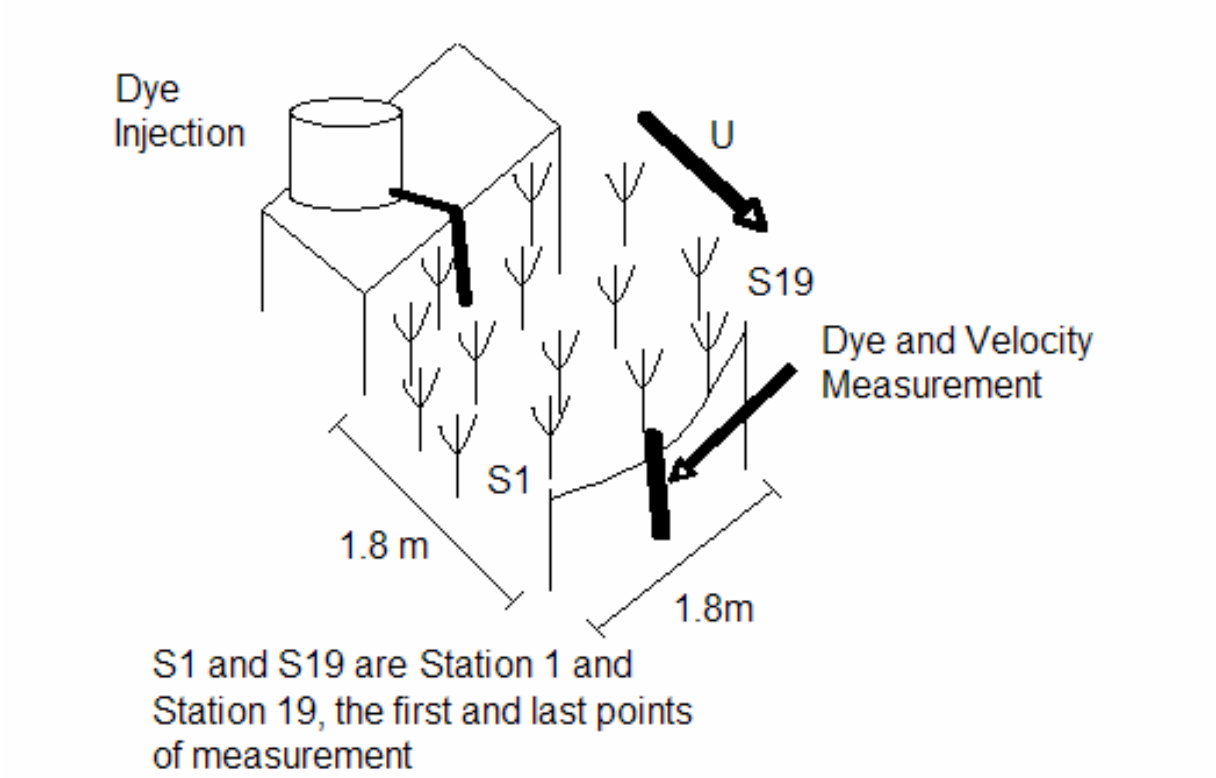

Figure 3.3: Diagram of Test Setup

3.1.3 Dye Preparation and Instrument Calibration

Rhodamine WT dye was used to measure diffusion. The Rhomdamine WT dye arrived at a 20% concentration. A stock solution of 100 mg/L was created (5 mL of the 20% Rhodamine WT was combined with 10 L of wetland water to produce a solution of 100 mg/L)

$$5ml \times \frac{1Liter}{1000ml} \times \frac{200g}{Liter} = 1gram \qquad \text{(Eq 3.1)}$$

$$\frac{1000mg}{10Liter} = \frac{100mg}{Liter} \qquad \text{(Eq 3.2)}$$

and used for calibration of the fluorometer and field procedures. The stock solution was made with water from the outlet of the wetland in order to have the same turbidity and

density to reduce any differences between the water/dye mixture injected into the wetland and the wetland water.

The YSI 600 OMS was calibrated using the stock solution of Rhodamine WT. The water for dilution was retrieved from the wetland. Concentrations of 100 mg/L, 50 mg/L and 25 mg/L were made using pipets and graduated cylinders. Communication with the flourometer was established using the Ecowatch software provided by SonTek YSI. The step by step calibration procedures are shown in Appendix C. This procedure was repeated every week from the stock solution.

The pump did not have to be calibrated, but a pump test was performed. The pump has ten levels of flow; a pump test was performed to determine the flow rate and velocity at each level. The mass of water traveling through the pump per unit time at each power level was recorded. The flow rate was used to calculate the velocity of the water leaving the pump through a ¼ inch diameter outlet at each power level. The calculations are shown in Appendix D, while results are shown in §4.2.1.

3.1.4 Daily Experimental Procedure

The field experiment was conducted in the months of June, July and August 2006 in the CSW on Villanova University's campus. Three different plant densities were examined 3.66, 6.88, and 10.24%; each was tested three to four times. The velocity and depth were measured along the measuring rope every 10 cm before each test run (Figure 3.3). A peristaltic pump was placed on top of the table and the ¼ inch diameter outlet was attached to the table leg at mid depth. A 1 mg/L dye solution was injected into the stream channel at mid-depth and at the in situ velocity. The dye concentration was

measured with the YSI 600 Optical Monitoring System (Flourometer) across the measuring rope 1.8 m downstream of the injection point. The velocity was measured again at the completion of the experiment to check for variations in flow. A detailed step by step procedure can be seen in Appendix E. The data was then downloaded to a lap top using Ecowatch and SonTek software (see §4.1.2 for results)

3.2 Numerical Analysis

Two methods of numerical modeling were used to calculate the diffusion coefficients from the field experiment and compare the results to the laboratory experiments: average and local. §3.2.1 reviews the average diffusivity calculations, §3.2.2 reviews the localized diffusivity calculations, §3.2.3 is the Reynolds number analysis, §3.2.4 analyzes Nepf's (1999) model and §3.2.5 examines the addition and sensitivity analysis of the dead zone term.

3.2.1 Simple Diffusivity Calculations

One method used to calculate the diffusion coefficient for the field data was also used by Nepf (1997)

$$\frac{\bar{c}_y}{c_{\max}} = \exp\left(-\frac{y^2 u}{4D_y x}\right) \qquad \text{(eq 3.3)}$$

$$u = \sqrt{u_x{}^2 + u_y{}^2} \qquad \text{(eq 3.4)}$$

where u_x and u_y are the longitudinal and lateral velocities to incorporate the effects of lateral velocities. The diffusion coefficients were within an order of magnitude when u and u_x were used. The method of least squares was used to create a composite diffusion

coefficient (Nepf, 1997). This was adequate for the laboratory studies as there was one-dimensional, uniform flow, but does not account for local velocity fluctuations that are present in the field experiment. The diffusion coefficients computed from (Eq 3.3) for the field data produced diffusion coefficients larger than the laboratory experiments (see §4.2.1 for results). An example calculation can be seen in Appendix F.

3.2.2 Diffusivity Calculations using Localized Velocity

A second numerical modeling method was used to incorporate the local velocity fluctuations. The velocity fluctuation is the deviation from the mean velocity

$$u'(y) = u(y) - u \qquad \text{(eq 3.5)}$$

where $u'(y)$ is the velocity fluctuation, and $u(y)$ is the local velocity. Fischer et al. (1979) accounts for local velocity fluctuations by substituting the local velocities fluctuations for average velocities and Fickian advection-diffusion becomes

$$\frac{\partial}{\partial t}\left(\bar{c} + c'\right)\Big) + (\bar{u} + u')\frac{\partial}{\partial x}(\bar{c} + c') = D\left[\frac{\partial^2}{\partial x^2}(\bar{c} + c') + \frac{\partial^2 c'}{\partial y^2}\right] \qquad \text{(eq 3.6)}$$

c(y) is the local concentration and c' is the velocity fluctuation. There are three *x* (main channel) locations for each measuring point along the cross section (Figure 3.4); X_0 is the location where dye is released, the dye concentration is measured at X_1 and X_2 is 1.8m downstream of X_1. There are also three time steps: T_0 is when the dye is released, T_1 is when the dye is measured across the cross section and T_2 is two T_1 so that the first wave of the dye will cross X_2 at T_2 assuming uniform velocity. The length and time derivates are independent of each other. At location X_0 and time T_0 the concentration is assumed to be 0, at location X_2 and time T_2 the concentration is assumed to be uniform

across the cross section (see §4.2.1 for results). An example calculation can be seen in Appendix G.

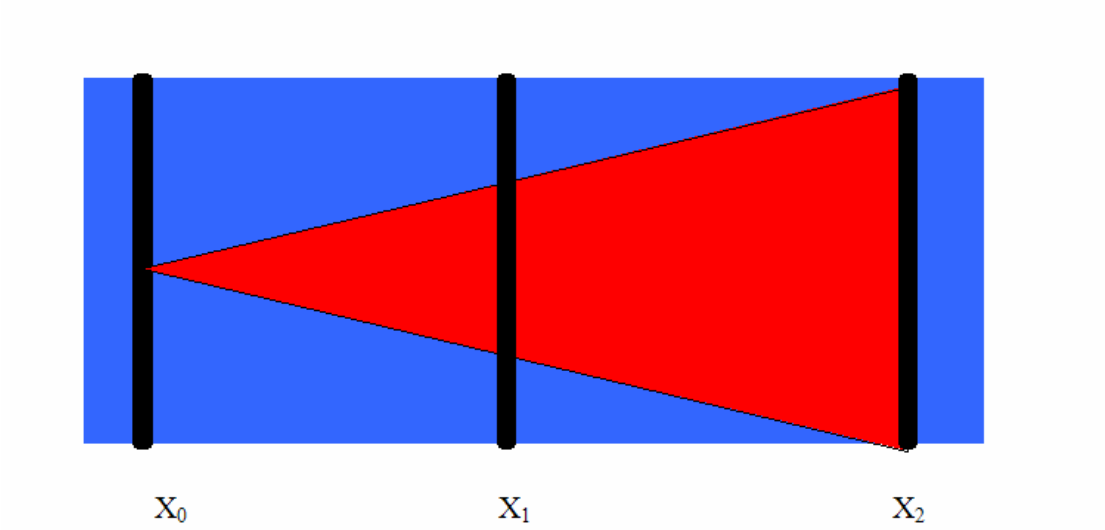

Figure 3.4: Diagram of Cross Section Locations.

3.2.3 Reynolds Number Analysis

The Re was computed in two separate fashions, Re_d (eq 2.4), Re_h (eq 2.5) using a ν of $1.14e^{-6}$ m^2/sec. The extreme and average value of stem diameter, channel width and velocity were used to obtain the range of Re seen in the wetland. The diffusion coefficients were also compared to Re (see § 4.2.2 for results).

3.2.4 Diffusion model

The plant density for the present field experiment, Nepf (1997), and Serra (2004) are given in percent plant density, which represents the percent of the plan area occupied by plant stems. The numerical model proposed by Nepf (1999) represents the plant density with the non-dimensional term *ad*, where $a = nd$, n is the number of plant stems per unit

area and *d* is the diameter. Serra and the present field study used the solid plant fraction percentages (*P*); to convert the ad term to P, *ad* was multiplied by a factor of π/4. $P\frac{4}{\pi}$ was subsituted into (eq 3.7) to form (eq 2.16).

$$\frac{D_y}{ud} = \alpha_n \left[C_d ad\right]^{\frac{1}{3}} + \left(\frac{B^2 n}{2}\right) ad \qquad \text{(eq 3.7)}$$

$$\frac{D}{ud} = \alpha_n \left[C_d \left(\frac{4P}{\pi}\right)\right]^{\frac{1}{3}} + \left(\frac{\beta^2 n}{2}\right)\left(\frac{4P}{\pi}\right) \qquad \text{(eq 2.16)}$$

The diffusion coefficients from Nepf (1997), Nepf (1999), Serra (2004) and the present field study were compared to the numerical model graphically. The numerical model was broken into its component parts of mechanical diffusion and turbulent diffusion, as well as kept as total diffusion (see §4.3.2 for results).

3.2.5 Addition and Sensitivity Analysis of Dead Zone Term

The dead zone term proposed by Pendersen et al. (1977) (eq 2.9 and eq 2.10) was incorporated into the local diffusion equation (eq 3.6) because they are both based on Fickian diffusion. The first three terms in (eq 3.6) and (eq 2.9) are the same except (eq 3.6) accounts for local velocity fluctuations while (eq 2.9) does not. The dead zone term from (eq 2.9) was added onto (eq 3.6) to produce

$$\frac{\partial}{\partial t}(\bar{c} + c') + (u + u')\frac{\partial}{\partial x}(\bar{c} + c') = D\left[\frac{\partial^2}{\partial x^2}(c + c') + \frac{\partial^2 c'}{\partial y^2}\right] + \in T^{-1}(c_d - c) \quad \text{(eq 3.8)}$$

The parameters $\in$, $\frac{\partial C_{dz}}{\partial t}$, *c* and c_{dz} are based on local conditions and will vary on a time and spatial basis. A sensitivity analysis was done to determine the impact field

conditions and the subsequent choice of numerical parameters has on the diffusion coefficient, the original parameters can be seen in Table 3.1. Each parameter was changed +/- 50% at 10% increments (example calculations can be seen in Appendix H). Visual observations and fluctuations in the dye and velocity profiles served as the basis for parameter estimation. The channel concentration was chosen as 25 ug/liter because it was approximately 75% of the maximum concentration. The dead zones of highest dye intensity appeared to be two to four times as concentrated as the average channel concentration and the concentration gradient was changing at a steady rate because flow conditions were continuously being altered. The $\in$ values were determined by observing the amount of debris removed between each plant density (see §4.2.4 for results).

Table 3.1: Dead Zone Parameter Estimation

Cd (ug/liter)	C (ug/liter)	t (seconds)	dCdz(ug/liter)	E (3.33)	E (6.66)	E (10.24)
75	25	30	-25	0.2	0.35	0.5

3.3 Model Procedure

This section reviews the procedure for the Mike 21 model. §3.3.1 reviews the model, options and inputs. §3.3.2 presents the stability calculations and §3.3.3 discusses how the model was used to analyze the effect of field conditions on diffusion in a CSW.

3.3.1 Model Creation

The hydrodynamic and advection dispersion modules were used to complete the Model. The input for the Model is divided into three areas: basic parameters, hydrodynamic parameters and advection dispersion parameters. In the basic parameters section, the hydrodynamic and advection-dispersion module were selected using the quickest AD scheme. The bathymetry consisted of a flat channel of height 0 m. The channel consists of a 30 x 300 grid with each grid area being 0.015 m^2 (Figure 3.5). The initial velocity field was set to zero (a cold start). UTM-30 Map Projection and Coriolis forcing were selected. The time step was 0.01 s; there were two open boundaries at the upstream and downstream ends of the channel (Figure 3.5) with closed boundaries along the sides. The dye was represented by a source at point (15, 290). Flooding and drying was not enabled.

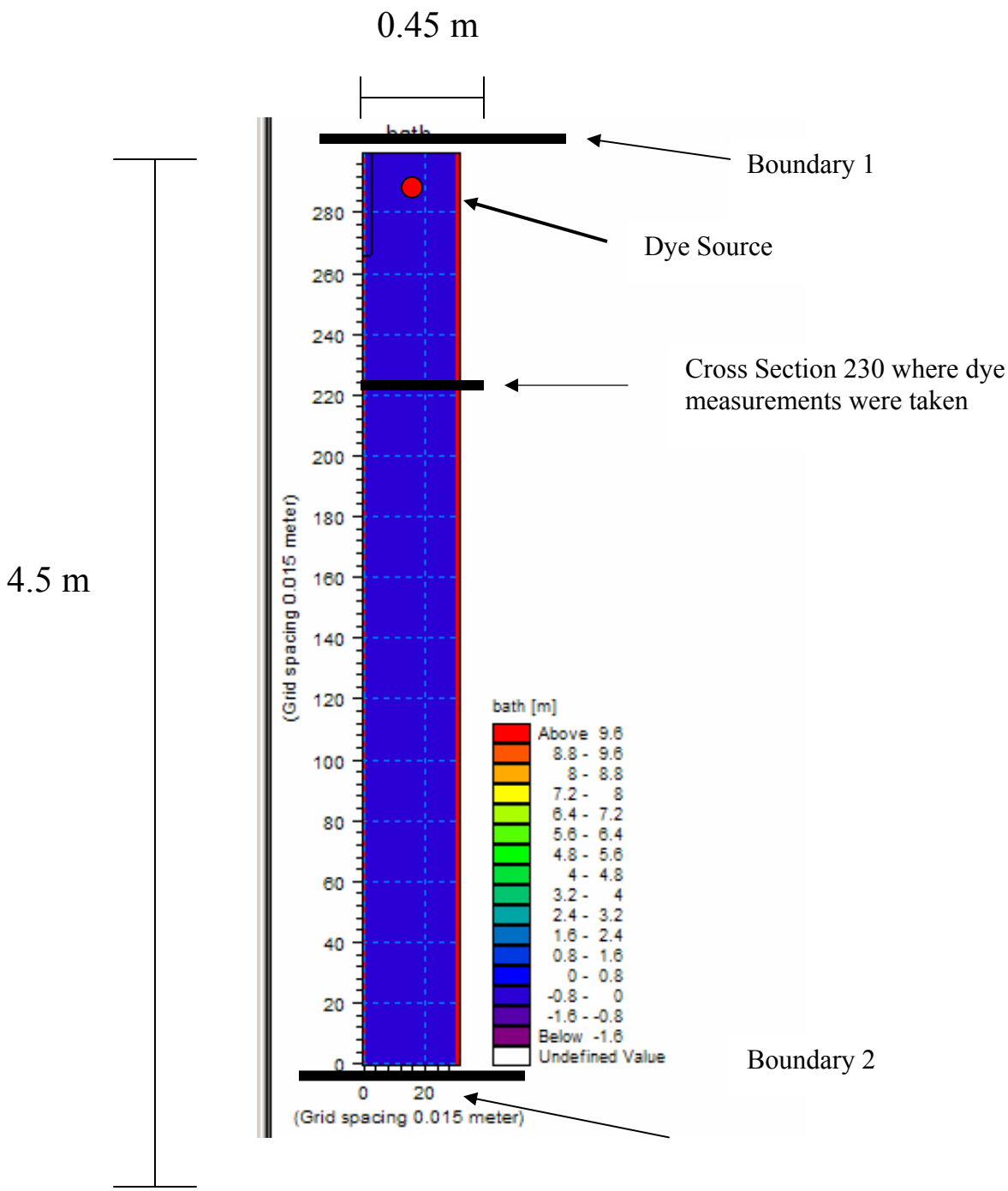

Figure 3.5: Bathymetry Input File

The hydrodynamic parameters were entered in a separate section in the model. The initial water surface elevation was 0.10 meters across the channel and a flux of 0.00045m^3/s travels through each open boundary, corresponding to a velocity of 0.01 m/s. The dye source discharges at the same velocity. The eddy viscosity is 0. The resistance is modeled using Manning number and a value of 32 is used to represent the

channel bottom as recommended by the DHI Reference Manual (see §2.5 for background information). Resistance has been used to represent vegetation in past research (Temmerman et al, 2005). There was no wave radiation or wind condition. The hydrodynamic results are computed at each cell and are written to a text file, following the grid in the form of flux and water height.

The advection dispersion parameters are entered in the last section of the Model. The simulation period spanned 25000 time steps, which is 250 s, and a cold start was used. The component was Rhodamine dye and it was a conservative component. The initial concentration of dye inside the channel and along the boundary was 0 mg/L. The concentration of the dye source was 750 mg/L; a concentration this high was used to give a greater concentration difference at the downstream cross section, making analysis more intuitive. Surface deposition was not included. The dispersion coefficient was $2.0e^{-6}$ m^2/s, which corresponds to a dimensionless diffusion coefficient of 0.013; this is in the range of Nepf's mechanical model (note: diffusion and dispersion may be used interchangeably with regards to the Model). The HD density feedback term is excluded, there is no line discharge or box simulation. The results are given in mg/L over a grid format. A step by step screen shot guide can be seen in Appendix H.

3.3.2 Stability Calculations

Model stability was calculated in three ways, as discussed in §2.5. The first is the Courant Number based on wave celerity, $\left(\sqrt{gh}\right)$ (eq 2.19). For the given grid, time step and channel setup, Cr_c is 0.66, which is less than 1 and is deemed stable (DHI, 2007). The Courant Number is also calculated using the current speed, U_{max} (eq 2.20). For the

given grid, time step and channel setup, Cr_u is 0.0066, which is less than one and is deemed stable. The dispersion coefficient is also a function of stability, where the dispersion coefficient is based on the spatial and temporal discretization (eq 2.21). For the given grid and time step, D_y is $2.0e^{-6}$ m^2/s, which is less than 0.0225 which is required for stability. Thus, all three conditions are met and the Cr_c is the limiting factor.

3.3.3 Model Calibration

In order to verify the hydrodynamic and advection dispersion modules, dye was released in a channel with no vegetation (resistance was constant) and the dye concentration was measured across cross section 230 at different time intervals (Figure 3.5). The cross-section dye concentrations were compared to each other and normal dye distributions were produced at different orders of magnitude. This is an expected result, verifying the model. The velocity across cross section 230 was also measured to make sure it was relatively uniform and reflected the target velocity of 0.01m/s; this was also affirmed, discussed further in §4.3.1.

3.3.4 Model Analysis

The first step in the analysis was to create resistance grids that reflected different plant densities. A Manning number of 32 represented the channel bottom and a Manning Number of 5 represented the stem stalks. Plant densities of 0, 3.5, 5.5 and 10% were created using random number generation in Excel. An example channel can be seen in Figure 3.6. These channels were then used in the Model created in §3.3.1. The dye concentration at cross section 230 and time step 379 was recorded for each plant density and used to compute the diffusion coefficient using (eq 3.3). This equation was chosen to replicate the Nepf (1997) laboratory experiment.

Once the diffusion coefficients were in the proper range for the laboratory simulation, the field conditions were created. Nonuniform resistance (NUR) was created at each plant density; the left hand side of the channel grid had twice as many plant stems as the right. The NUR cases simulated the field conditions where one side of the wetland had a greater plant density than the other, due to the clumping effect often seen in Phragmites stands. The debris and rough channel bottom present in field stormwater wetlands were simulated by increasing bed resistance (IR). The Manning number representing the channel bottom was changed from 32 to 20. Nonuniform velocities (NUV) across the cross section were also used (Table 3.2). The field conditions of NUR, NUV and IR were combined to predict the total effect of both of these elements. The adjusted model field conditions were applied to the 3.5, 5.5 and 10% plant densities. The concentrations across a cross section were recorded and the diffusion coefficients were calculated for each plant density and field condition variation.

One limitation of the Model is that the diffusion coefficient must be specified by the user. Thus, the calculated diffusion coefficients should match the specified diffusion coefficient. If the calculated diffusion coefficient is the same as that specified, then the model is behaving as expected. However, if the calculated diffusion coefficient varies from that specified, it could indicate that the channel characteristics are affecting the flow and diffusion. A second diffusion coefficient was analyzed ($\frac{D}{ud_{stem}} = 0.5$ as found in the field study) to assess the effect of the specified diffusion coefficient and channel characteristics (see §4.3.2 and §4.3.3 for results).

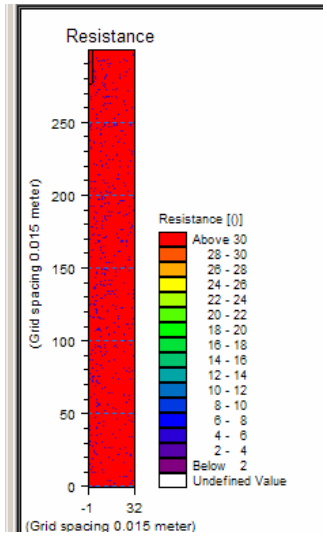

Figure 3.6: Example of Resistance Cell.

The channel bottom is shown in red with a Manning's number of 32, while the plant stems are represented by the blue dots with Manning's *M* of 5.

:

Table 3.2 Nonuniform Velocity Boundary Condition

Station	1	2	3	4	5	6	7	8	9	10	11	12	13	14	15	16	17	18	19	20	21	22	23	24	25	26	27	28	29	30
Velocity (cm/sec)	0.0	0.1	0.2	0.4	0.5	0.7	0.8	0.9	1.1	1.3	1.4	1.6	1.7	1.9	2.0	1.9	1.7	1.6	1.4	1.3	1.1	1.0	0.8	0.7	0.5	0.4	0.2	0.1	0.0	0.0

Chapter 4: Results and Discussion

This chapter presents the results and analysis of the present study. §4.1 presents the results of the field study. §4.2 discusses the results of the numerical analysis and §4.3 presents and discusses the Modeling effort. The combination of the results and analysis shows that field conditions cause pockets of turbulence and variation in the diffusion coefficients and the mechanical diffusion model, Nepf (1999), is not sufficient for field conditions. It is suggested to use the total diffusion model to predict diffusion coefficients and variation should be expected and accounted for in design.

4.1 Results of Field Experiment

In §4.1, the results of the field experiment are presented and discussed. §4.1.1 discusses general site characteristics such as plant diameter and plant density. §4.1.2 gives an example of the results from an experimental run. This data serves as a basis for the numerical modeling and analysis in §4.2.

4.1.1 Plant Diameter and Density

The average plant diameter was determined by sampling 47 stem stalks (all Phragmites) from the area directly upstream of the field test site, measuring and recording each diameter (see Table 4.1). The mean vegetation diameter was 1.52 cm, the minimum diameter was 0.4 cm, the maximum diameter was 4.2 cm and the standard deviation was 0.94 cm. In the laboratory experiments one or two stem diameters were used (e.g. 0.6 cm

and 1.2 cm, Nepf, 1997; 1 cm, Serra, 2004). The differences in stem diameter in the field caused variations in flow paths and Reynolds numbers that were not present in the lab. This discussion is continued in §4.2.

Table 4.1: Stem Stalk Statistical Information

Mean	1.52	cm
Standard Error	0.14	cm
Median	1.10	cm
Mode	0.90	cm
Standard Deviation	0.95	cm
Sample Variance	0.90	cm
Skewness	1.29	
Range	3.80	cm
Minimum	0.40	cm
Maximum	4.20	cm
Count	47.00	

The field plant density was extrapolated from several samples taken in the wetland. The number of plant stems contained in each plant box was measured and recorded five times for each plant density

$$P = \frac{n\frac{{d_{ave}}^2\pi}{4}}{A_{box}} \qquad \text{(eq 4.1)}$$

where n is the average number of stems contained in the plant box, d_{ave} is the average stem diameter and A_{box} is the area inside the measuring box (96 cm^2). Example calculations can be seen in Table 4.2. Each replicate to obtain the plant density is a sample representation of the entire test area, so there is slight variation in each n. These variations produce a plant density that is an estimation rather than an exact measurement, in addition Phragmites reproduce by their root structure creating areas with a higher plant density (Saltonstall, 2001), which may account for some of the discrepancies between the field and laboratory experiments.

Table 4.2: Example Calculation of Plant Density

Trial	n	
1	6	
2	6	
3	6	
4	5	
5	4	
ave d	1.52	cm
ave plant density	5.40	plants
ave stem area	1.82	cm^2
P%	10.24	

4.1.2 Example of Daily Results

The data collected on July 17th, 2006 at a plant density of 6.8% is used as an example (data from all runs is in Appendix J, note Run 1 was discarded to inaccurate readings). Measurements were taken at two locations in the test site: at the table where the dye was injected and across the downstream cross section. Before the experiment began the velocity was taken at the table to match the dye discharge rate to the in situ conditions. A SonTek Velocimeter FlowTracker measured the velocity in the x, y and z directions. A reference coordinate system can be seen in Figure 4.1, example table velocities are in Table 4.3. The lateral velocity (u_y) has a magnitude greater than the longitudinal velocity (u_x), which will affect the dye distribution by physically moving the dye in the lateral direction. The lateral velocities will also increase the total velocity increasing the Re and creating pockets of turbulent diffusion. Vertical velocities were also present; the maximum vertical velocity (u_z) was approximately one order of magnitude less than the maximum lateral and longitudinal velocities and were ignored. An interesting future

study would examine the influence of vertical velocities on the diffusion coefficient (see chapter 5 for more information).

Table 4.3: Example of Table Velocities

U_x	U_y	U_z
0.79	-1.12	-0.85

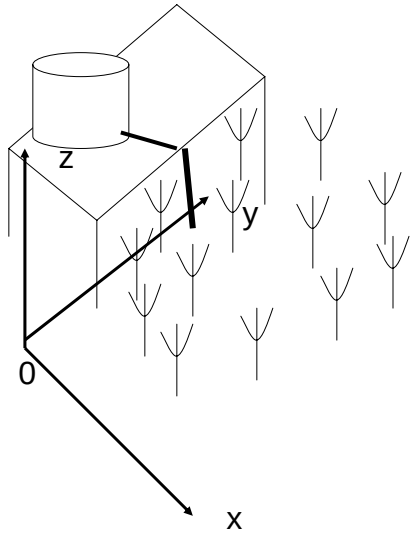

Figure 4.1: Coordinate Diagram

The depth, velocity and dye concentration were measured at the downstream cross section. The channel depth was measured before the start of each run (Figure 4.2). The channel is shaped like a traditional stream cross section with the deepest section in the middle. The variation in the depth will result in variations in Re_h that are primarily in the transitional flow regime; this is discussed in more detail in §4.2.2. The velocity was measured before (u_{x1}) and after the experiment (u_{x2}). The data from 7/17/06 can be seen in Figures 4.3, 4.4, and 4.5 and Table 4.4. The lateral velocities peak in magnitude in the

center (Figure 4.4), the same location where the concentration peaks (Figure 4.5) indicating that the lateral velocites may influence the flux of dye. The velocities u_{x1} and u_{x2} follow the same curve indicating that the velocity was relatively constant over the time period of each experiment. The first velocity reading (u_{x1}) was used in eq 3.3 in §3.2.1 and is referred to as u in the rest of the document. The velocity variation across the cross section will affect the Re_d; §4.2 provides more discussion on the subject. The negative u_x indicate the presence of dead zones, which is explained in more detail in §4.2. The concentration was measured when the first wave of dye passed the cross section (C_1) and again two minutes later to see how the dye concentration patterns and diffusion changed over time (C_2). C_2 was not used for analysis because dye recirculation was occurring off the weir on some runs; dye traveling on the right side of the channel (S19) came in contact with the weir creating a standing pool, lateral velocities then carried the flux of dye to the left side of the channel. Example raw data is shown in Figure 4.5 and Table 4.5. The dye pattern of C_1 peaks sharply in the center. This pattern is not consistent throughout the data sets, some runs (i.e. Run 3, 7/10/06) show little variation between the first and second Rhodamine WT readings. Wall affects are not the same on a day to day basis highlighting the variability of field conditions.

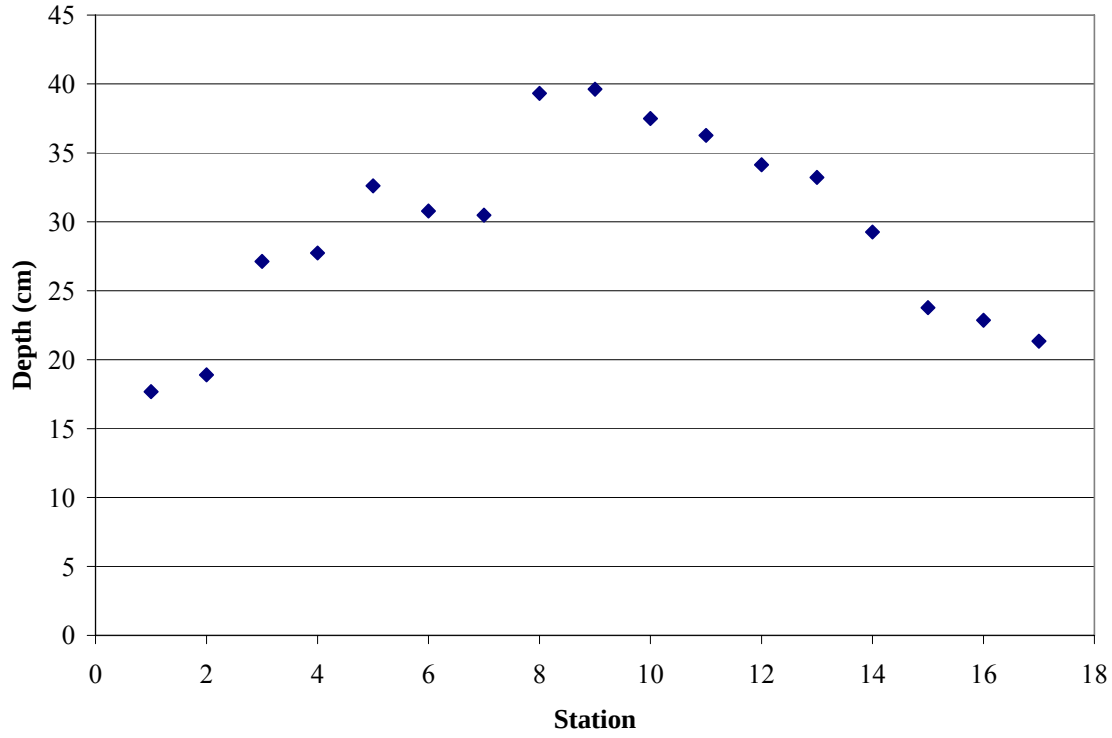

Figure 4.2: Depth on 7/17/06 across the cross section.

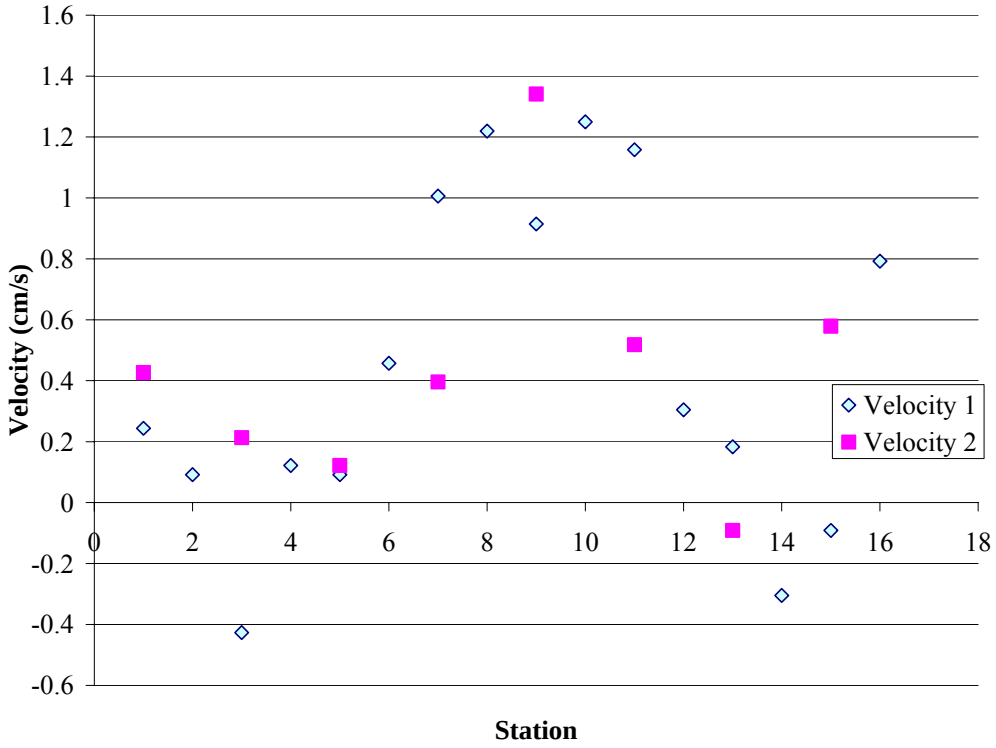

Figure 4.3: Longitudinal Velocity Results on 7/17 across cross section

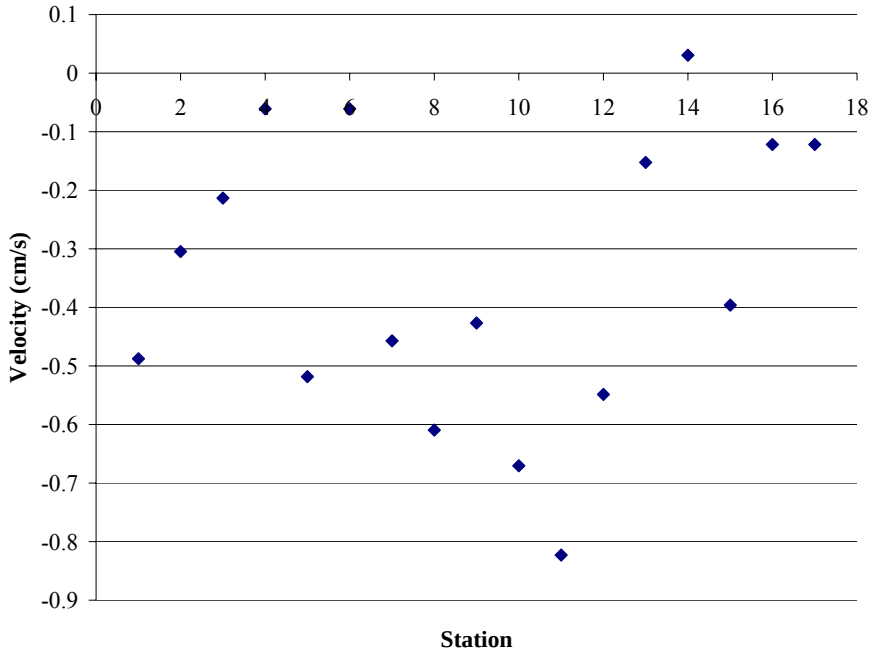

Figure 4.4: Lateral Velocity Results on 7/17 across the cross section

Table 4.4: Sample Velocity Results

Station	Vx_1 (cm/sec)	Vy_1 (cm/sec)	Vz_1 (cm/sec)	Vx_2 (cm/sec)	Vy_2 (cm/sec)	Vz_2 (cm/sec)
1	0.24	-0.49	0.03	0.43	0.30	-0.34
2	0.09	-0.30	0.15			
3	-0.43	-0.21	-0.15	0.21	-0.18	-0.15
4	0.12	-0.06	-0.30			
5	0.09	-0.52	0.06	0.12	-1.22	-0.30
6	0.46	-0.06	-0.43			
7	1.01	-0.46	-0.34	0.40	-0.37	-0.30
8	1.22	-0.61	-0.06			
9	0.91	-0.43	0.00	1.34	-0.49	-0.06
10	1.25	-0.67	-0.12			
11	1.16	-0.82	-0.06	0.52	-0.73	0.06
12	0.30	-0.55	-0.40			
13	0.18	-0.15	0.00	-0.09	-0.49	-0.06
14	-0.30	0.03	-0.21			
15	-0.09	-0.40	-0.21	0.58	-0.03	-0.18
16	0.79	-0.12	-0.06			
17	-0.18	-0.12	0.24			

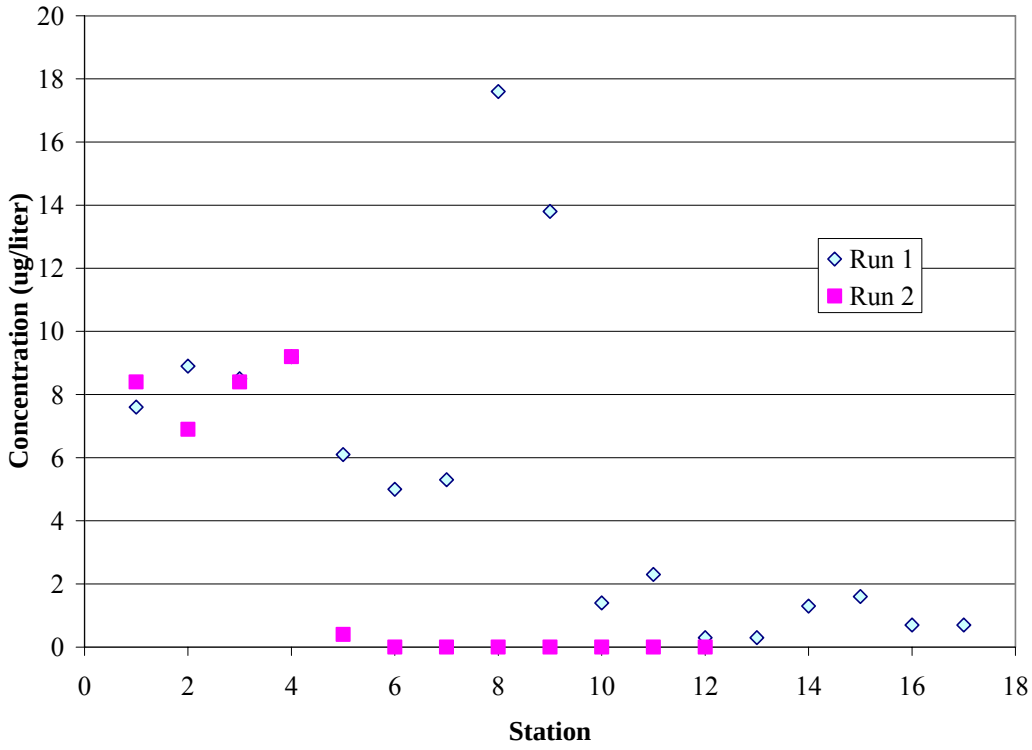

Figure 4.5: Concentration Results

Table 4.5: Dye Results

Station	Run 1 (ug/liter)	Run 2 (ug/liter)
1	7.6	8.4
2	8.9	6.9
3	8.5	8.4
4	9.2	9.2
5	6.1	0.4
6	5	-2.1
7	5.3	-2
8	17.6	-2.8
9	13.8	-2.7
10	1.4	-2.8
11	2.3	-3.7
12	0.3	-5.2
13	0.3	
14	1.3	
15	1.6	
16	0.7	
17	0.7	

The concentration and longitudinal velocity are nondimensionalized for Run 5, (C/C_{max} and V/V_{max}) and plotted together in Figure 4.6 to show that the dye concentration follows the same pattern as the velocity distribution, indicating that the hydrodynamics significantly affect the dye distribution; this statement is supported by the Model analysis of §4.3.

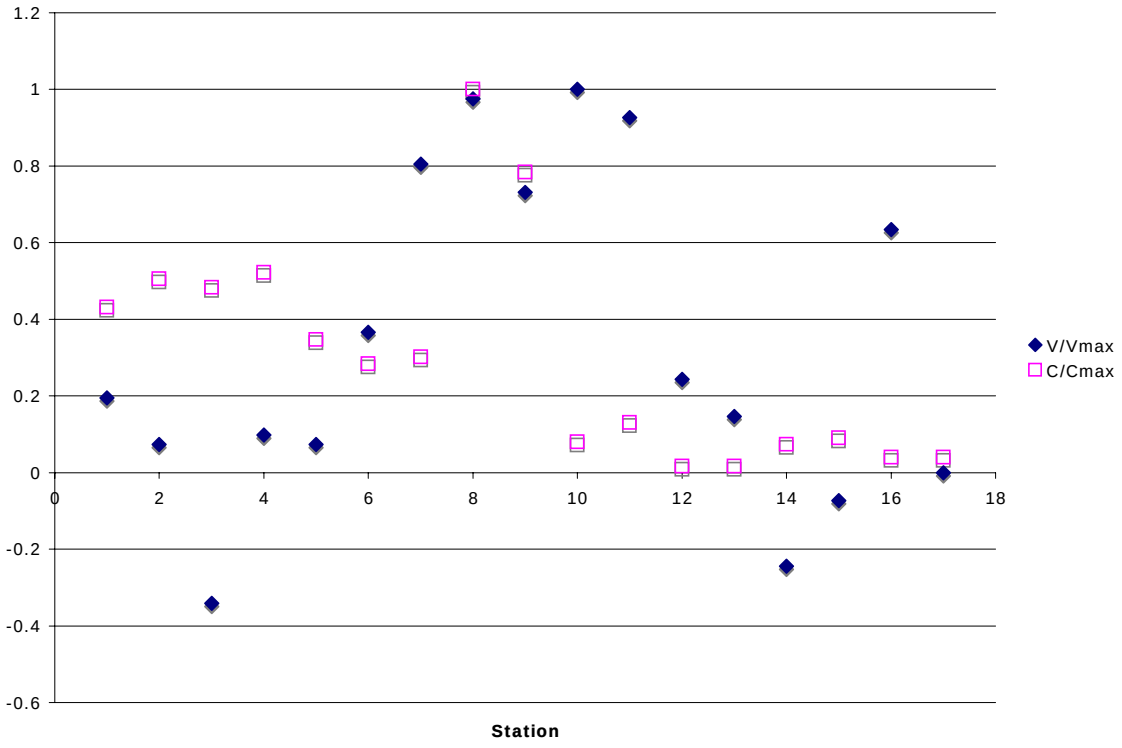

Figure 4.6: Non-dimensional Longitudinal Velocity and Concentration

4.2 Numerical Modeling Results

§4.2 presents and discusses the results of the numerical analysis. §4.2.1 briefly discusses the results on the diffusion coefficient calculations, §4.2.2 discusses the Reynolds number analysis, §4.2.3 applies the results in §4.2.1 and §4.2.2 to Nepf's 1999 model and §4.2.4 discusses the results of the sensitivity analysis for the dead zone model. The combination of the results show that Nepf's total diffusion model (1999) is a better prediction of diffusion in low flow CSWs under field conditions; however the range of values between the mechanical and total diffusion model should be considered due to variations in field conditions.

4.2.1 Diffusion Calculation Results

Two methods of numerical modeling were used to calculate to the diffusion coefficients from the field experiment (§3.1 and §3.2.), which are compared the diffusion coefficients of Nepf (1997), and Serra. One method (Eq 3.3) was used by Nepf (1997) and Serra and is adequate for the laboratory studies as there was one-dimensional, uniform flow, but does not account for local velocities that are present in the field experiment. A second numerical modeling method was used to incorporate the local velocity fluctuations (eq 3.6). The results of this analysis can be seen in Figure 4.7; Nepf (1997) and (1999) are grouped together under the title of Nepf and all results are non-dimensionalized so they can be compared against each other. In the two laboratory calculations the velocity is solely the longitudinal velocity, the total velocities (eq 3.4) were used in both field diffusion calculations.

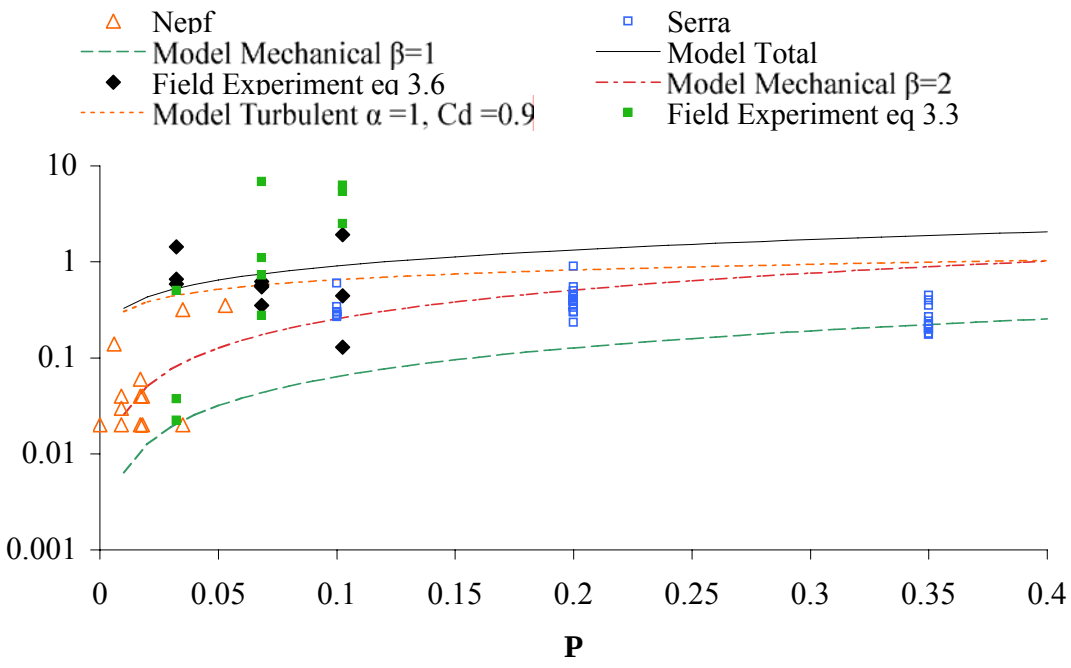

Figure 4.7: Diffusion Coefficient Results.
Nepf's data is shown by red open triangles, while Serra's data is shown blue open by squares (taken from the literature). The highest three Nepf values have Reynolds numbers of 192 and are considered in the transitional zone. The field experiment is shown with black closed diamonds (eq 3.3) and green closed squares (eq 3.6). The mechanical model is shown by a dashed line ($\beta = 1$) and a dot-dashed line ($\beta = 2$) while the turbulent diffusion model is shown be the dotted line and the total diffusion model is shown be the solid line.

The field diffusion coefficients calculated using (eq 3.3) contain extreme values, ranging from the same order of magnitude as Nepf, to three orders of magnitude higher and two orders of magnitude higher than Serra's. These extreme values, along with the absence of local velocity fluctuations in (eq 3.3), make the validity of the calculated diffusion coefficients questionable. The diffusion coefficients calculated using (eq 3.6) account for local velocity fluctuations and are within a smaller range of values: one to two orders of magnitude higher than Nepf's and in the same order of magnitude or one

order of magnitude higher than Serra's results. The field diffusion coefficients calculated (absolute values) using equation (eq 3.6) will be used in the rest of the analysis.

Possible reasons for the discrepancies between the field and laboratory data include debris in the field (e.g. dead plant matter) and bottom shear stress. The debris present in the wetland produces preferential flow paths, which block uniform diffusion through the wetland and also increase the velocity and Re in patches with more flow. The bottom shear stress can produce turbulence and increased diffusion. These concepts are discussed in more detail in §4.2.3.

4.2.2 Reynolds Number Analysis

As discussed in §2.2, the Re is used to represent the type of flow regime within the wetland; in the present study the focus is on Re_d and Re_h. While the laboratory studies suggested calculating Re with the average velocity and characteristic length, it is instructive here to calculate Re with the average, minimum and maximum velocity, stem diameter and channel depth as there are a range of conditions in the field experiment (Table 4.6). The Re_d ranges from 10 to 1952 with a value of 74 when the average velocity and stem diameter are used. The boundary between laminar and turbulent flow is approximately 200 (Nepf, 1997); on average, it appears that the flow would be characterized as laminar, however there could be patches of flow that lie in the turbulent flow regime if greater than average velocities or stem diameters are present. The preferential flow paths carry the majority of the flux traveling through the CSW. The velocity in these flow paths is greater in magnitude than the average velocity. It is

reasonable to assume that a proportion of the flux is turbulent flow when the diameter is the characteristic length.

Table 4.6: Reynolds Number Results

	Minimum Velocity 0.003 (m/s)	**Average Velocity 0.0056 (m/s)**	**Max Velocity 0.053 (m/s)**
Minimum Diameter 0.004 (m)	11	20	186
Average Diameter 0.0152 (m)	40	75	707
Maximum Diameter 0.042(m)	111	206	1953
Minimum Depth 0.17 (m)	**447**	**835**	**7904**
Average Depth 0.28 (m)	**737**	**1375**	**13018**
Maximum Depth 0.36 (m)	**947**	**1768**	**16737**

When the channel depth was the characteristic length, Re_h ranged from 447 to 16737 with 1375 as the average. The transitional zone between laminar and turbulent flow ranges from 600 to 12,500 (Leonard and Luther, 1995). Thus, the present work spans from laminar through the transitional zone and into the turbulent regime, however most of the flow scenarios place the flow in the transitional regime, similar to the work of Kadlec (1990) and Leonard and Luther (1995). The fact that the water depth is shallow enough for the flow to be characterized as transitional will affect diffusion through bed-generated turbulence (Leonard and Luther, 1995) and how the diffusion coefficients characterize the wetland as a whole. The diffusion coefficient was compared to the average Re_d and no relationship was found (Figure 4.8); Re_h was not displayed because the channel depth remained constant over time and there was no variation in Re_h.

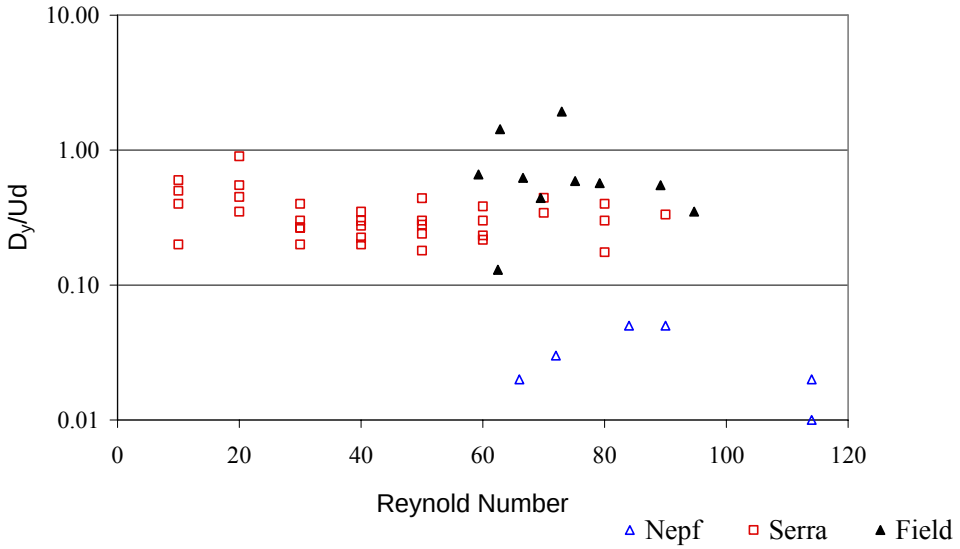

Figure 4.8: Reynolds Number Analysis
The diffusion coefficient is plotted against Re_d Nepf's data is represented by open triangles and Serra's data is represented by open squares and the field data is shown by closed triangles.

4.2.3 Diffusion Model Analysis

The field diffusion coefficients were compared to the numerical model produced by Nepf (1999) (eq 2.16); the results can be seen in Figure 4.7. The diffusion models (mechanical, turbulent and total) plotted in Figure 4.7 use values of the coefficients (α = 0.9, C_d = 3 and β =1 and 2) as suggested by Nepf (1999), see §2.4. The values for the field experiment are a better fit for the total diffusion model than the mechanical diffusion model, which can be attributed to the variation in Reynolds number. Pockets of turbulent flow are present in the field, as seen from the range of Re_d (10 – 1952) and Re_h (447 – 16737) values. Flow traveling around the stem stalks with increased velocity will exhibit more wakes and turbulence than flow with the average velocity. The presence of

turbulence increases the overall diffusion coefficient. In addition, the laboratory experiments had a smooth channel bottom and the model neglects the effects of bed shear stress. In the natural conditions of a stormwater wetland there is the microtopography of the channel bottom and abundant debris on the channel bottom creating additional turbulence. Re_h indicates that the majority of the flow is in the transitional regime. The bed shear stress can also create pockets of turbulence and turbulent diffusion. It is observed that the total diffusion model proposed by Nepf (1999) better predicts diffusion in natural wetlands than simply the mechanical diffusion model. However, Nepf's (1999) model may not always precisely represent the diffusion within a wetland due to variations in field conditions. Perhaps another model that accounts for variations in the velocity field, bathymetry and channel characteristics may provide a better prediction of the diffusion coefficient.

4.2.4 Dead Zone Sensitivity Analysis

The increased diffusion coefficients and the apparent turbulent pockets found in the field are supported by the dead zone concept, as proposed by Pendersen et al. (1977). Pendersen added the dead zone term to the traditional Fickian advection-diffusion equation (e.g. Fischer, 1967) to more closely examine the range of diffusion coefficient values that could result from variations in field conditions. In the present study field diffusion coefficients were calculated using (eq 3.8), to incorporate the dead zone effect. A sensitivity analysis was performed to quantify what effect each parameter had on the diffusion coefficient. Results are shown in Figure 4.9.

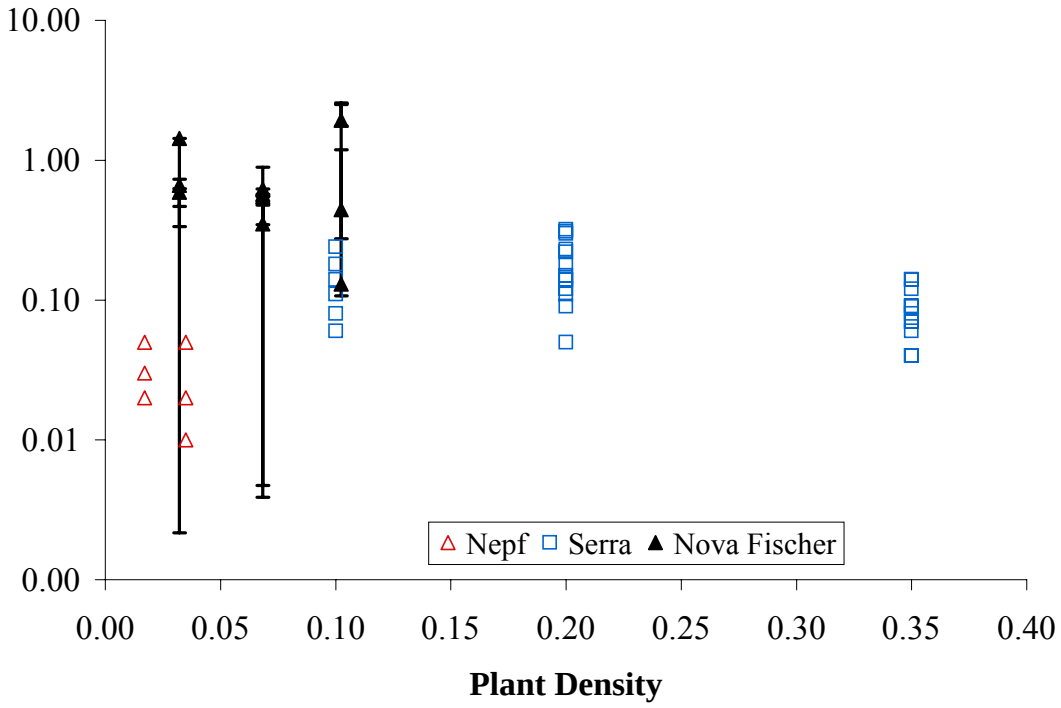

Figure 4.9: Sensitivity Analysis for the dead zone model.
Nepf's data is shown by open triangles, Serra's data is shown by open squares (taken from literature). The field experiment is shown with closed triangles. There is an error bar on each triangle, showing the maximum and minimum diffusion values for that run.

The diffusion coefficient was calculated 31 times (e.g. choosing an original $\in$ and then varying it in 10% increments from -50% to +50%; similar variations were done for dC_{dz}) for each field run in the sensitivity analysis and the maximum and minimum diffusion coefficients for each run were recorded. These values are shown with error bars in Figure 4.9. The sensitivity analysis shows that variation due to dead zones encompasses the entire range of data sets including Nepf's, Serra's and the field experiment. There is more dead zone variability at the higher plant densities due to $\in$, the percentage of the cross sectional area occupied by dead zones, which is intuitive because at higher plant densities, there are more impediments to the through flow. As $\in$ increases, so does the

magnitude of the dead zone term increasing the effect it will have on the diffusion coefficient from (eq 3.8). This analysis indicates that dead zones can significantly change diffusion characteristics and affirms the diffusion coefficient differences between the laboratory studies and field study are due to local field conditions not present in the laboratory. The laboratory studies tended to show good reproducibility in the diffusion coefficients, that is, for a repeated run with the same plant density and velocity, the diffusion coefficient was nearly the same as the original run. Whereas in the field study, repeated runs at the same plant density were performed on different days, where there may be slight variations in the velocity and differences in the field condition (e.g. a storm came through and cleared out some debris, new plant material had been washed into the test area, etc); thus, there was a much wider range of diffusion coefficients for the field condition that may change on a spatial and time basis.

The present study attempted to quantify the effect of each parameter on the diffusion coefficient. The results can be seen in Figures 4.10, 4.11 and 4.12. Figure 4.10 shows the effect of $\in$ on the diffusion coefficient. At the 10.24% plant density, decreasing $\in$ decreases the diffusion coefficient. At the 6.68% plant density, three of the four trials show that a decrease in $\in$ causes an increase in the diffusion coefficient. At the 3.22% plant density there is no defined pattern. When c and c_d are changed there is no change in the diffusion coefficient because the values cancel out when (eq 2.11) is substituted into (eq 10). Figure 4.11 shows the effect of T^{-1} on the diffusion coefficient. At the 10.24% plant density, decreasing T^{-1} increases the diffusion coefficient. At the 6.68% plant density, three of the four trials show that a decrease in T^{-1} causes a decrease in the diffusion coefficient. At the 3.22% plant density there is no defined pattern.

Figure 4.12 shows the effect of $\frac{dC_{dz}}{dt}$ on the diffusion coefficient. At the 10.24% plant density, increasing $\frac{dC_{dz}}{dt}$ increases the diffusion coefficient. At the 6.68% plant density, three of the four trials show that a decrease in $\frac{dC_{dz}}{dt}$ causes an increase in the diffusion coefficient. At the 3.22% plant densities there is no defined pattern.

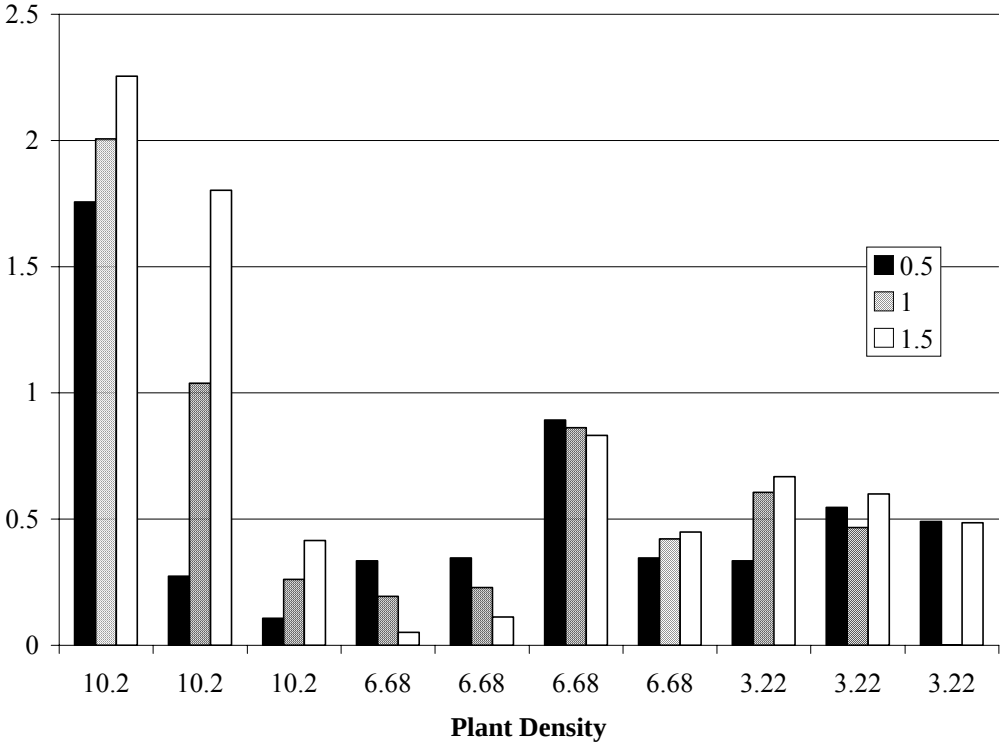

Figure 4.9: Effect of $\in$ on Diffusion Coefficient
The diffusion coefficient values for each run using different $\in$ values are shown.

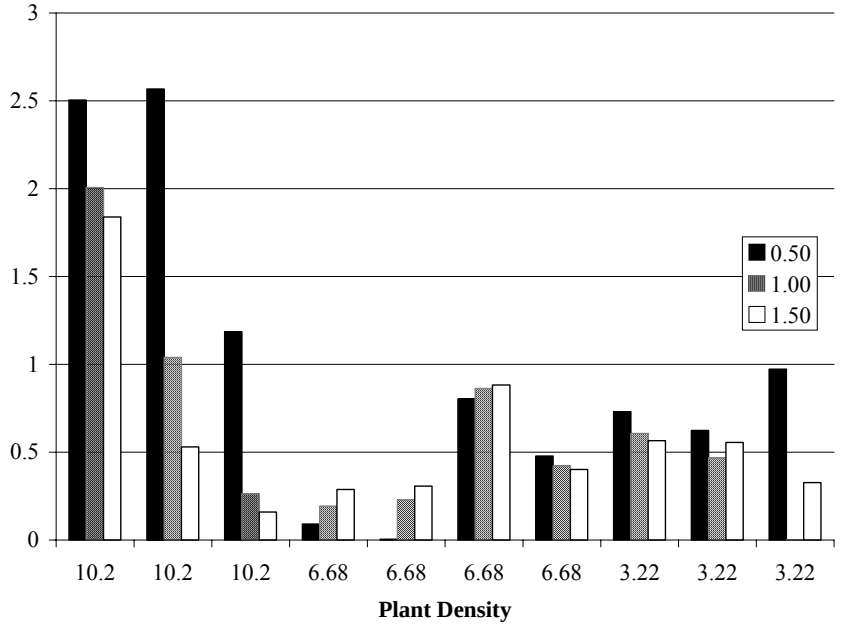

Figure 4.10: Effect of T^{-1} on Diffusion Coefficient.
The diffusion coefficient values for each run using different T^{-1} values are shown.

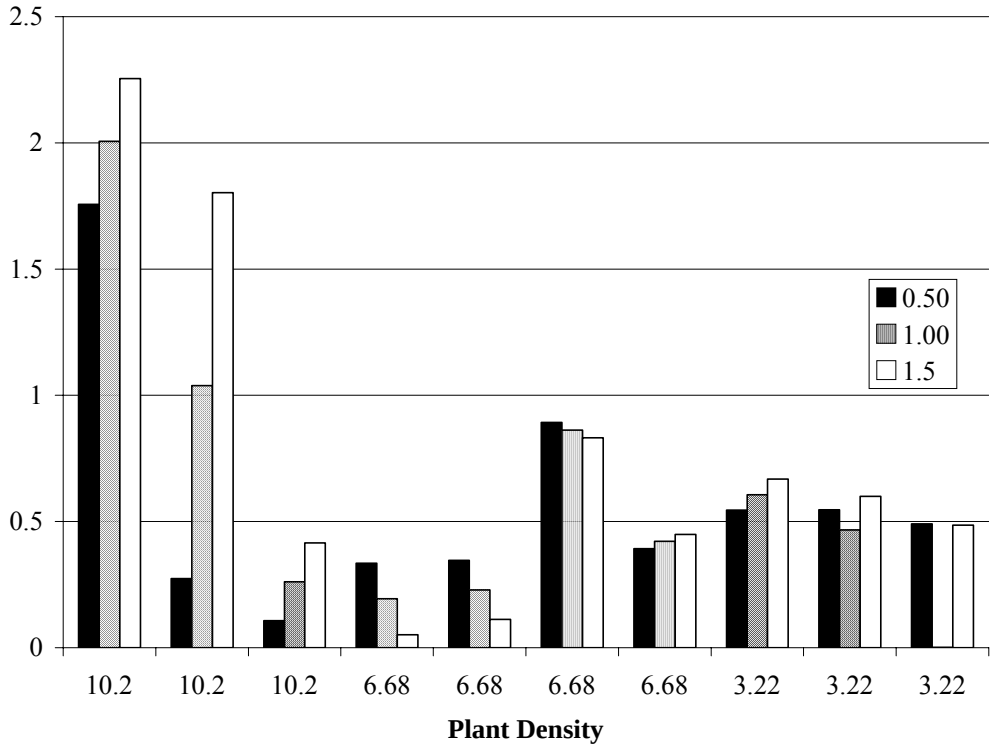

Figure 4.11: Effect of $\frac{dC_{dz}}{dt}$ on Diffusion Coefficient.

The diffusion coefficient values for each run using different $\frac{dC_{dz}}{dt}$ values are shown.

While the results of the sensitivity analysis do not give a clear picture of how the dead zone terms affect the diffusion coefficient, it is interesting to note that there is a trend for each different density, where the highest density had the most clear pattern and the lowest density had no pattern at all; this goes back to the idea of a more dense vegetation will create more opportunity for dead zones to occur. The inconclusive results of the sensitivity analysis are a reflection of the complexity and variance of each diffusion calculation. The composite diffusion coefficient has many contributing factors such as concentration, velocity distribution, and error resulting from the method of least

squares. Varying a factor such as $\in$ has unique effects on the diffusion coefficient in each run. This reflects the conditions that are present in field CSWs. Increasing the volume of dead zones can increase or decrease the diffusion coefficient depending on flow conditions such as flow speed, solute concentration and other variables. Some field conditions will increase diffusion while others will decrease it. The present study recommends that a range of values be considered when designing a CSW. An appropriate range would be values between Nepf's mechanical and total diffusion model because this is where Nepf's, Serra's, and the present field study's values fall between.

4.3 Model Results and Analysis

This section provides the results and analysis of the Mike 21 modeling. §4.3.1 provides the basic hydrodynamic model verification. §4.3.2 demonstrates that the selected Manning's numbers are an appropriate way to represent plant density. §4.3.3 discusses the results and analyzes the effects of changing the channel to represent field conditions. §4.3.4 discusses the effect of the user defined diffusion coefficient and other model limitations. The trends observed in this modeling process provide potential insight into the effect field conditions have on diffusion. The differences between the Model and field CSW prevents definitive conclusions from being formed, however do provide ideas for future research.

4.3.1 Hydrodynamic verification

As discussed in §3.3 the concentration across cross section 230 (Figure 4.12) was measured at seven different computational time steps at a 0% plant density. Cross section 230 was chosen because downstream of this point sidewall affects become significant. The Model writes the results every 25 time steps. Using a time step of 0.01 s each computational period represents 0.25 s; for example, at computational period 400, 100 seconds had passed. Results of the calibration study can be seen in Figure 4.12. A normal Gaussian distribution with some oscillations on the tails is produced for the first five measurements, which is the expected results based on traditional Fickian diffusion. The oscillations are due to variations in the ADIT used for integration. At the later time steps larger oscillations caused by wall effects accelerate the mixing and a flatter distribution is observed.

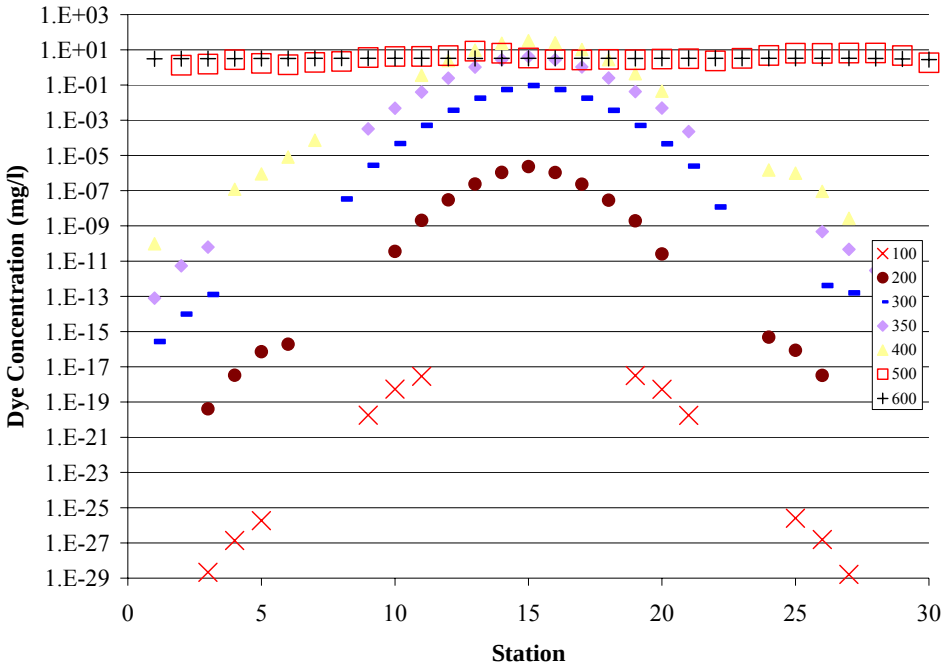

Figure 4.12: Dye Results of Model Hydrodynamic Calibration.

The velocity across cross section 230 was also recorded at seven different time steps (Figure 4.13). At the first five time steps the velocity distribution across the cross section is constant for each time interval. Differences between the velocities for the first five time intervals can be attributed to the oscillations due the ADIT. Larger variations are observed in the last two time steps and can be attributed to the presence of a wall and the mixing that is induced. The dye and velocity profiles are the expected results indicating that basic model is valid and it is acceptable to proceed to modeling stem stalks.

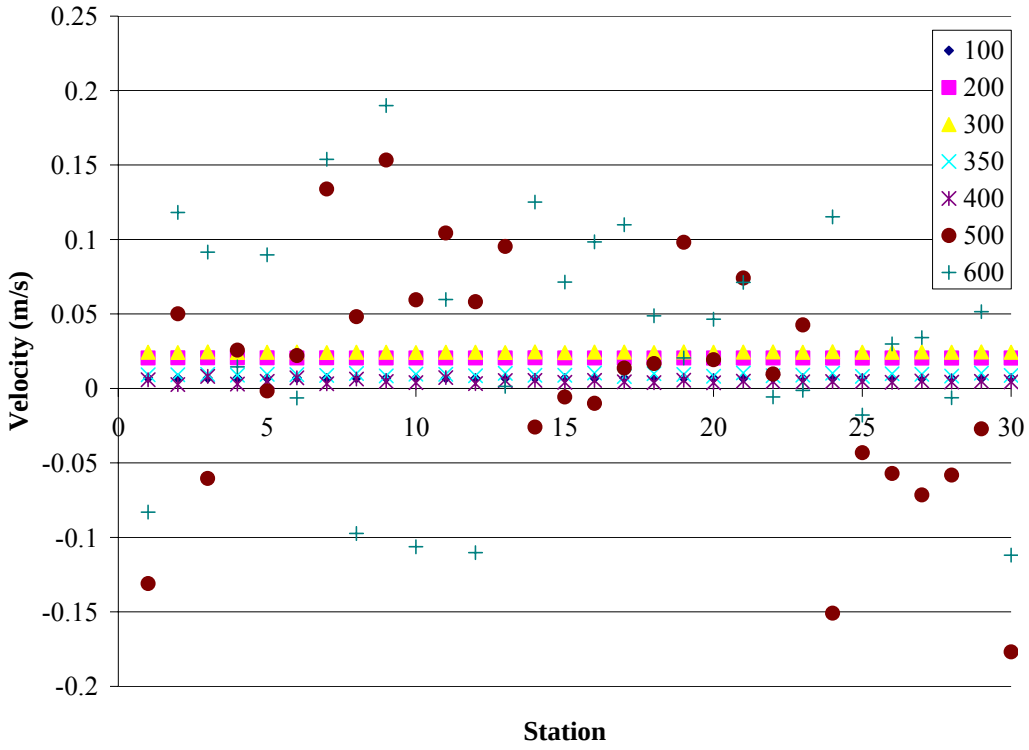

Figure 4.13: Velocity Results of Hydrodynamic Calibration

4.3.2 Resistance Calibration and Verification

The plant stems were represented with a Manning number of 5 while the channel bottom was represented with a Manning number of 32. Channels with four different plant densities were assessed within the model (see §3.3 for more detail). The dye distributions across cross section 230 at computational step 379 can be seen in Figure 4.14. The greatest peak concentration occurs at 0% plant density and the peak concentration decreases as the plant density increases. The reduction in peak concentration is expected as the dye travels through the channel it encounters resistance, representing the stem stalks, which temporarily slows the flow allowing more time for lateral transport. This is illustrated in Figure 4.15, where as the plant density increases so does the velocity variation across cross section 320 at computational step 379; the standard deviations are shown in Table 4.7 and increase with plant density with the exception of the 5.5% plant density. In the field the stem stalks would physically block the path of the dye forcing it to move in a lateral direction before continuing downstream.

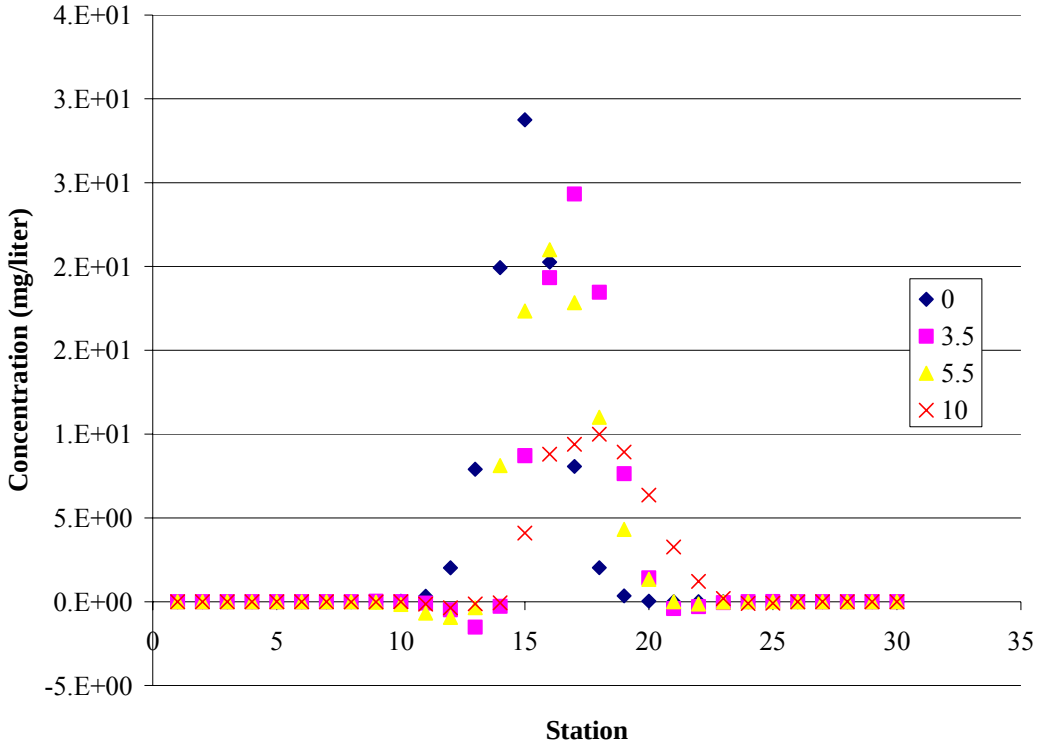

Figure 4.14: Dye Concentrations at different simulated densities.

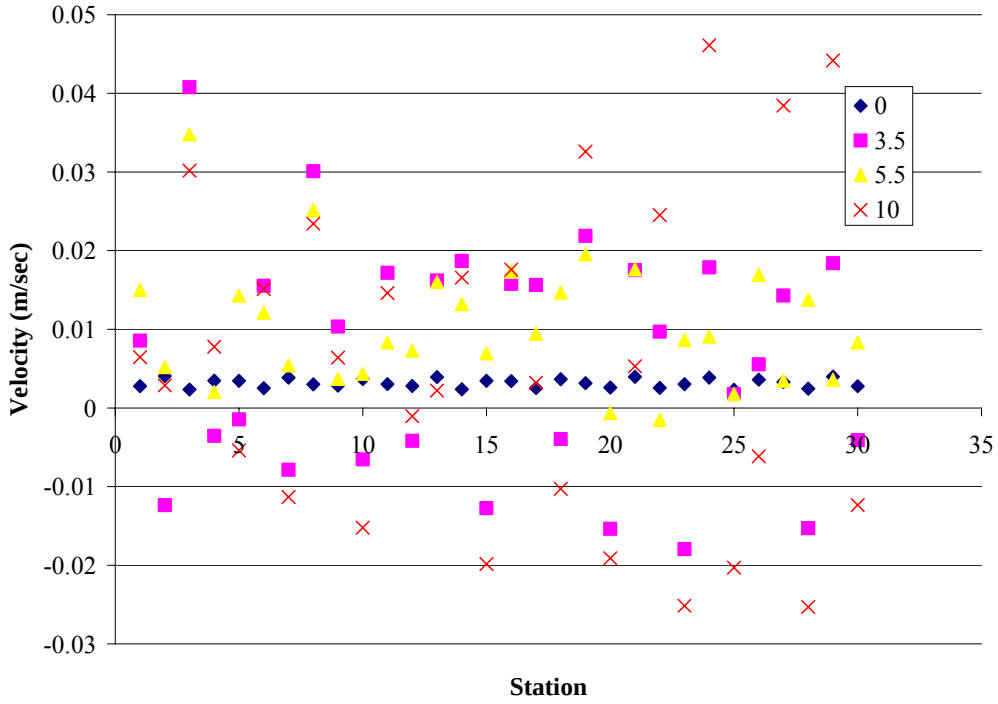

Figure 4.15: Velocity Distribution at different plant densities

Table 4.7: Average Velocity and Standard Deviation at Different Plant Densities

Plant Density	Average Velocity (m/sec)	Standard Deviation (m/s)
0	0.0032	0.0006
3.5	0.0064	0.0136
5.5	0.0105	0.0063
10	0.0055	0.0232

Although the peaks vary in magnitude the curves share the same basic shape, however as the peak decreases the curves get slightly wider. The tailends of the curve are relatively flat with a sharp peaking center of approximately (8-10) stations and the peaks are around station 15. The similarly shaped curves produce similar diffusion coefficients. The diffusion coefficients for the Model are plotted against Nepf's (1999) model in Figure 4.16. There is no increase in the diffusion coefficient as the plant density increases in the Model as predicted by Nepf's 1999 model. In field conditions plant stems physically block flow and create wakes, causing diffusion and mixing. Resistance representing vegetation in the Model creates variation in the flow profile, but does not physically create boundaries or wakes, thus, not fully mimicking the laboratory scenario and the effect simulated plants have on diffusion. In addition the user specifies a diffusion coefficient for the Model. This user defined diffusion coefficient may be the dominating factor, as opposed to the channel characteristics.

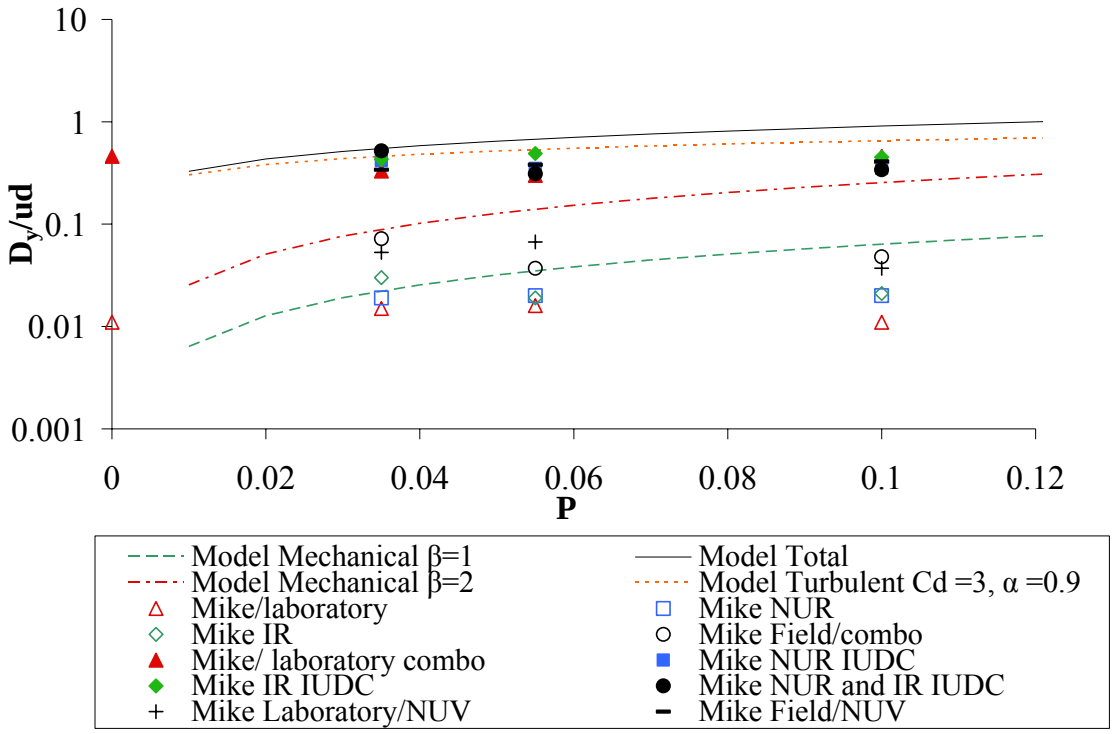

Figure 4.16: Model Results Plotted with Nepf's 1999 model.
IUDC is increased user diffusion coefficient. NUR is nonuniform resistance where the left hand side of the channel has twice as many simulated stem stalks and IR is increased resistance where the Manning number of the channel is changed from 32 to 20. The combo channel combines the IUDC, NUR and IR field conditions.

4.3.3 Effect of Simulated Field Conditions on Diffusion in the Mike 21

Three different field conditions were simulated for 3.5, 5.5 and 10% plant densities. The first field condition, NUR, had plants twice as dense on the left side as the right side. The second field condition, IR, increased the bed resistance from a Mannings number of 32 to 20. The third field condition had nonuniform velocities and the fourth combined the NUR, NUV and IR channels. The resulting dye profiles can be seen in Figures 4.17. 4.18, 4.19; an example velocity profile for the 3.5% plant density can be seen in Figure 4.20. It should be noted that the field variations for the 5.5% plant density were taken at

computational step 360 to reduce the effect of wall oscillations, this was not necessary for the 3.5 and 10 plant densities.

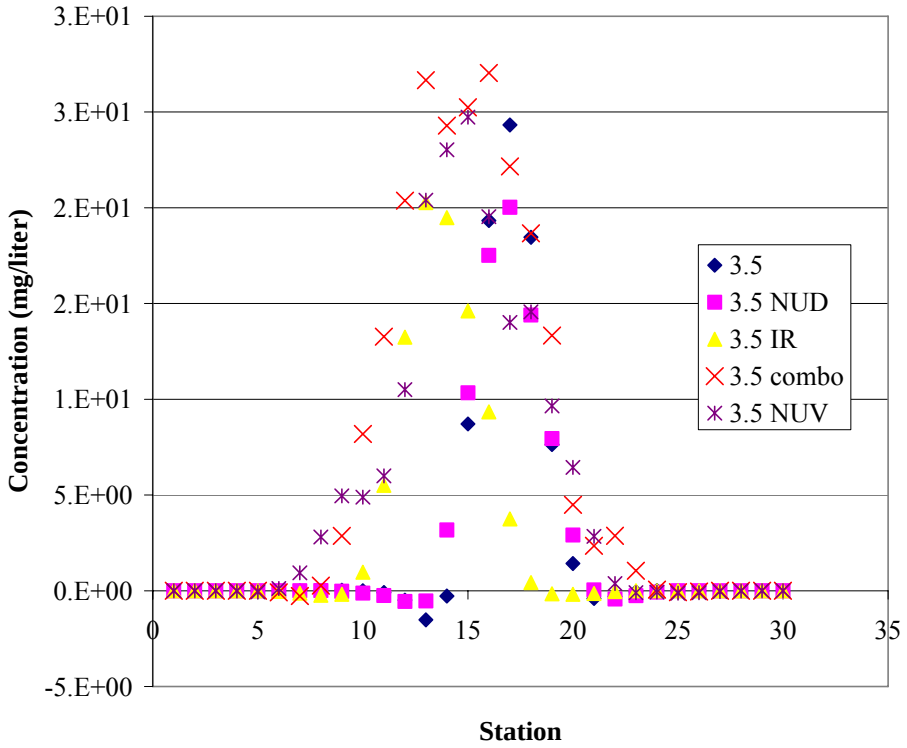

Figure 4.17: Effect of Simulated Field Conditions on the 3.5% plant density.

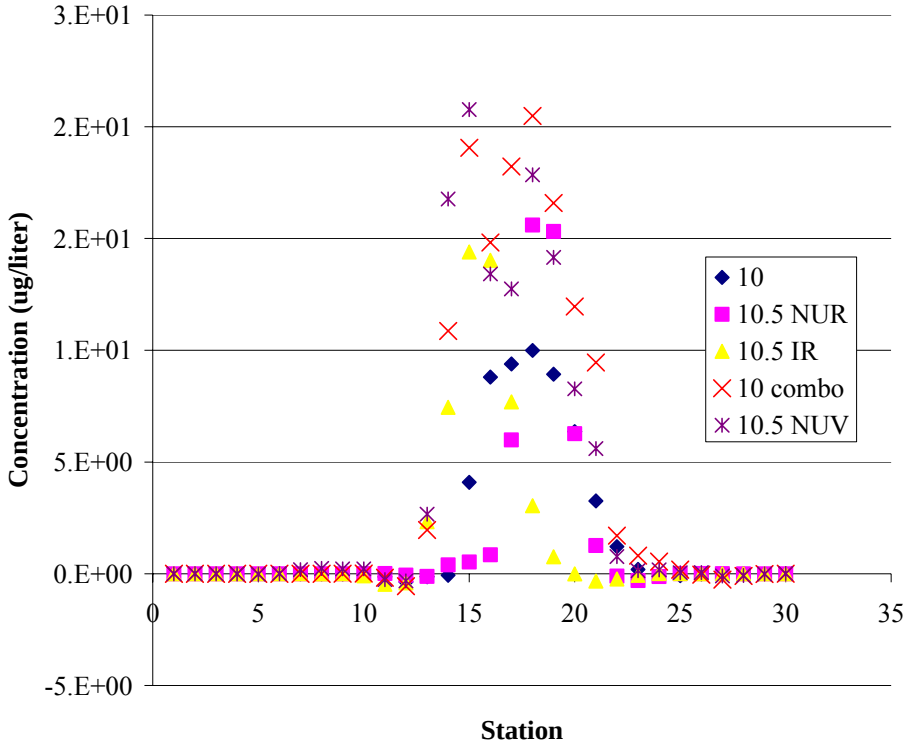

Figure 4.18: Effect of Simulated Field Conditions of the 5.5% plant density.

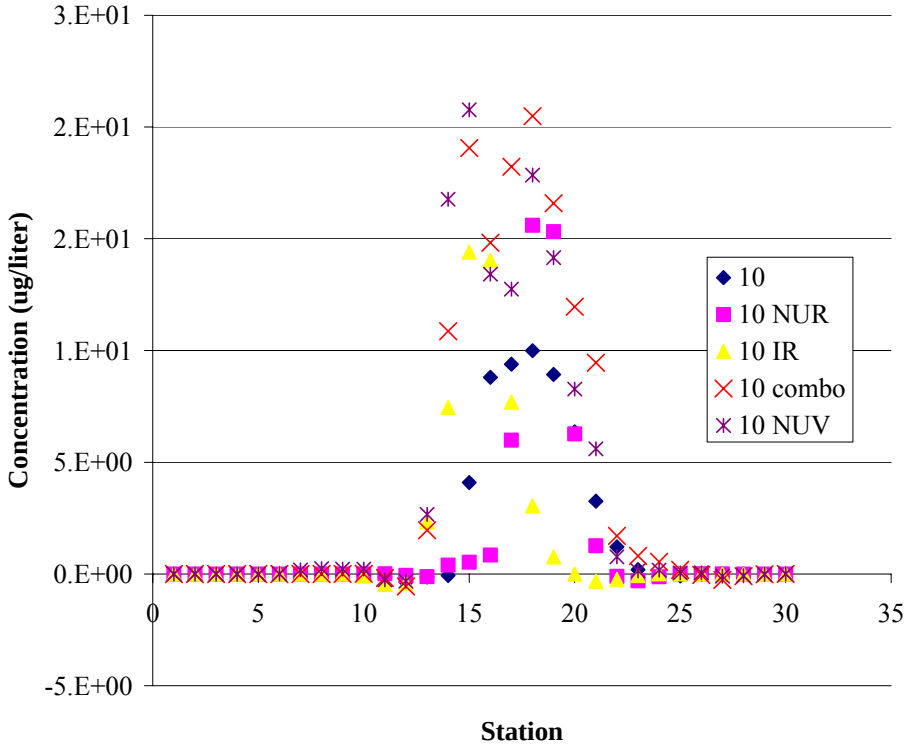

Figure 4.19: Effect of Simulated Field Conditions on the 10% plant density.

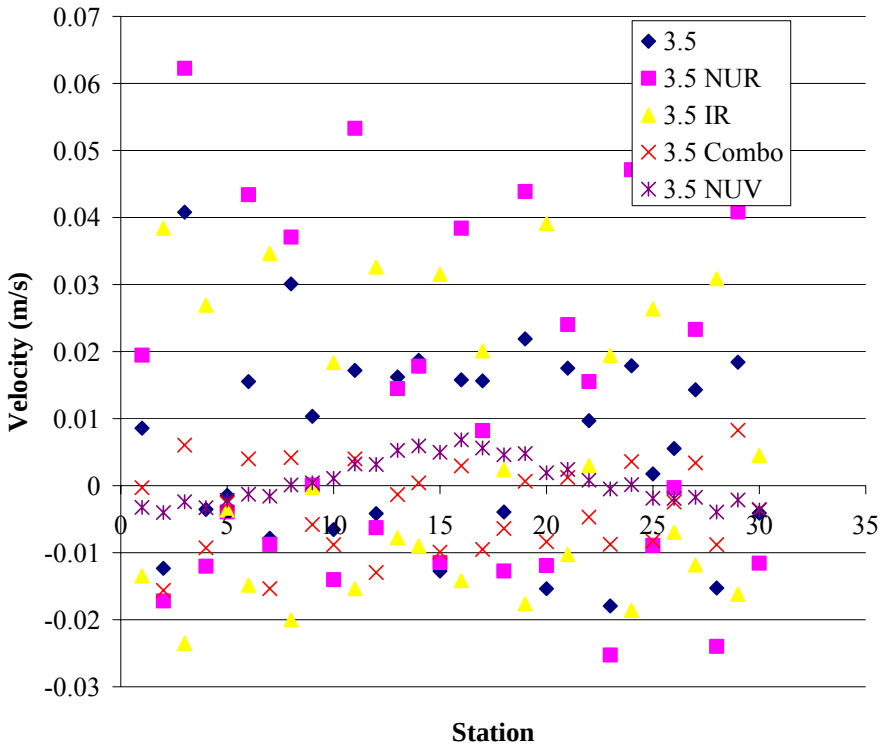

Figure 4.20: Effect of Simulated Field Conditions on Velocity at the 3.5% Plant Density.

The Model simulations of field conditions do not show distinct patterns, and the changes for different field conditions are not as dramatic as the observed differences in the diffusion coefficients between the laboratory flume and field experiments. The NUR channel decreased the peak at the 3.5 and 5.5% plant densities while it increased the peak and shifted it to the right at the 10% plant density. The IR channel shifted the peak to the left at all three plant densities. There was a small increase, 0.01, in the diffusion coefficient at all three plant densities for the NUR and IR channels (Figure 4.17). The NUV channel showed a similar magnitude peak, but flatter curve for all three plant densities and an increase of approximately 0.04 in the diffusion coefficient which is the greater than the other simulated field conditions in the Model but not the same order of magnitude as the field conditions. The combined channel had the same magnitude peak

and a broader base with a diffusion coefficient increase of 0.07 at the 3.5% plant density, an increased peak and diffusion coefficient increase of 0.05 at the 5.5% plant density and a double peak and diffusion coefficient increase of .04 at the 10% plant density. The nonuniform velocity is the most significant factor influencing the diffusion coefficient in the model. The combined channel differences do not result in the magnitude of variation seen in the field conditions. The velocity variations in the field were different than the velocity variations present in the Mike 21 (Figure 4.16). A normal profile was produced to simulate typical channel flow. In the field conditions the velocity profile was skewed towards one bank affecting the flux of dye and diffusion.

4.3.4 Variations between the Mike 21 Model and Field Experiments

There are several important differences between the model and the conditions present in the field experiment. The first is the use of increased resistance to represent stem stalks due to stability problems. The presence of physical obstructions and their wakes is not present in the model. Past research has refined the resistance term (e.g. Tennerman et al., 2005). The Delft3d model has developed a specified friction term based on plant diameter and density to represent plant stem stalks, however it was not able to physically model the plant stems as solid objects in the water (Tennerman et al., 2005). The present study attempted to change the bathymetry to represent cells with stems as a land cell instead of simply with increased resistance, but this led to an unstable model and simulations were not executed. The inability to model stem wakes on the correct scale is an important limitation of computer models when examining diffusion in CSWs. The model created in the present study also lacks skewed velocity variation and negative

velocities observed in the field. In §4.2, it was proposed that pockets of turbulence were produced when flow with an increased velocity encountered stem stalks creating larger than average wakes, increased turbulent diffusion and increased mixing. In the model, neither the increased velocities nor wakes are present to create pockets of turbulence (note: the maximum velocity of 0.01m/s was used in the nonuniform velocities due to Courant number limitations).

The user defined diffusion coefficient also affects the diffusion in the Model. To quantify the effect the analysis was repeated with a defined diffusion coefficient of 0.5, within the range of the field experiment. The dye distribution profiles can be seen in Figure 4.21 and have lower peaks and greater width, or spread, to the distribution curve than the curves representing the laboratory diffusion conditions in Figure 4.13. The diffusion coefficients for the increased user diffusion coefficient, IUDC, can be seen in Figure 4.17 and are compared with Nepf's (1999) model. The IUDC diffusion coefficients are an order of magnitude higher than the diffusion coefficients with a user defined diffusion coefficient of $\frac{D}{ud} = 0.013$ and there is little variation with the exception of nonuniform velocities; indicating the nonuniform velocities are is important, but the user defined diffusion coefficient is the dominant factor. This questions the accuracy of the results concerning the simulated field conditions.

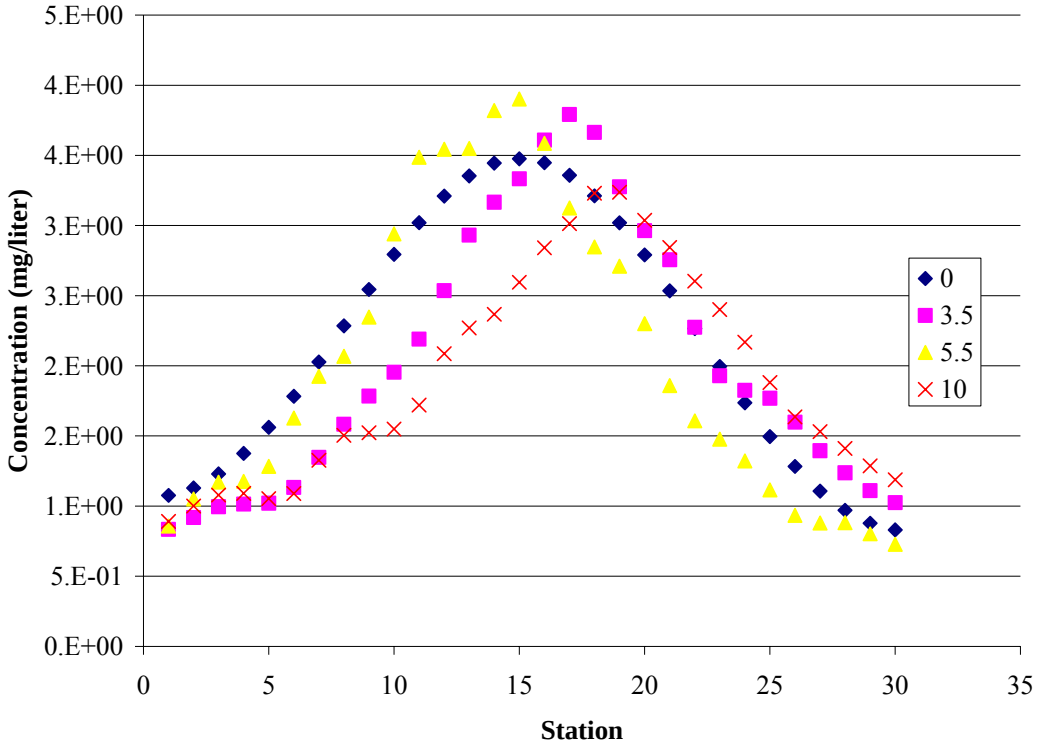

Figure 4.21: Dye Distribution Profiles with a defined diffusion coefficient of 0.5, IUDC.

Chapter 5: Summary and Conclusions

The present study examined the effect of plant density on diffusion in low Reynolds number stormwater wetlands. This topic has been studied primarily in the laboratory and the results of two laboratory experiments Nepf (1997) and Serra are examined (Figure 2.2) where the dimensionless diffusion coefficients were related to plant densities. Serra's diffusion coefficients are an order of magnitude higher than Nepf's and there is a gap in plant densities studied. Nepf (1999) proposed a model which predicts diffusion based on plant density (eq 2.16); total diffusion is composed of mechanical and turbulent diffusion which are independent of each other. In laminar flow only mechanical diffusion is expected. The purpose of the present study was to examine discrepancies between Nepf (1997 and 1999) and Serra, fill in the gap in plant densities and examine the effect of field conditions such as nonuniform flow, bed shear stress and debris. The validity of Nepf's (1999) model was also examined for field conditions. To accomplish this, a field experiment at Villanova University's CSW was conducted in the summer of 2006 where diffusion and plant density were measured. Numerical calculations were performed and a model was produced to quantify the effect of field conditions.

The field diffusion coefficients were one to two orders of magnitude larger than the laboratory because field conditions play an important role in diffusion in a CSW. There is variation in stem diameter standard deviation of (0.94cm), channel depth (5cm) and velocity (1.28cm/s) due to preferential flow paths and channel characteristics; this causes variation in Reynolds number and flow regimes. Although the average Re_d lies within the laminar flow regime, there are pockets of turbulent flow and diffusion. Nepf's (1999) mechanical diffusion model is not sufficient for field conditions and the total

diffusion model should be used to estimate diffusion. There is a large amount of variation between the laboratory studies and field experiment and within the field data range. Similar discrepancies have been documented in the past and attributed to dead zones (Beltaos, 1980). A sensitivity analysis of a dead zone term added to traditional Fickian diffusion proposed by Pendersen et al. (1977) showed that dead zones can create a wide range of diffusion coefficients. A Mike 21 model was produced to quantify the effect of specific field conditions. Model limitations prevent any theories or conclusions from being drawn; however it was observed that nonuniform velocities are the most significant factor when determining diffusion coefficients.

The present study has limitations which could provide the foundation for future research. If field conditions and procedures had reflected the laboratory experiment more, the differences in diffusion could have been more strongly attributed to field conditions not differences in procedures. The weir located at the end of the test channel, caused recirculation and ponding affecting the hydrodynamics and subsequently the diffusion. Concentrations were only taken along one cross section, where as in the laboratory experiment they were taken at several. If the field experiment were to be redone, a straight channel should be used and the concentrations taken at 2 or 3 cross sections.

A laboratory flume experiment could also be created to reflect field conditions. This would have the advantage of being a controlled environment where the effects of each field condition can be isolated and quantified. A nonuniform distribution of plant stems could be simulated along with the presence of debris. An increased bed resistance

could be modeled using simulated organic matter instead of a plexiglass bottom. Each simulated condition should be applied individually and in combination.

Improvements in modeling could also be realized by representing the plant stems as land cells rather than areas of increased resistance. This would cause wakes and eddies that are not present in the model, increasing mixing and diffusion. There are also vertical velocities present in field conditions which could be modeled. The user defined diffusion coefficient is also a model limitation in the present study, a greater sensitivity analysis of this number could provide greater insight into its effect on the diffusion results.

Even with the limitations the results concluded from this study can be applied to the design and analysis of CSWs. The diffusion in field conditions has shown to be greater than laboratory and empirical equations have suggested, which increases the retention time and treatment capacity. The variation in field diffusion coefficients and dead zone analysis show that diffusion in a CSW varies on a day to day basis based on changing field conditions. Engineers and scientists should consider a range of diffusion coefficients when designing treatment in a low Reynolds number wetland.

Works Cited

Ackerman and Okubo. (1993). "Reduced Mixing in a Marine Macrophyte Canopy." Functional Ecology **7**(3): 305-309.

Adams and Papa (2000). Stormwater Management Planning with Analytical Probalistic Models, Wiley.

Baek and Seo. (2004). "Estimation of the Longitudinal Dispersion Coefficient using the Velocity Profile in Natural Streams." Journal of Hydraulic Engineering(March): 227-236.

Basha, H. A. (1997). "Analytical Model of Two-Dimensional Dispersion in Laterally Nonuniform Axial Velocity Distributions." Journal of Hydraulic Enginering **123**: 853-862.

Beltaos, S. (1980). "Longiudinal Dispersion in Rivers." Journal of the Hydraulics Division **HY1**: 151-171.

Carleton and Montas (2006). "A Modeling Approach for mixing and reaction in wetland with continuously varyin flow." Ecological Engineering **1083**.

Carlson, T. N. (2004). "Analysis and Prediction of Surface Runoff in an Urbanizing Watershed Using Satellite Imagery." Journal of the Americal Water Resources Association **40**(4): 1087-1098.

Center for Low Impact Development. (2007). Introductin to Low Impact Development.

Chadderton and Traver. (2000). Section 319 Nonpoint Source Implementation Grand Final Project Report. Villanova, PA, Villanova University.

DHI, w. a. e. (2005). Model & Mike 3 Flow model CWC Scemes Scientific Documentation. Horsholm ,Denmark.

DHI, w. a. e. (2007). Model Environmental Hydraulics, Advection-Dispersion Module Refernce Manual. Horshol Denmark.

Fischer, H. B. (1967). "The Mechanics of Dispersion in natural Streams." Journal of the Hydraulics Division **HY6**: 187-215.

Fischer, List, Koh, Imberger, Brooks (1979). Mixing in Inland and Coastal Waters, Academic Press.

Fox, McDonald and Pritchard. (2004). Introduction to Fluid Mechanics, John Wiley and Sons, Inc.

Groffman, N. L. L., Kenneth T. Belt, Lawrence E. Band and Gary T. Fishcher (2004). "Nitrogen Fluxes and Retention in Urban Watershed Ecosystems." Ecosystems **7**: 393-403.

Kadlec and Knight. (1996). Treatment Wetlands. New York, Lewis Publishers.

Kadlec, R. H. (1990). "Overland flow in wetlands. Vegetation resistance." Journal of Hydraulic Engineering **116**(5): 691-706.

Kashelipour and Falconer, S. M. K. a. R. A. (2002). "Longitudianl dispersion coefficients in natural channels." Water Research **26**: 159-1608.

Ichimura, M. (2003). "Urbanization, Urban Environment and Land Use: Challenges and Opportunites." Asia-Pacific Forum for Environment and Development(APFED3/EM/03/Doc.5).

Laxen and Harrison. (1977). "Highway as a Source of Water Pollution: An Appraisal with the Heavy Metal Lead." Water Research **11**(1): 1-11.

Leonard and Luther. (1995). "Flow Hydodynamics in tidal marsh canopies." Limnol Oceanogr **40**: 1474-`484.

Nicolini, E. P. a. C. S. (1999). Landsat TM images as sea-truth data for calibrating dispersion coefficients in a two-dimensional river plume numberical model. Conference on Remote Sensing of the Ocean and the Sea Ice, Florence, Italy.

Nepf, H. M. (1999). "Drag, Turbulence, and diffusion in flow through emergent vegetation." Water Resrouces Research **35**: 479-489.

Nepf, Sullivan and Zavistoski (1997). "A model for diffusion within emergent vegetation." Limnology and Oceanography **42**(8): 1735-1745.

NRCS (2003). National Resources Inventory 2003 Annual NRI.

Nunnari, G. (2003). "A 3D CNN-based approach to integrate the air pollution diffusion equation." Advances in Air Pollution **13**: 43-52.

PA DEP. (2006). Pennslyvania Stormwater Best Management Practices.

Pennsylvania Department of Community and Economic Development, 2005. "2005 State Land Use and Growth Management Report". Pennsylvania Governor's Center for Local Government Services.

Purnama (1988). "The effect of dead zones on longitudinal dispersion." Journal of Fluid Mechanics **186**: 351-357.

Roberson, Cassidy and Chaudhry (1998). Hydraulic Engineering, John Wiley & Sons, Inc.

Saltonstall, K. (2001). "Cryptic invastion by a non-native genotype of the common reed, Phragmites australis, into North America." PNAS **99**(4): 42445-2449.

Seo and Cheong. (1998). "Predicting Longtiudianl DispersionCoefficients in Natural Streams." Journal of Hydraulic Enginering **124**.

Serra et al. (200). "Effecs of emergent vegetation on lateral diffusion in wetland." Water Research **38**: 139-147.

Streeter, Wiley and Bedford (1997). Fluid Mechanics, WCB/McGraw-Hill.

Temmerman, T. J. B., G. Govers, Z.B. Wang, M.B. De Bries and P.M.J. Herman (2005). "Impact of vegetation on flow routing and sedimentation patterns: Three-dimensional modeling for a tidal marsh." Journal of Geophysical Research **110**.

The Interstate Technology & Regulatory Council Mitigation Wetlands Team. (2005). Characterization, Design, Construction and Monitoring of Mitigation Wetlands. Washington DC, Interstate Technology & Regulatory Council.

Traver, D. R. (2007). CEE 8502: Watershed Modeling, Villanova University, Civil and Environmental Engineering**:** Slides 20-30.

VUSP (2005). Villanova University Stormwater Best Management Practice 319 Report. National Monitoring Program Project. EPA.

Whipple and Hunter. (1979). "Petroleum Hydrocarbons in Urban Runoff." Water Resources Bulletin **15**(4): 1096-1105.

YSI (2006). YSI Environmental Operations Manual 6-Series.

Appendix

Table of Appendices

Appendix A: Mike Hydrodynamic Diffusion Equations 97
Appendix B: Equipment List 98
Appendix C: Step by Step Calibration Procedure 104
Appendix D: Pump Calculations 105
Appendix E: Field Procedure Directions 106
Appendix F: Average Diffusion Calculations 107
Appendix G: Local Diffusion Calculations 108
Appendix H: Dead Zone Sensitivity Analysis Calculation 109
Appendix I: Step by Step Mike 21 110
Appendix J: Daily Field Data 125

Appendix A: Mike Hydrodynamic Diffusion Equations

$$\frac{\partial \zeta}{\partial t} + \frac{\partial p}{\partial x} + \frac{\partial q}{\partial y} = \frac{\partial d}{\partial t}$$

$$\frac{\partial p}{\partial t} + \frac{\partial}{\partial x}(\frac{p^2}{h}) + \frac{\partial}{\partial y}\left(\frac{pq}{h}\right) + gh\frac{\partial \zeta}{\partial x} + \frac{gp\sqrt{p^2+q^2}}{C^2 \bullet h^2} - \frac{1}{p_w}\left[\frac{\partial}{\partial x}\left(h\tau_{xy}\right)\right] - \Omega_q - fVV_x + \frac{h}{\rho_w}\frac{\partial}{\partial x}(p_a) = 0$$

$$\frac{\partial p}{\partial t} + \frac{\partial}{\partial y}(\frac{p^2}{h}) + \frac{\partial}{\partial x}\left(\frac{pq}{h}\right) + gh\frac{\partial \zeta}{\partial y} + \frac{gp\sqrt{p^2+q^2}}{C^2 \bullet h^2} - \frac{1}{p_w}\left[\frac{\partial}{\partial y}\left(h\tau_{xy}\right)\right] - \Omega_q - fVV_y + \frac{h}{\rho_w}\frac{\partial}{\partial xy}(p_a) = 0$$

Symbols are as follows:

h(x,y,t)	water depth (m)
d(x.y,t)	time varying water depth (m)
ζ (x,y,t)	surface elevation (m)
p,q(x,y,t)	flux densities in x-and y-directions ($m^3/s/m$) =(uh,vh); (u,v) = depth averaged velocities in x-y-directions
C(x,y)	Chezy resistance ($m^{1/2}/s$)
g	acceleration due to gravity (m^2/s)
f (V)	wind friction factor
V,V_x,V_y,(x,y,t)	wind speed and components in x- and y- directions (m/s)
Ω (x,y)	Coriolis parameter, latitude dependent (s^{-1})
p_a (x,y,t)	a tmospheric pressure ($kg/m/s^2$)
ρ_w	density of water (kg/m^3)
x,y	spacing coordinates (m)
t	time (s)
τ_{xx}, τ_{xy}, τ_{yy}	components of effective shear stress

Appendix B: Equipment List

The equipment list provides a detailed description of the materials used in the field experiment at Villanova University during the summer of 2006. Pictures and descriptions of specific instruments are provided at the end of the section. General supplies such as rubber gloves and measuring tape will not be explained.

Site Preparation and Initial Measurement

The Plant Box (Figure A.1)
Rags
Cutters/Scissors
2 hedge trimmers
Measuring Tape
Plywood (2)
Philadelphia Rod
Bobber
Stop Watch

The plant box was used to measure the plant density, rags were used for cleaning, cutter/scissors and hedge trimmers were used to clear and prune the Phragmites. The plywood and Philadelphia rods were used to measure the drop in surface water elevation although this information was not used. The bobber and stop watch were used to measure preliminary velocities.

Calibration

2 Empty One Gallon Containers
Graduated Cylinders
Pipettes
Rhodamine WT Dye
Rubber Gloves

The empty one gallon containers were used to obtain water from the wetland for calibration; Rhodamine WT, pipettes and graduated Cylinders were used for

instrumentation calibration and rubber gloves were used for safety purposes. Calibration procedures can be seen in §3.1.4

Dye Injection
5 Gallon Bucket
Table
Peristalic Pump (Figure A.2), Cole Parme Instrument Co. model # 7553030
¼ inch plastic tubing
Outlet (1/4 inch)
Duct Tape
Extension Cord

The 5 Gallon bucket filled with dye solution was placed on a table in the field test area with the Peristalic Pump. The tubing carried the dye to the outlet which was attached to the table leg at mid depth with duct tape. An extension cord provided power to the Peristalic Pump.

Measurement
Rope
Velocimeter (Figure A.3, A.4 and A.5), SonTek FlowTracker
Flourometer (Figure A.6) YSI 600 Optical Monitoring System
Lap Top Computer (Must have Serial Port)

Measurement points were marked along the rope, placed along the downstream location (Figure 3.10). Velocity was measured with the velocimeter and dye concentrations were measured with the flourometer which was controlled by the lap top computer.

References and General Supplies
Key to Power
Extra Batteries
Manuals
First Aid Kit
Instructions
Instrumentation Manuals

The power key unlocked the instrumentation box where the power access was stored. Extra batteries and a first aid kit were taken as a precaution; daily instructions and the instrumentation manuals were taken as a reference.

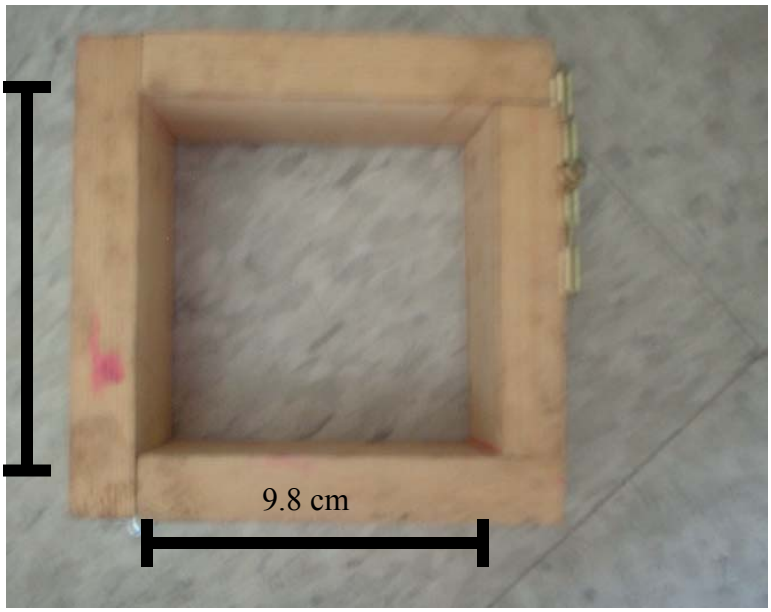

Figure A.4.22: Plant Box.

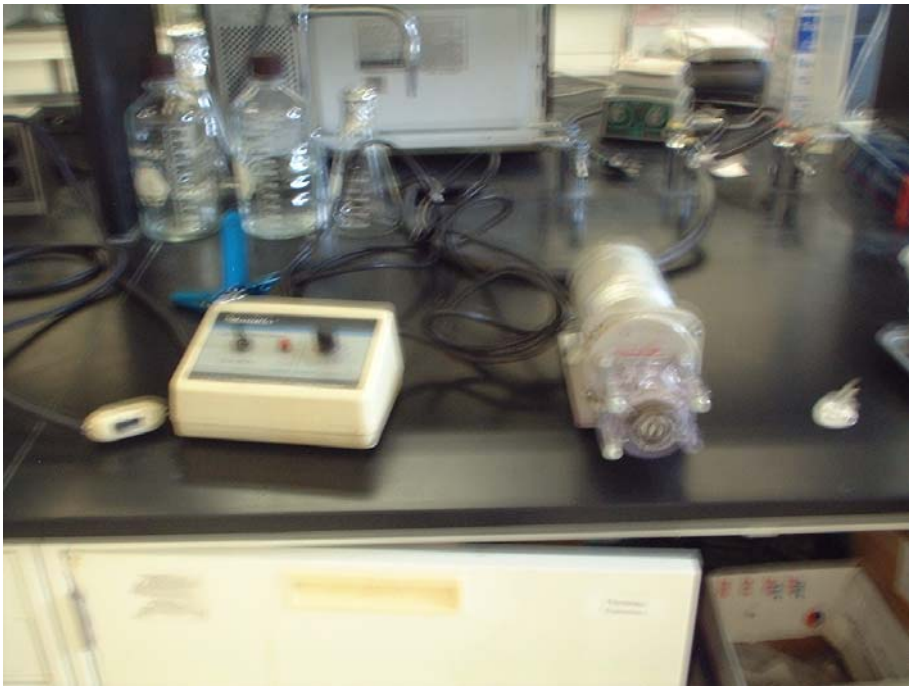

Figure A.4.23: Peristalic Pump.
The Peristalic pump used was produced by Cole-parme Instrament Co. The system model number was 7553-30. The Control device was the Masterflex Solid State Speed Control.

Figure A.4.24: Velcomimeter, SonTrek FlowTracker.

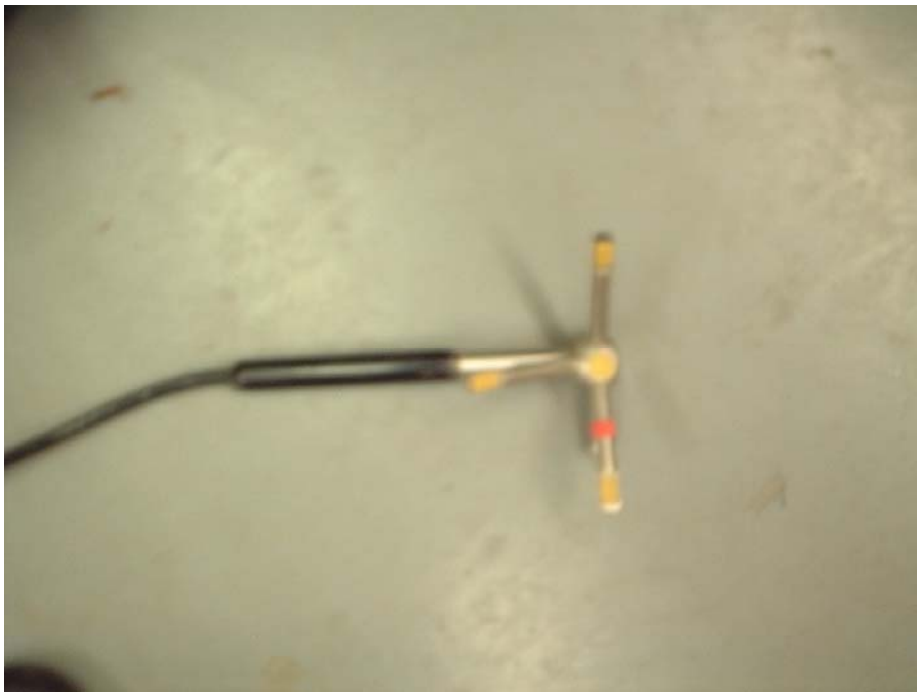

Figure A.4.25: Probe that entered the water for SonTek FlowTracker.

Figure A.4.26: Hand held control device for SonTek FlowTracker.

Figure A.4.27: Flourometer, YSI 600 OMS optical monitoring system**.**

Appendix C: Step by Step Calibration Procedure

Select Rhodamine from the Calibrate Menu and then 2-2 Point

Note: One standard must be μg/L in Rhodamine WT, and this standard must be calibrated first.

To begin the calibration, place the 0 standard (clear dionized or distilled water) into a calibration cup provided with the sonde and immerse the sonde in the water. Input the value 0 ug/L at the prompt, and press Enter. The screen will display real-time readings that will allow you to determine when the readings have stabilized. Activate the wiper 1-2 times by pressing #-Clean Optics as shown on the screen, to remove any bubbles. After stabilization is complete, press Enter to "confirm" the first calibration and then, as instructed, press Enter to continue.

Dry the sonde carefully and then place the sonde in the second Rhodamine WT standard (200 ug/L is recommended) using the same container as for the 0 ug/L standard. Input the correct Rhodamine WT concentration in ug/L, press Enter, and view the stabilization of the values on the screen in real-time. As above, activate the wiper with the "#" key or manually rotate the sonde to remove bubbles. After the readings have stabilized, press Enter to confirm the calibration and then press Enter to return the calibration menu.

Thoroughly rinse and dry the calibration cups for future use. (YSI, 2006)

Appendix D: Pump Calculations

Pump Calculation

Pump Level	Start Time (minutes and second)	End Time (minutes and seconds)	Total Time	ml/second	ft^3/second	ft/second (using 1/4 diameter Pump)	cm/second
10	46:40	46:59	19	1.316	0.000	0.136	4.157
9	49:36	49:54	18	1.389	0.000	0.144	4.388
8	51:37	51:57	20	1.250	0.000	0.130	3.949
7	53:59	54:25	34	0.735	0.000	0.076	2.323
6	55:29	55:57	28	0.893	0.000	0.093	2.821
5	57:07	57:42	35	0.714	0.000	0.074	2.257
4	3:56	4:39	43	0.581	0.000	0.060	1.837
3	5:26	6:27	61	0.410	0.000	0.042	1.295
2	10:11	12:20	129	0.194	0.000	0.020	0.612
1	N/A	N/A	N/A	N/A	N/A	N/A	0.000

Appendix E: Field Procedure Directions

Part A Site Preparation

1) Bring Pump and Dye out to Table
2) Secure Pump to Table using Duct Tape
3) Secure outlet to end of table at Mid Depth pointing at direction of primary velocity
4) Assemble Velocimeter
5) Open power box with key and plug in the two extension cords
6) Attach one extension cord to lap top and duct tape second to table
7) Assemble Flourometer and attach to computer

Part B Preliminary Measurements

1) Use Philadelphia Rod to measure longitudinal distance between outlet and testing site
2) Mark each piece of plywood as upstream or downstream.
3) Place the plywood at the corresponding upstream and downstream ends of the testing site and mark the water surface elevation
4) Use the Philadelphia Rod to create a line perpendicular to the downstream piece of plywood that connects with the upstream piece of plywood. Mark where the Philadelphia Rod intersects with each piece of plywood.

Part C Velocity and Depth Measurements

1) Use the Velocimeter to measure the velocity of the water in the primary direction of flow next to the table leg.
2) Measure the depth and velocity every 10cm along the testing site. Record the depth velocity by hand

Part D Dye Test Procedure

1) Plug power into pump.
2) Use velocity measured in Part C to set the power settings for the pump, see chart in Appendix C.Turn Pump on.
3) Take Rhodamine WT concentrations every 10 cm once the dye becomes visible. Repeat this procedure 3 times

Appendix F: Average Diffusion Calculations

Date	7/31/2006		Average Velocity	0.01	m/second
Plant Density	3.22		x	1.83	m
Reynolds Number	62.82				
Original Concentration	100000	ug/liter	Dopt	0.00	
Run #	11			0.61	

Station	Concentration (mg/liter)	y	C/Cmax	ln(C/Cmax)	y^2	D	In Bracket	sq_bracket
1	2	-0.85	0.05	-3.06	0.72	1.49E-04	-0.22	0.05
2	5.7	-0.75	0.13	-2.01	0.56	1.77E-04	-0.22	0.05
3	10.6	-0.65	0.25	-1.39	0.42	1.92E-04	-0.21	0.04
4	11.2	-0.55	0.26	-1.34	0.30	1.43E-04	-0.31	0.10
5	17.4	-0.45	0.41	-0.90	0.20	1.43E-04	-0.28	0.08
6	24.5	-0.35	0.58	-0.55	0.12	1.40E-04	-0.22	0.05
7	24.3	-0.25	0.57	-0.56	0.06	7.04E-05	-0.32	0.10
8	22	-0.15	0.52	-0.66	0.02	2.15E-05	-0.44	0.20
9	40.1	-0.05	0.94	-0.06	0.00	2.62E-05	-0.05	0.00
10	41.3	0.05	0.97	-0.03	0.00	5.10E-05	-0.03	0.00
11	39	0.15	0.92	-0.09	0.02	1.61E-04	-0.04	0.00
12	41.4	0.25	0.97	-0.03	0.06	1.38E-03	0.08	0.01
13	32.5	0.35	0.76	-0.27	0.12	2.86E-04	-0.04	0.00
14	33.2	0.45	0.78	-0.25	0.20	5.14E-04	0.09	0.01
15	42.6	0.55	1.00	0.00	0.30	#DIV/0!	0.43	0.18
16	39.2	0.65	0.92	-0.08	0.42	3.21E-03	0.46	0.21
17	26.4	0.75	0.62	-0.48	0.56	7.44E-04	0.26	0.07
18	20.7	0.85	0.49	-0.72	0.72	6.33E-04	0.22	0.05
							SUM	1.20
							e	0.26

$$\text{where } e = \sqrt{\frac{1}{N}\sum_{\forall y}\left[\frac{c_y}{c_{\max}} - \exp\left(-\frac{y^2 u}{4D_y}x\right)^2\right]}$$

Appendix G: Local Diffusion Calculations

Date	Average Velocity (cm/sec)	x (cm)	C average (ug/liter)	Delta t	Dopt	Dy/Ud
7/17/2005	0.41	190	5.33	460.74	-0.39	-0.62

Station	Concentration (mg/liter)	C'	Velocity (cm/second)	U'	d^2 (C')	d^2(C+C')	First Term	Second Term	Third Term	D	In Bracket	sq Bracket
1	7.6	2.27	0.24	-0.17	-0.97	-9.87	0.016	0.010	-0.010	-2.630	2.24E-02	5.00E-04
2	8.9	3.57	0.09	-0.32	-1.70	-12.47	0.019	0.004	-0.017	-1.361	1.69E-02	2.84E-04
3	8.5	3.17	-0.43	-0.84	1.10	-11.67	0.018	-0.019	0.011	-0.060	3.51E-03	1.23E-05
4	9.2	3.87	0.12	-0.29	-3.80	-13.07	0.020	0.006	-0.038	-0.674	1.09E-02	1.20E-04
5	6.1	0.77	0.09	-0.32	2.00	-6.87	0.013	0.003	0.020	0.817	2.39E-02	5.70E-04
6	5	-0.33	0.46	0.04	1.40	-4.67	0.011	0.012	0.014	1.650	2.83E-02	8.00E-04
7	5.3	-0.03	1.01	0.59	12.00	-5.27	0.012	0.028	0.120	0.330	8.62E-02	7.43E-03
8	17.6	12.27	1.22	0.81	-16.10	-29.87	0.038	0.113	-0.162	-0.934	8.82E-02	7.77E-03
9	13.8	8.47	0.91	0.50	-8.60	-22.27	0.030	0.066	-0.087	-1.113	6.27E-02	3.93E-03
10	1.4	-3.93	1.25	0.84	13.30	2.53	0.003	0.009	0.133	0.092	6.40E-02	4.10E-03
11	2.3	-3.03	1.16	0.75	-2.90	0.73	0.005	0.014	-0.029	-0.656	7.74E-03	5.98E-05
12	0.3	-5.03	0.30	-0.11	2.00	4.73	0.001	0.000	0.020	0.056	8.97E-03	8.04E-05
13	0.3	-5.03	0.18	-0.23	1.00	4.73	0.001	0.000	0.010	0.093	4.88E-03	2.38E-05
14	1.3	-4.03	-0.30	-0.72	-0.70	2.73	0.003	-0.002	-0.007	-0.106	-1.96E-03	3.84E-06
15	1.6	-3.73	-0.09	-0.50	-1.20	2.13	0.003	-0.001	-0.012	-0.226	-1.94E-03	3.78E-06
16	0.7	-4.63	0.79	0.38	0.90	3.93	0.002	0.003	0.009	0.487	7.98E-03	6.37E-05
17	0.7	-4.63	0.00	-0.41	-4.63	3.93	0.002	0.000	-0.046	-0.033	-1.65E-02	2.71E-04
											SUM	0.026
											E	0.039

Appendix H: Dead Zone Sensitivity Analysis Calculation

Terms Used							
					E		
t (seconds)	C (ug/liter)	$dC_{dz\ (ug/liter*sec)}$	Cd (ug/liter)	T^{-1} (1/sec)	3.33%	6.66%	10.24%
30	25	-25	75	0.02	0.20	0.35	0.50

Date	Average Velocity (cm/s)	x (cm)	C average (ug/liter)	Delta t (s)	Dopt	Dy/Ud
7/31/2006	0.66	190.00	11.01	287.29	0.0022	0.0022

Station	Concentration (ug/liter)	C'	Velocity(cm/second)	U'	d^2 (C')	d^2(C+C')	First Term	Second Term	Third Term	Dead zone	D	In Bracket	sq Bracket
1	7.6	-3.41	0.37	-0.29	9.31	-4.19	0.03	0.01	0.09	0.17	0.44	-0.13	0.016
2	13.5	2.49	0.45	-0.21	-7.70	-15.99	0.05	0.03	0.04	0.17	-1.02	-0.09	0.008
3	11.7	0.69	0.13	-0.53	3.10	-12.39	0.04	0.01	0.01	0.17	1.59	-0.12	0.014
4	13	1.99	0.34	-0.32	-0.80	-14.99	0.05	0.02	0.01	0.17	-8.15	-0.10	0.010
5	13.5	2.49	0.33	-0.33	-4.20	-15.99	0.05	0.02	0.06	0.17	-1.66	-0.10	0.009
6	9.8	-1.21	0.86	0.20	4.50	-8.59	0.03	0.04	0.02	0.17	1.75	-0.09	0.008
7	10.6	-0.41	1.35	0.69	20.40	-10.19	0.04	0.08	0.22	0.17	0.55	-0.05	0.003
8	31.8	20.79	1.33	0.67	-24.40	-52.59	0.11	0.22	0.24	0.17	-1.36	0.17	0.027
9	28.6	17.59	2.11	1.44	-10.00	-46.19	0.10	0.32	0.31	0.17	-4.11	0.25	0.062
10	15.4	4.39	1.04	0.38	6.50	-19.79	0.05	0.08	0.11	0.17	2.14	-0.03	0.001
11	8.7	-2.31	0.29	-0.37	2.20	-6.39	0.03	0.01	0.02	0.17	1.99	-0.12	0.015
12	4.2	-6.81	0.59	-0.07	4.60	2.61	0.01	0.01	0.07	0.17	0.60	-0.14	0.019
13	4.3	-6.71	0.38	-0.28	0.00	2.41	0.01	0.01	0.07	0.17	353.41	-0.14	0.021
14	4.4	-6.61	0.30	-0.36	-0.10	2.21	0.02	0.01	0.07	0.17	-23.83	-0.14	0.021
15	4.4	-6.61	0.95	0.29	-1.10	2.21	0.02	0.02	0.06	0.17	-3.41	-0.13	0.017
16	3.3	-7.71	0.24	-0.42	0.20	4.41	0.01	0.00	0.07	0.17	7.36	-0.15	0.023
17	2.4	-8.61	0.19	-0.48	-7.71	6.21	0.01	0.00	0.17	0.17	-0.14	-0.16	0.024
												SUM	0.30
												E	0.13

Appendix I: Step by Step Mike 21

Model Appendix:
This Appendix is designed to give step by step instructions about how to create the Mike 21 used in the present study. The actual input files can be viewed in the electronic submission of the thesis.

The parameter input box is shown below:

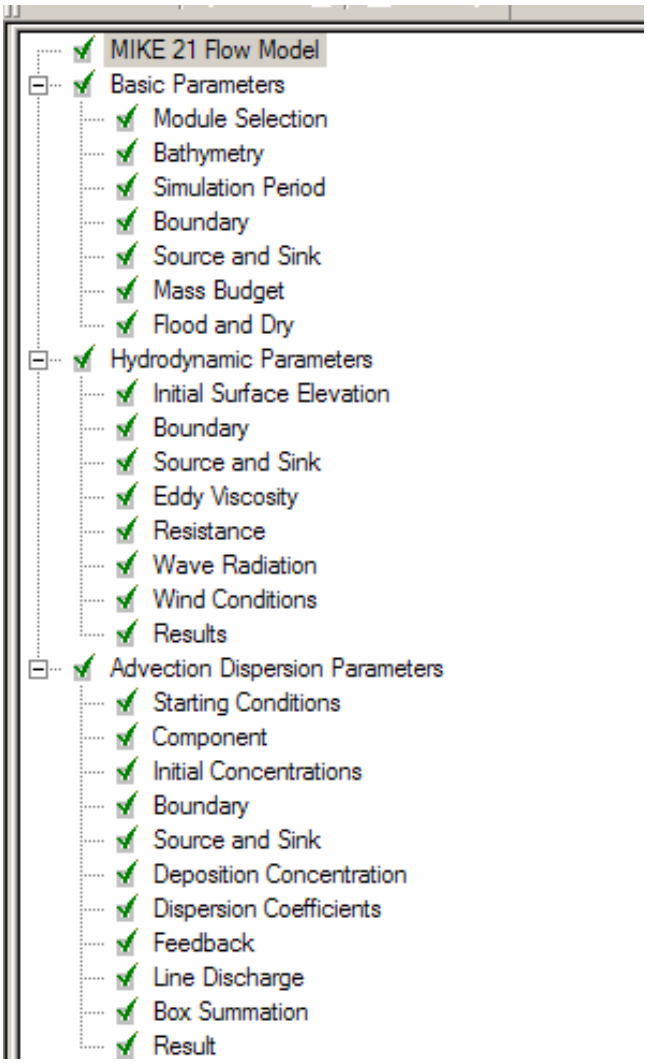

Basic Parameters:

-Module Selection

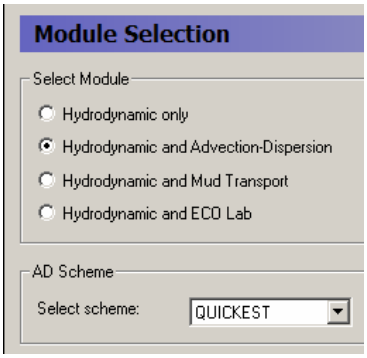

-Bathymetry

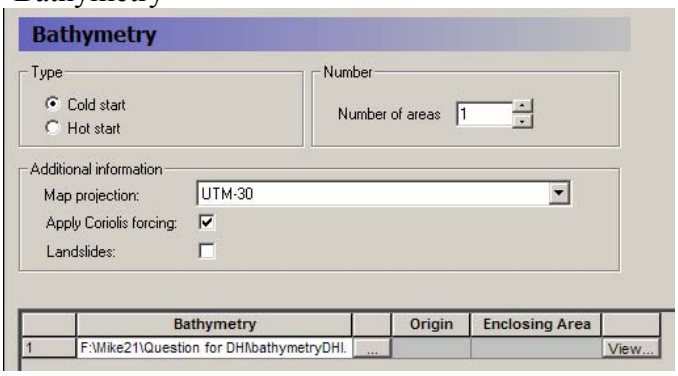

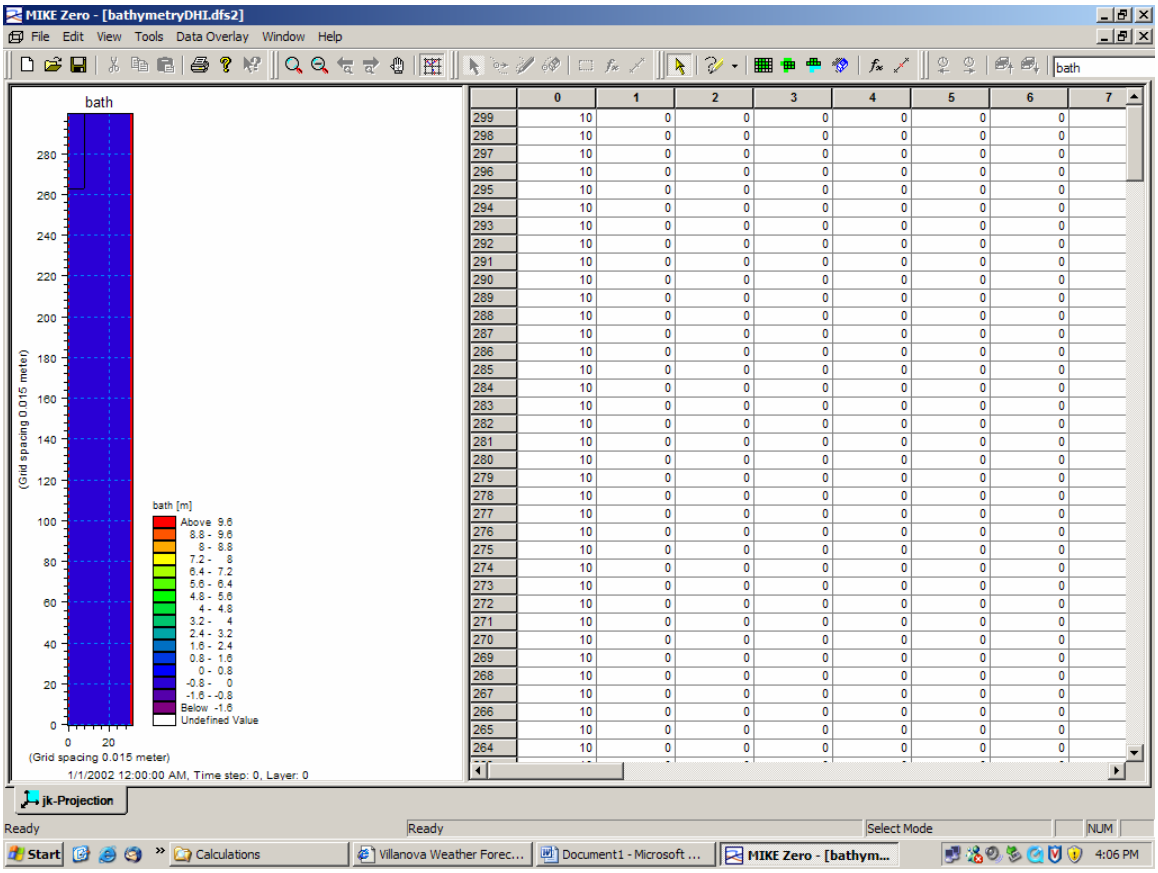

-Simulation Period

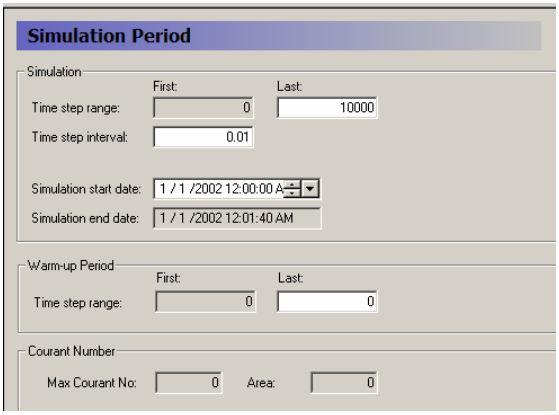

-Boundary

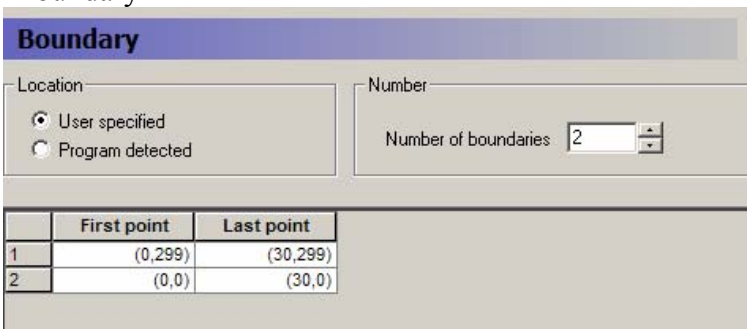

-Source and Sink

	Type	Source		Sink	
		Point	Area	Point	Area
1	Isolated Source	(15,290)	1	(0,0)	1

-Mass Budget

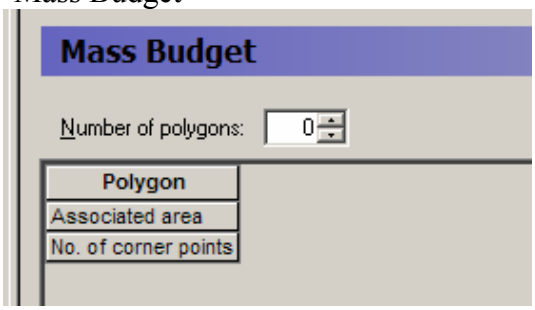

-Flood and Dry

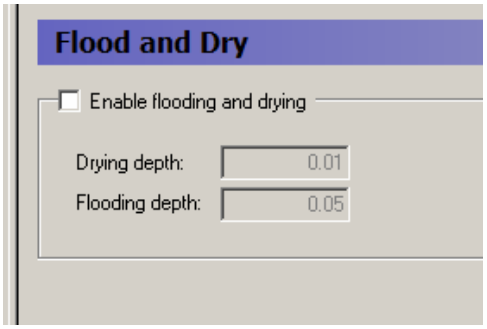

Hydrodynamic Parameters:

-Initial Surface Elevation

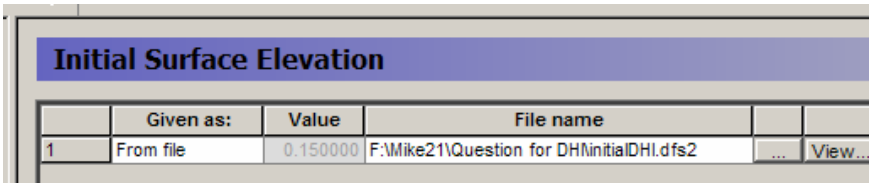

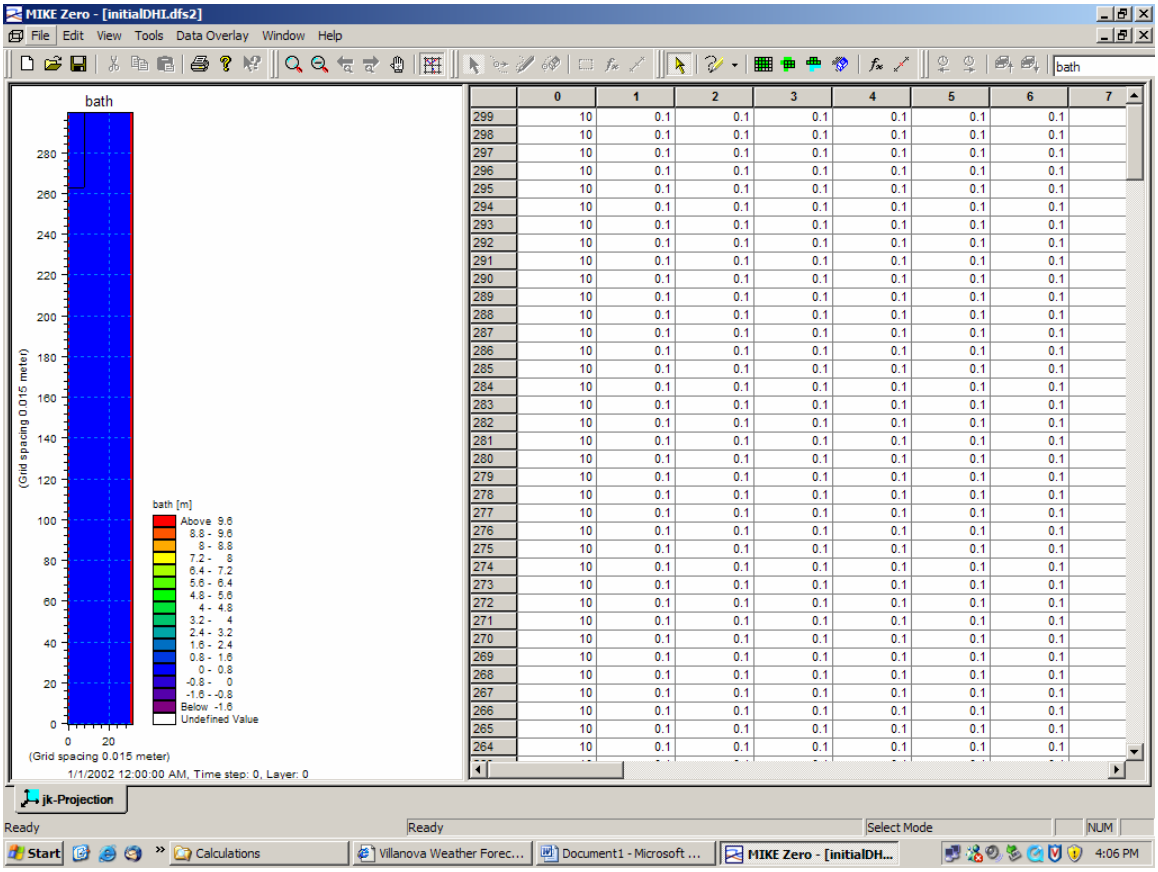

-Boundary

Boundary

Boundary 1 : (0,299) - (30,299)			
Formulation:	Flux		
Type 1 Data file:	F:\Mike21\Question for DH\non uniform velocities	...	View
FAB type:	12		
No tilting	0		
No user defined flow direction			View
Boundary 2 : (0,0) - (30,0)			
Formulation:	Flux		
Type 1 Data file:	F:\Mike21\Question for DH\non uniform velocities	...	View
FAB type:	12		
No tilting	0		
No user defined flow direction			View

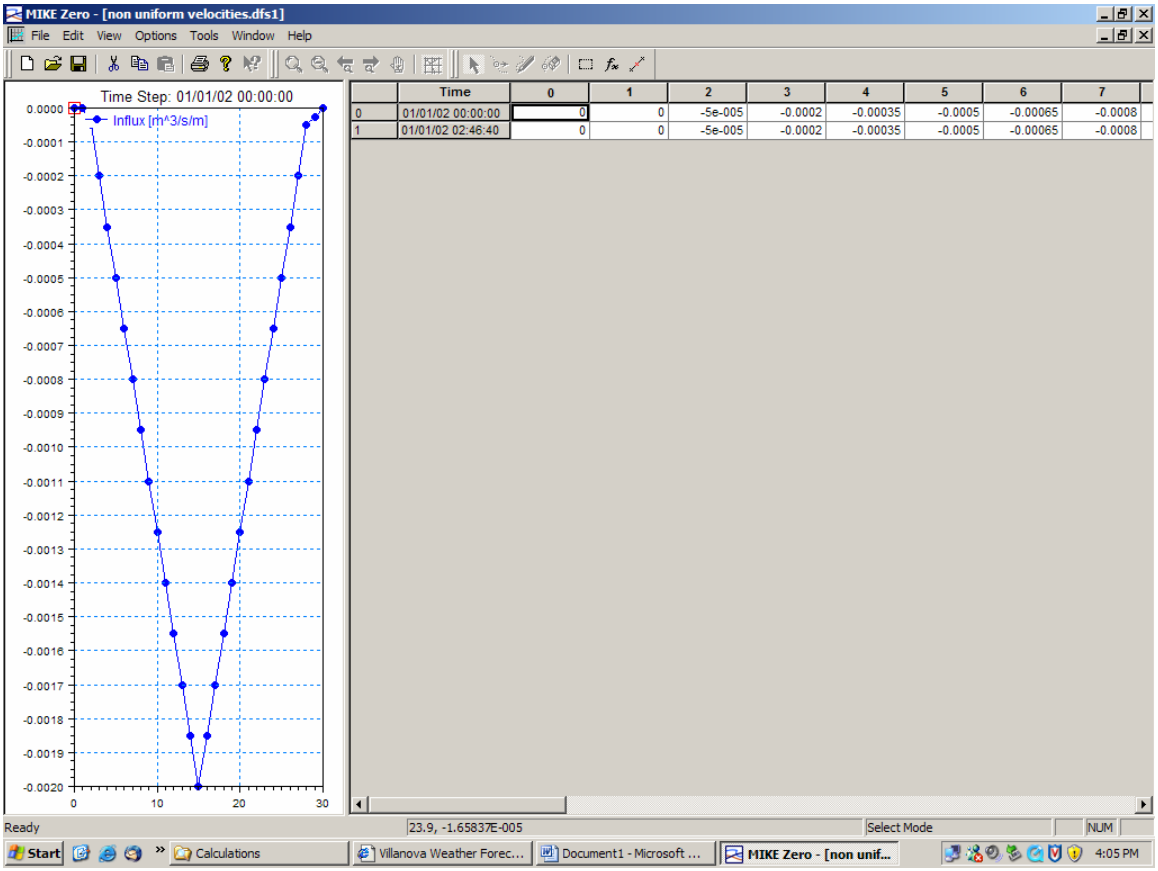

-Source and Sink

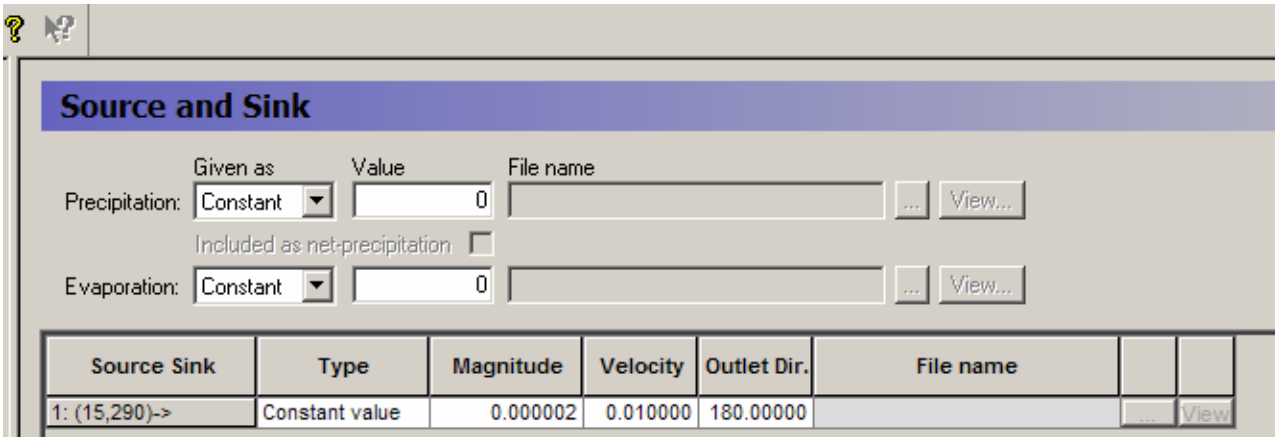

-Eddy Viscosity

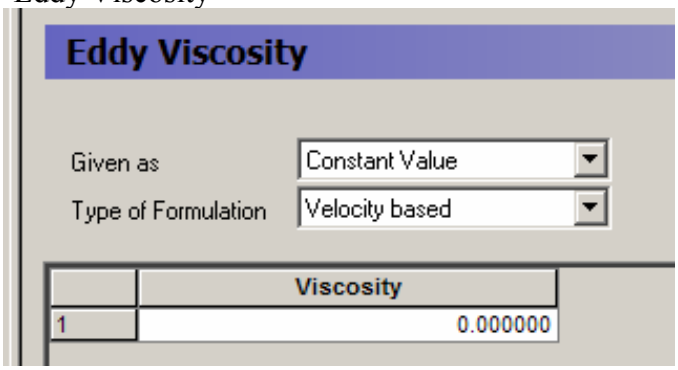

-Resistance

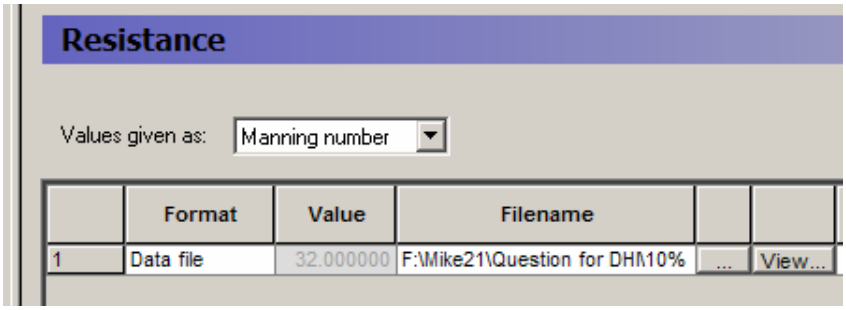

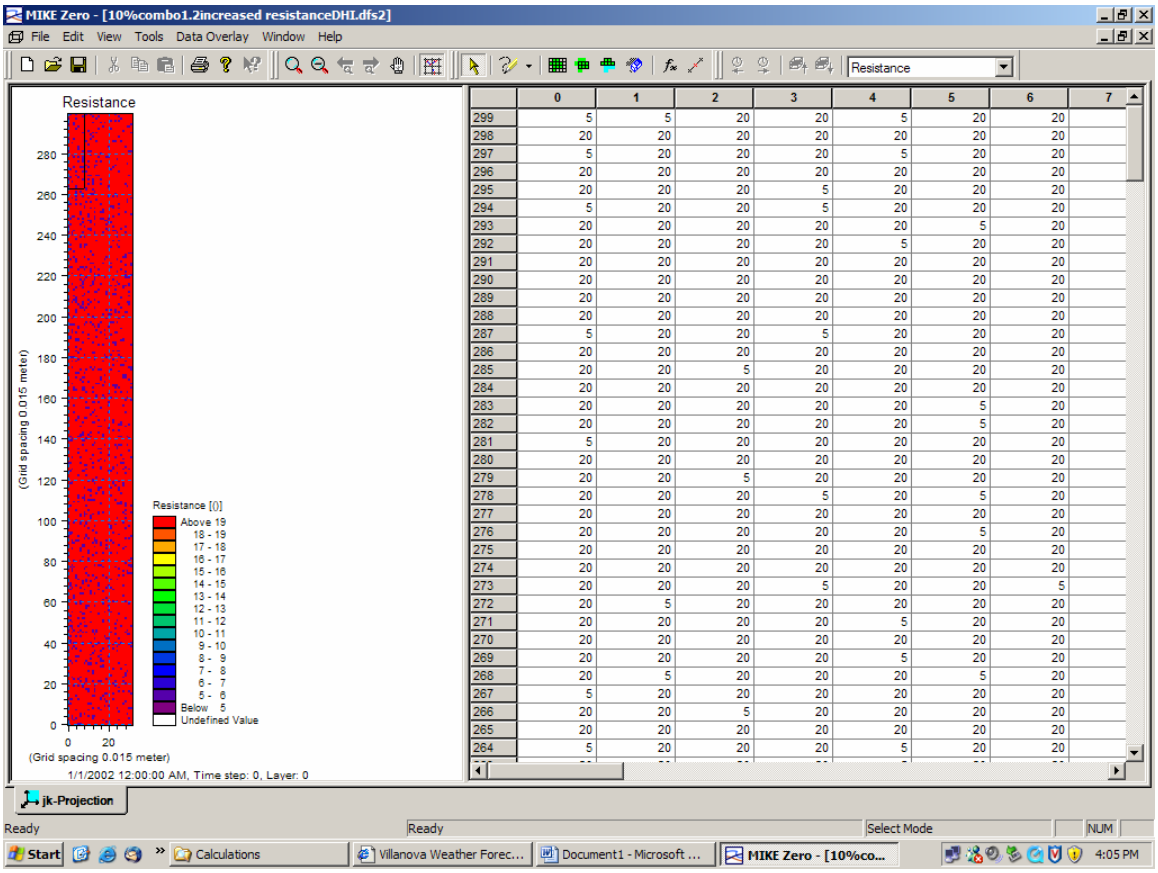

	0	1	2	3	4	5	6	7
299	5	5	20	20	5	20	20	
298	20	20	20	20	20	20	20	
297	5	20	20	20	5	20	20	
296	20	20	20	20	20	20	20	
295	20	20	20	5	20	20	20	
294	5	20	20	5	20	20	20	
293	20	20	20	20	20	5	20	
292	20	20	20	20	5	20	20	
291	20	20	20	20	20	20	20	
290	20	20	20	20	20	20	20	
289	20	20	20	20	20	20	20	
288	20	20	20	20	20	20	20	
287	5	20	20	5	20	20	20	
286	20	20	20	20	20	20	20	
285	20	20	5	20	20	20	20	
284	20	20	20	20	20	20	20	
283	20	20	20	20	20	5	20	
282	20	20	20	20	20	5	20	
281	5	20	20	20	20	20	20	
280	20	20	20	20	20	20	20	
279	20	20	5	20	20	20	20	
278	20	20	20	5	20	5	20	
277	20	20	20	20	20	20	20	
276	20	20	20	20	20	5	20	
275	20	20	20	20	20	20	20	
274	20	20	20	20	20	20	20	
273	20	20	20	5	20	20	5	
272	20	5	20	20	20	20	20	
271	20	20	20	20	5	20	20	
270	20	20	20	20	20	20	20	
269	20	20	20	20	5	20	20	
268	20	5	20	20	20	5	20	
267	5	20	20	20	20	20	20	
266	20	20	5	20	20	20	20	
265	20	20	20	20	20	20	20	
264	5	20	20	20	5	20	20	

-Wave Radiation

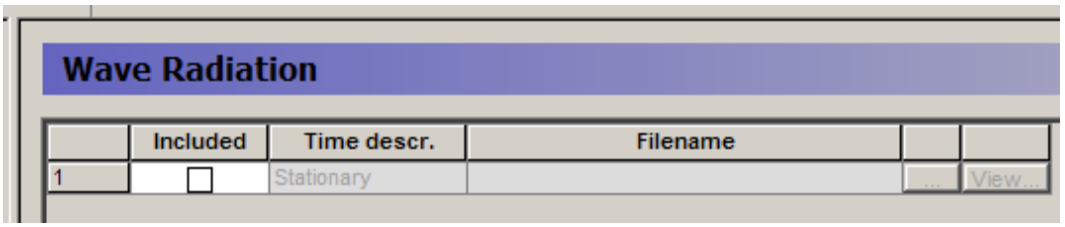

-Wind Conditions

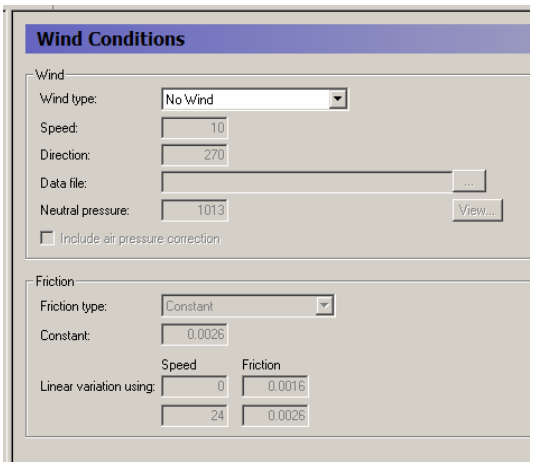

-Results

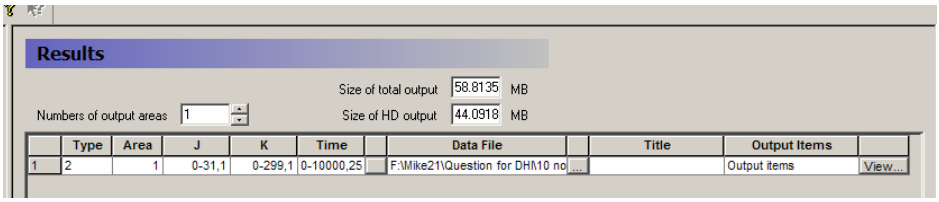

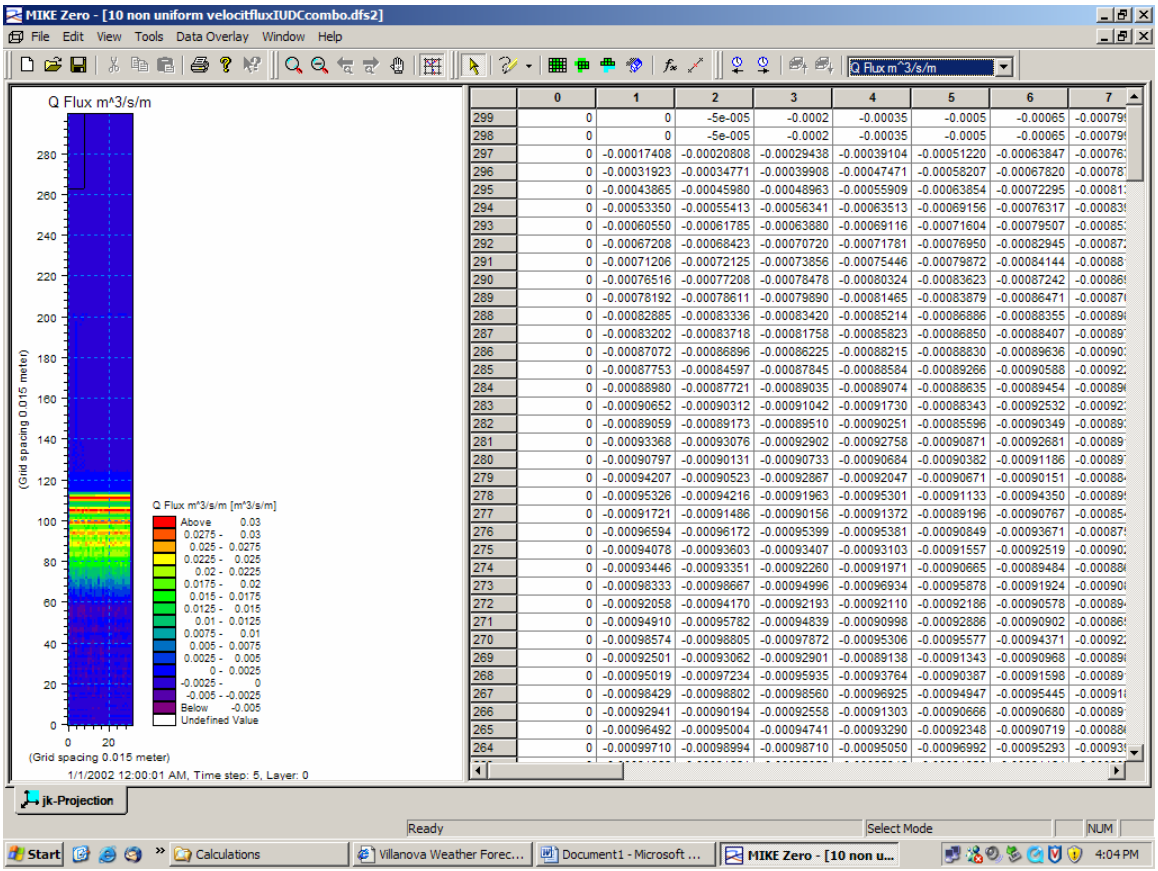

Advection Dispersion Parameters:

-Starting Conditions

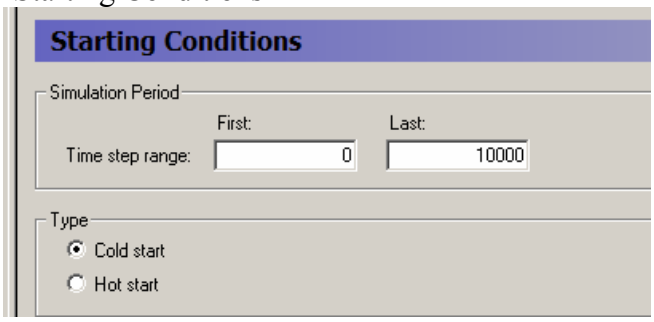

-Component

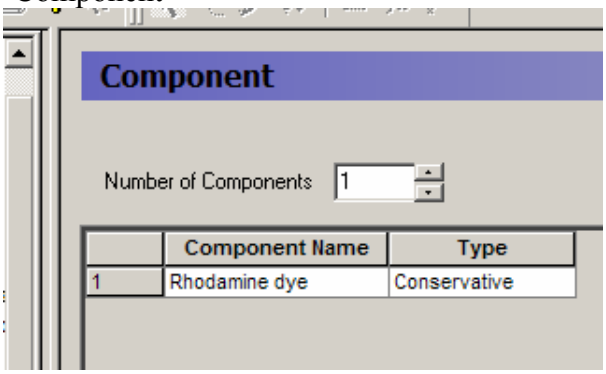

-Initial Concentrations

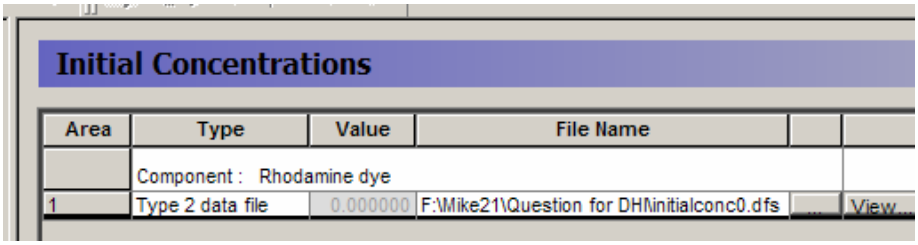

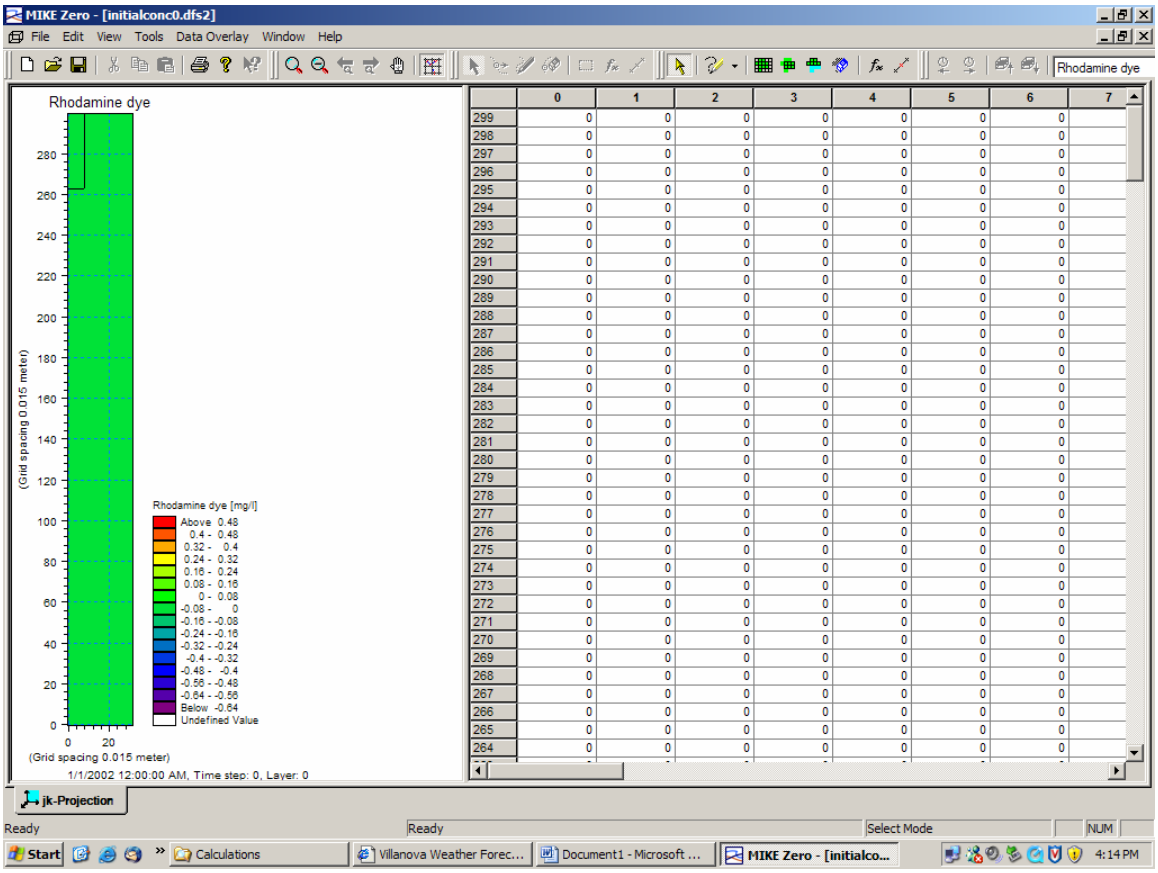
MIKE Zero - [initialconc0.dfs2]
File Edit View Tools Data Overlay Window Help
Rhodamine dye
Rhodamine dye
(Grid spacing 0.015 meter)
Rhodamine dye [mg/l]
Above 0.48
0.4 - 0.48
0.32 - 0.4
0.24 - 0.32
0.16 - 0.24
0.08 - 0.16
0 - 0.08
-0.08 - 0
-0.16 - -0.08
-0.24 - -0.16
-0.32 - -0.24
-0.4 - -0.32
-0.48 - -0.4
-0.56 - -0.48
-0.64 - -0.56
Below -0.64
Undefined Value
(Grid spacing 0.015 meter)
1/1/2002 12:00:00 AM, Time step: 0, Layer: 0
jk-Projection
Ready
Ready
Select Mode
NUM
Start
Calculations
Villanova Weather Forec...
Document1 - Microsoft ...
MIKE Zero - [initialco...
4:14 PM

-Boundary

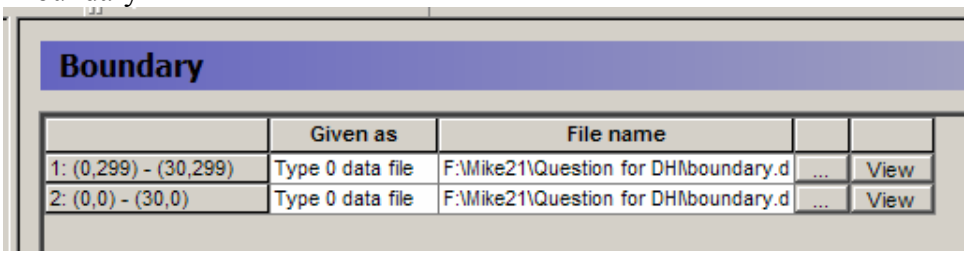
Boundary
Given as
File name
1: (0,299) - (30,299)
Type 0 data file
F:\Mike21\Question for DH\boundary.d
...
View
2: (0,0) - (30,0)
Type 0 data file
F:\Mike21\Question for DH\boundary.d
...
View

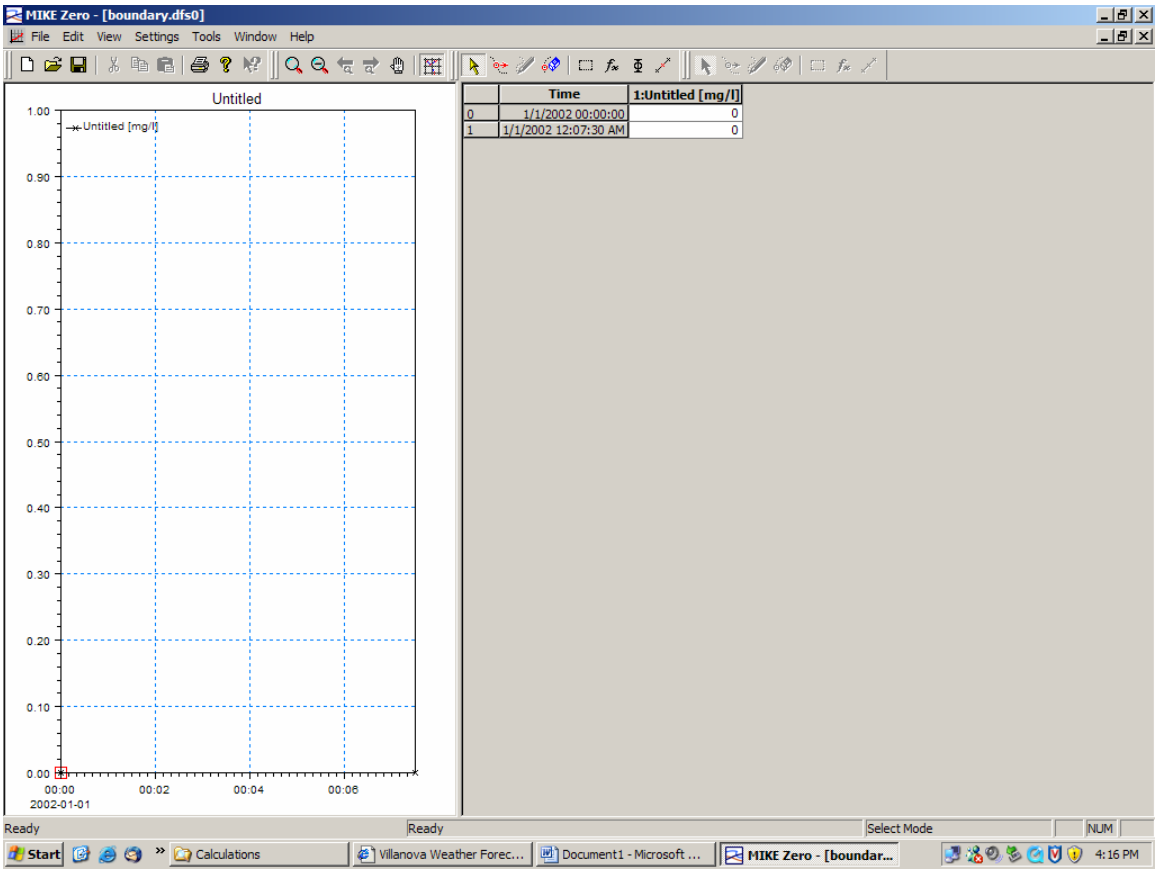

-Source and Sink

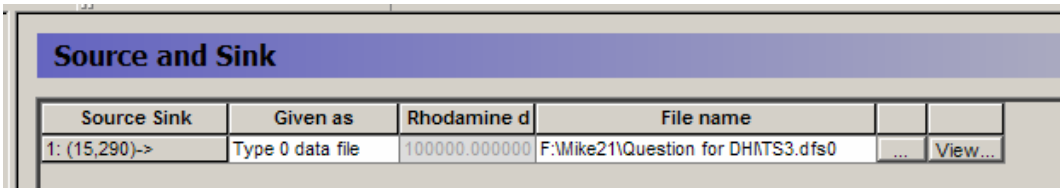

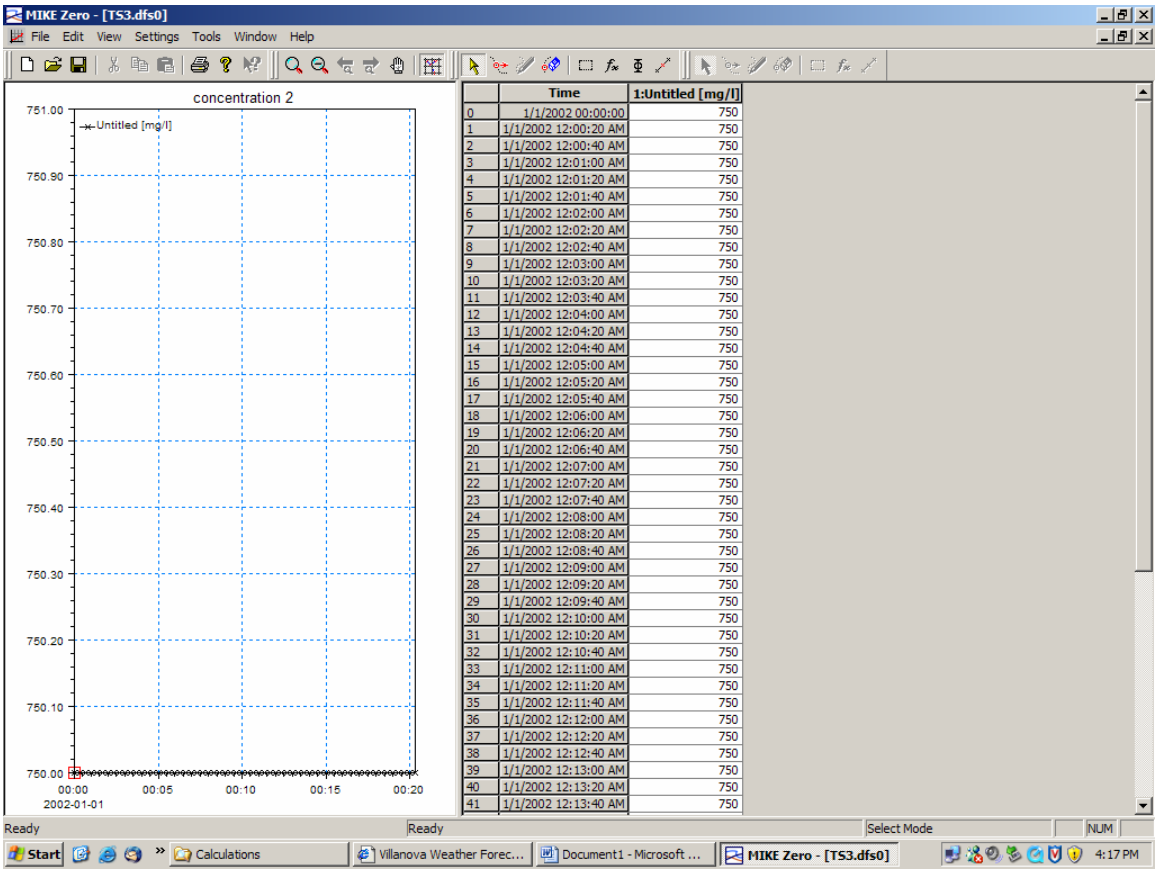

-Deposition Concentration

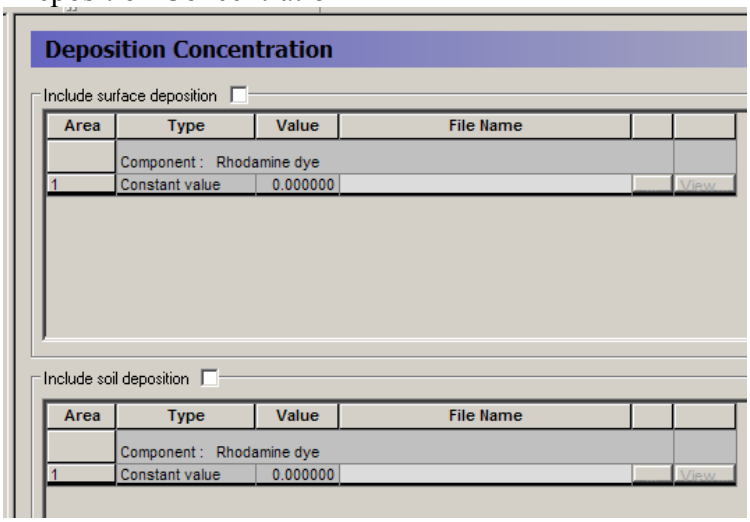

-Dispersion Coefficients

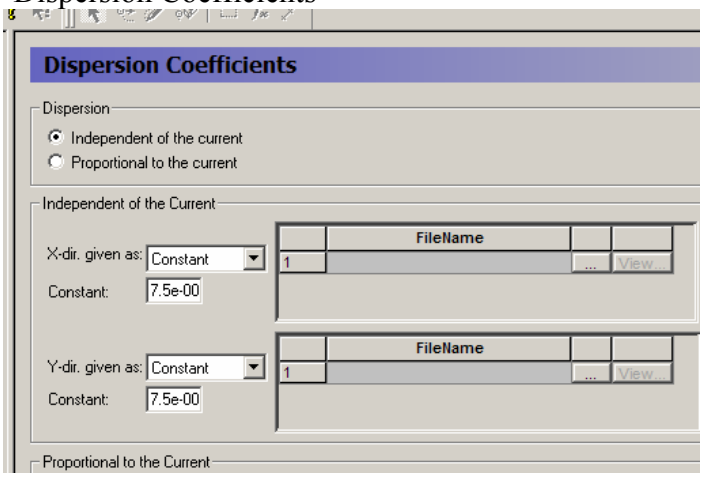

-Feedback

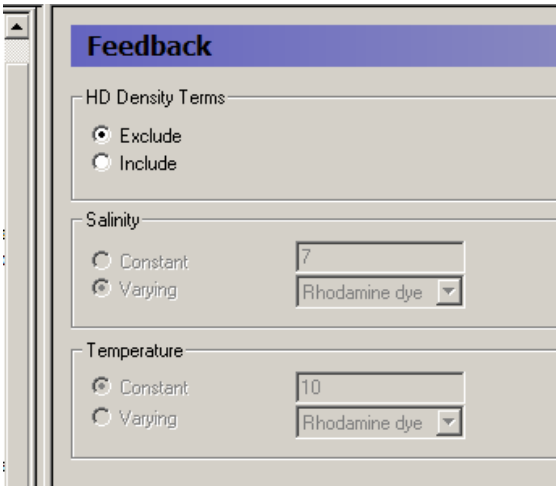

-Line Discharge

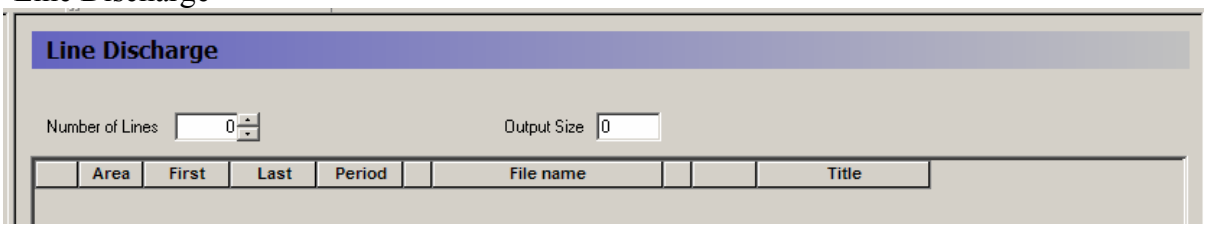

-Box Simulation

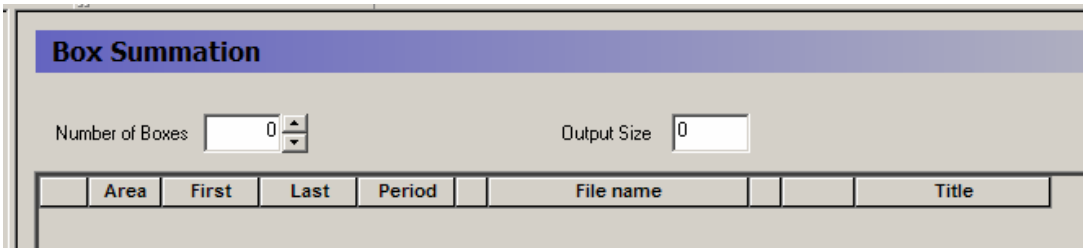

-Result

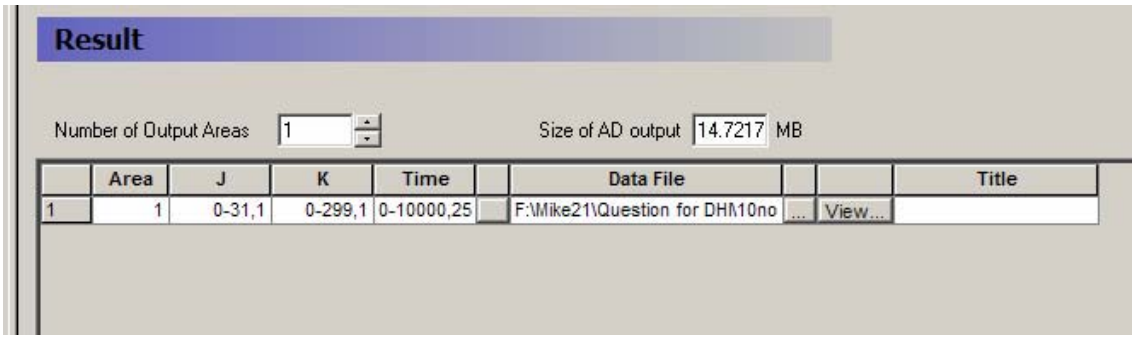

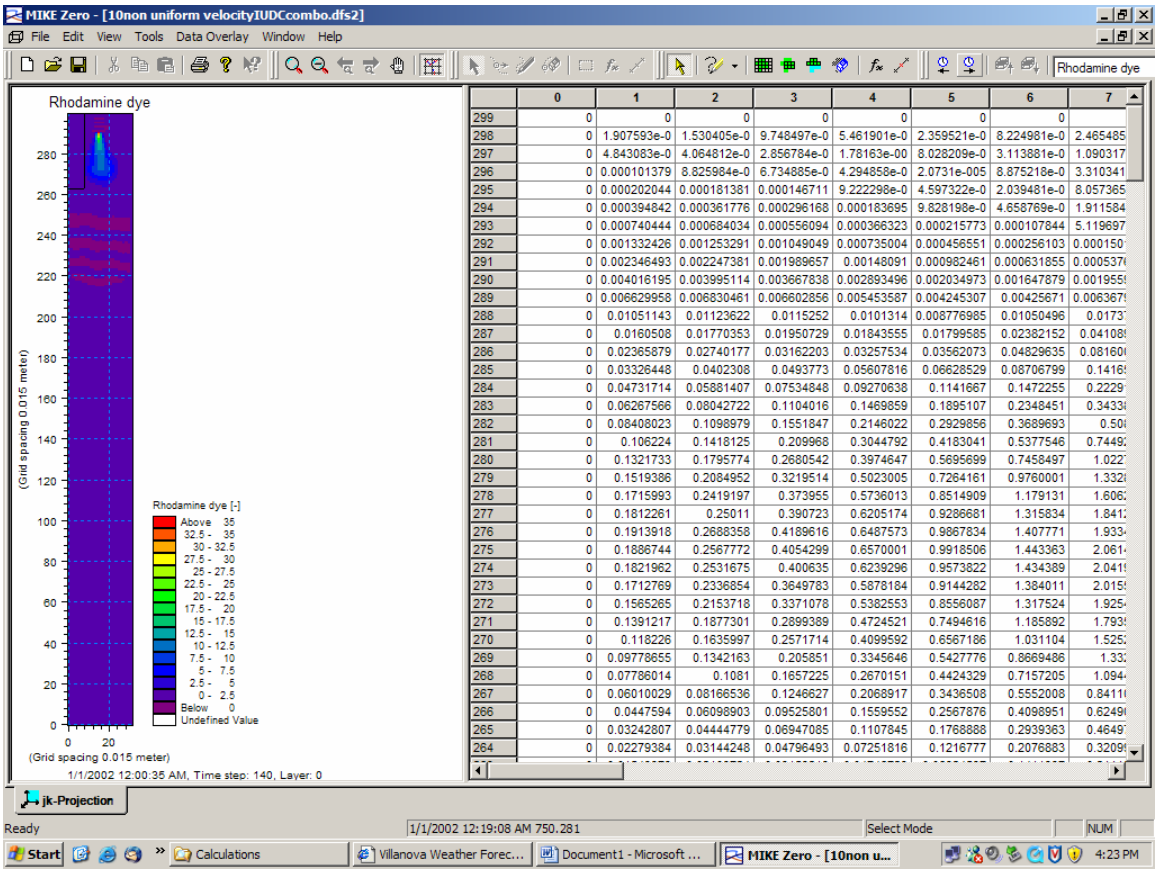

	0	1	2	3	4	5	6	7
299	0	0	0	0	0	0	0	
298	0	1.907593e-0	1.530405e-0	9.748497e-0	5.461901e-0	2.359521e-0	8.224981e-0	2.465485
297	0	4.843083e-0	4.064812e-0	2.856784e-0	1.78163e-00	8.028209e-0	3.113881e-0	1.090317
296	0	0.000101379	8.825984e-0	6.734885e-0	4.294858e-0	2.0731e-005	8.875218e-0	3.310341
295	0	0.000202044	0.000181381	0.000146711	9.222298e-0	4.597322e-0	2.039481e-0	8.057365
294	0	0.000394842	0.000361776	0.000296168	0.000183695	9.828198e-0	4.658769e-0	1.911584
293	0	0.000740444	0.000684034	0.000556094	0.000366323	0.000215773	0.000107844	5.119697
292	0	0.001332426	0.001253291	0.001049049	0.000735004	0.000456551	0.000256103	0.000150
291	0	0.002346493	0.002247381	0.001989657	0.00148091	0.000982461	0.000631855	0.000537
290	0	0.004016195	0.003995114	0.003667838	0.002893496	0.002034973	0.001647879	0.001955
289	0	0.006629958	0.006830461	0.006602856	0.005453587	0.004245307	0.00425671	0.006367
288	0	0.01051143	0.01123622	0.0115252	0.0101314	0.008776985	0.01050496	0.0173
287	0	0.0160508	0.01770353	0.01950729	0.01843555	0.01799585	0.02382152	0.04108
286	0	0.02365879	0.02740177	0.03162203	0.03257534	0.03562073	0.04829635	0.08160
285	0	0.03326448	0.0402308	0.0493773	0.05607816	0.06628529	0.08706799	0.1416
284	0	0.04731714	0.05881407	0.07534848	0.09270638	0.1141667	0.1472255	0.2229
283	0	0.06267566	0.08042722	0.1104016	0.1469859	0.1895107	0.2348451	0.3433
282	0	0.08408023	0.1098979	0.1551847	0.2146022	0.2929856	0.3689693	0.50
281	0	0.106224	0.1418125	0.209968	0.3044792	0.4183041	0.5377546	0.7449
280	0	0.1321733	0.1795774	0.2680542	0.3974647	0.5695699	0.7458497	1.022
279	0	0.1519386	0.2084952	0.3219514	0.5023005	0.7264161	0.9760001	1.332
278	0	0.1715993	0.2419197	0.373955	0.5736013	0.8514909	1.179131	1.606
277	0	0.1812261	0.25011	0.390723	0.6205174	0.9286681	1.315834	1.841
276	0	0.1913918	0.2688358	0.4189616	0.6487573	0.9867834	1.407771	1.933
275	0	0.1886744	0.2567772	0.4054299	0.6570001	0.9918506	1.443363	2.061
274	0	0.1821962	0.2531675	0.400635	0.6239296	0.9573822	1.434389	2.041
273	0	0.1712769	0.2336854	0.3649783	0.5878184	0.9144282	1.384011	2.015
272	0	0.1565265	0.2153718	0.3371078	0.5382553	0.8556087	1.317524	1.925
271	0	0.1391217	0.1877301	0.2899389	0.4724521	0.7494616	1.185892	1.793
270	0	0.118226	0.1635997	0.2571714	0.4099592	0.6567186	1.031104	1.525
269	0	0.09778655	0.1342163	0.205851	0.3345646	0.5427776	0.8669486	1.33
268	0	0.07786014	0.1081	0.1657225	0.2670151	0.4424329	0.7157205	1.094
267	0	0.06010029	0.08166536	0.1246627	0.2068917	0.3436508	0.5552008	0.8411
266	0	0.0447594	0.06098903	0.09525801	0.1559552	0.2567876	0.4098951	0.6249
265	0	0.03242807	0.04444779	0.06947085	0.1107845	0.1768888	0.2939363	0.4649
264	0	0.02279384	0.03144248	0.04796493	0.07251816	0.1216777	0.2076883	0.3209

Appendix J: Daily Field Data

Run 2 6/29/06

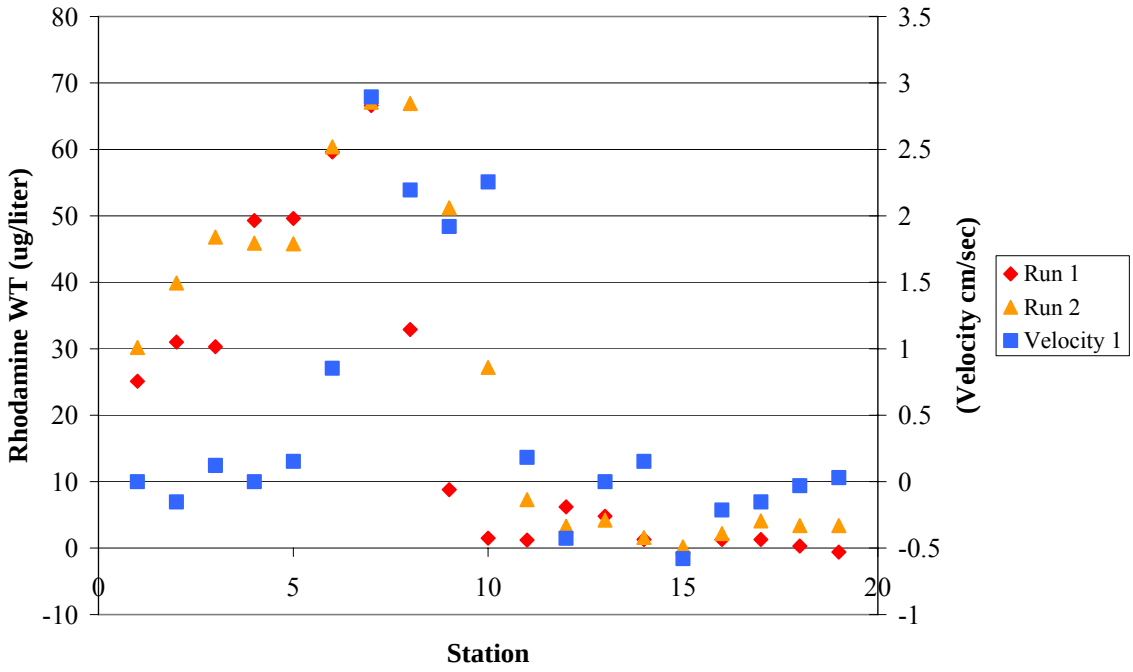

Run 3 7/10/2006

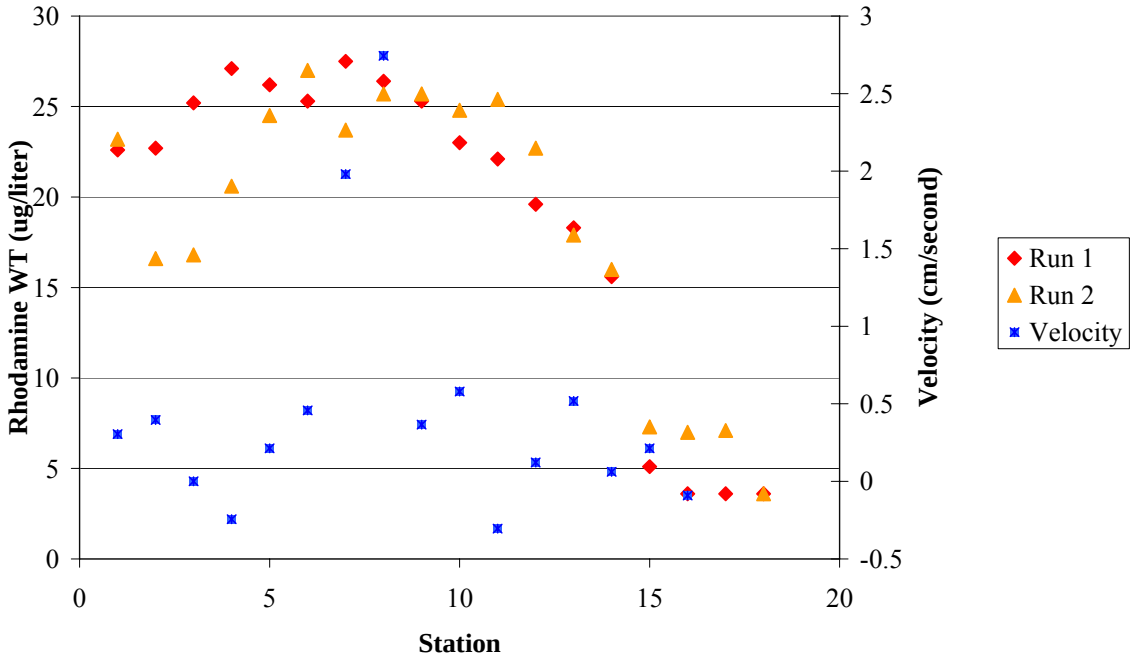

Run 4 7/12/2006

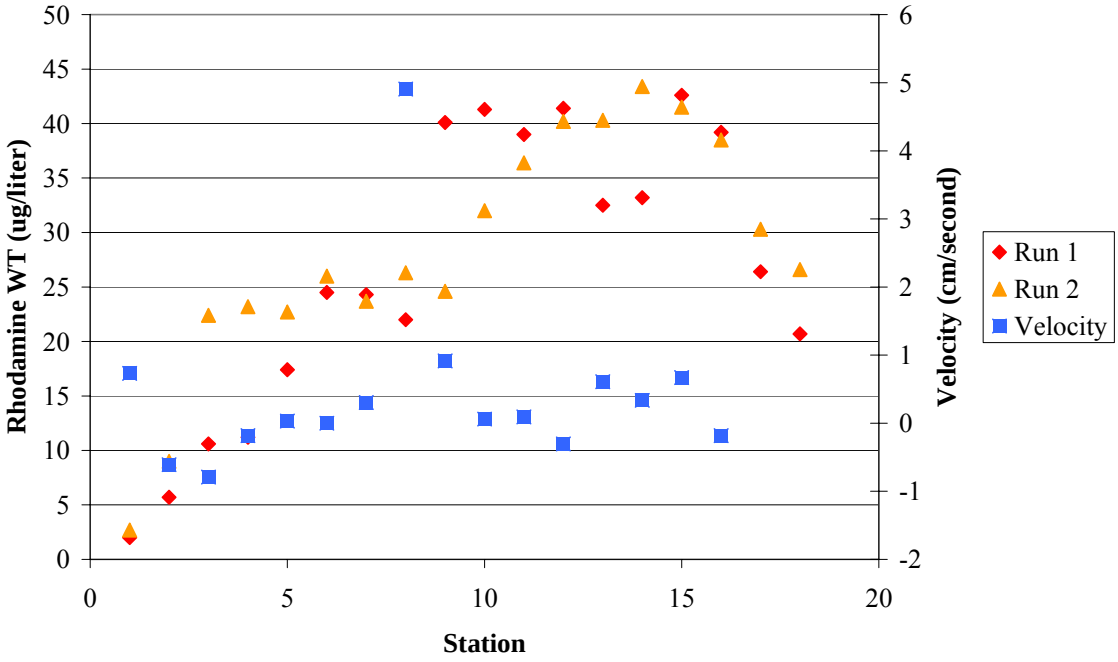

Run 5 7/17/2006

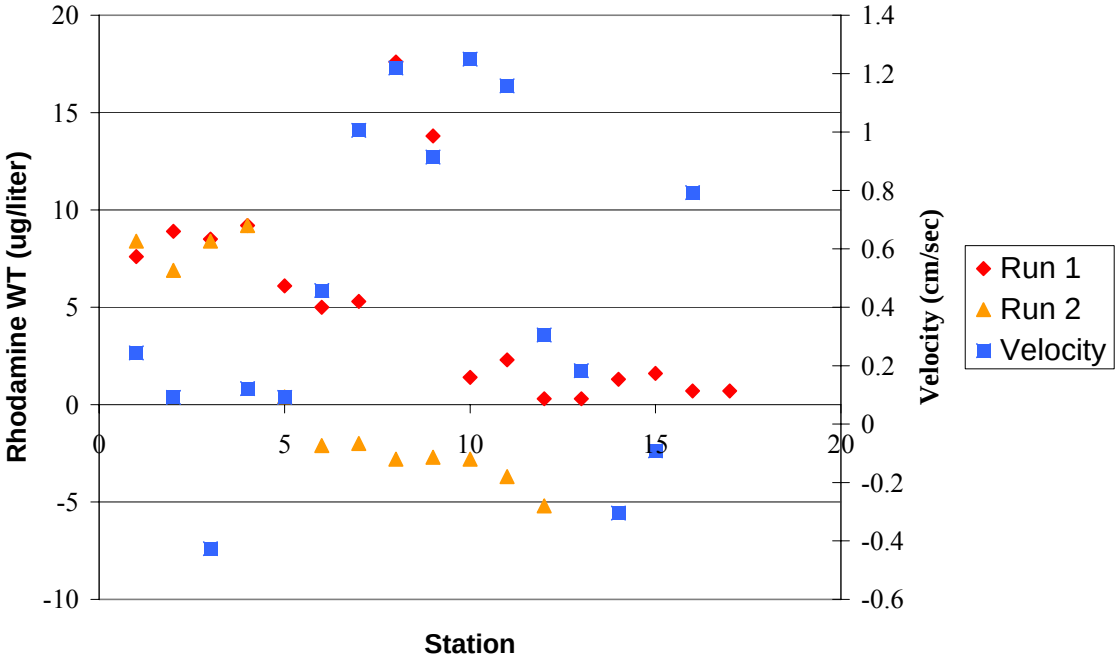

Run 6 7/19/2006

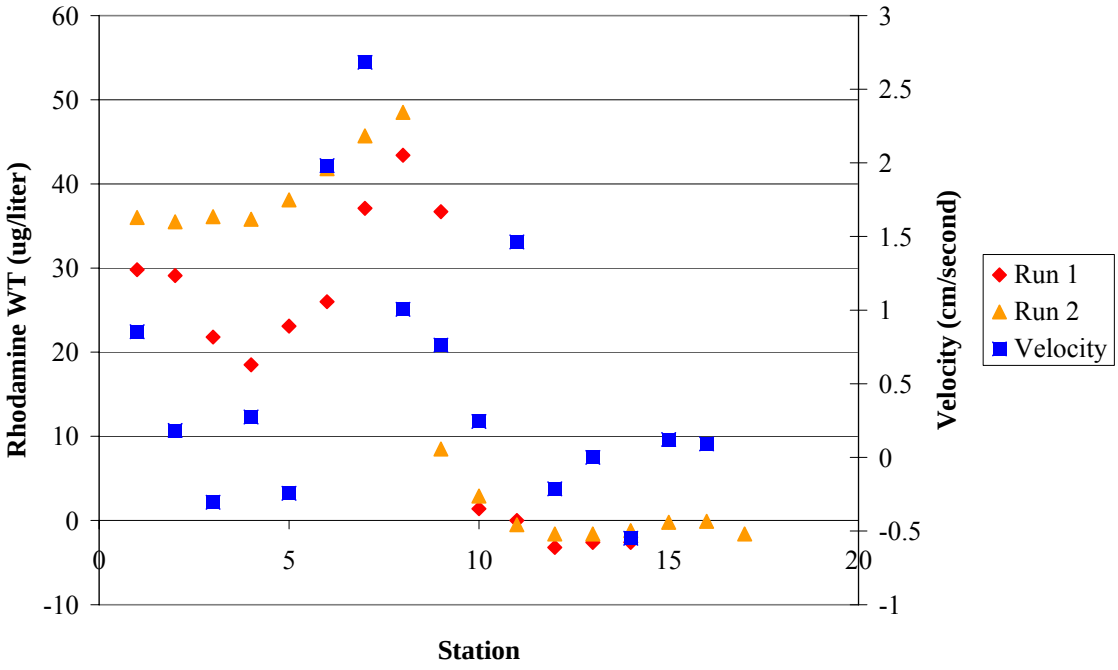

Run 7 7/21/2006

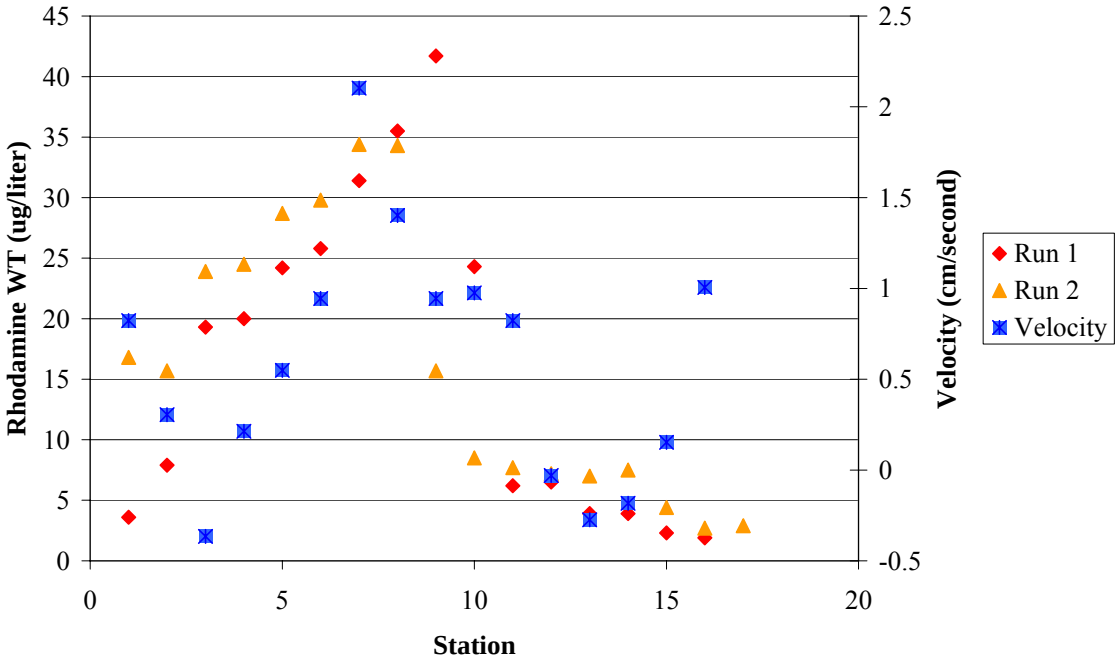

Run 8 7/21/2006

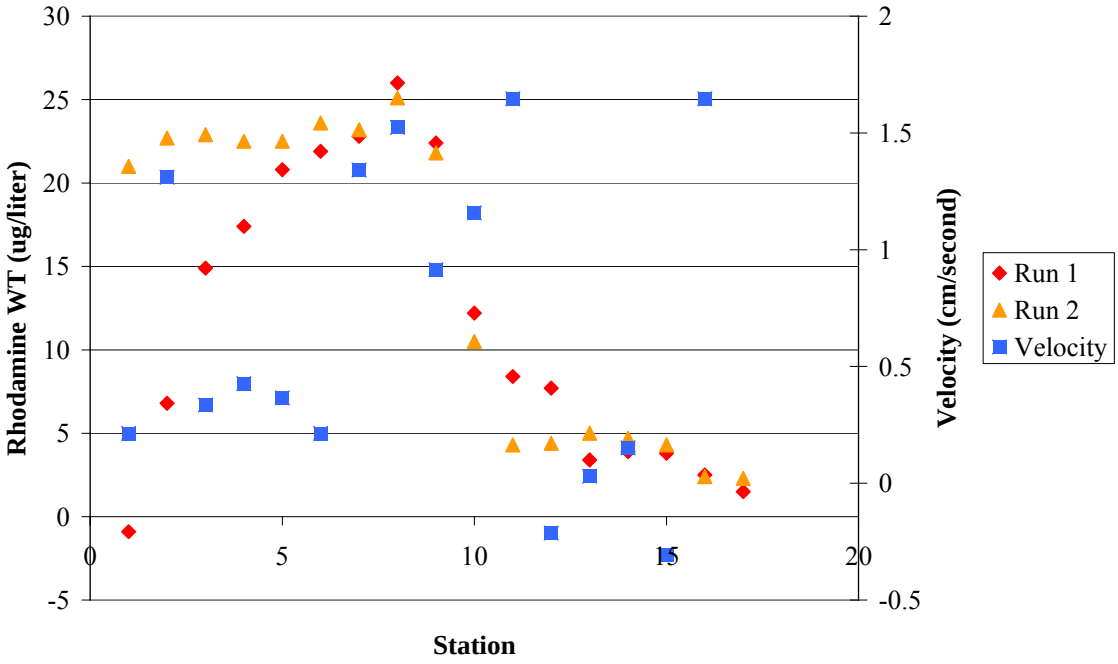

Run 9 7/26/2006

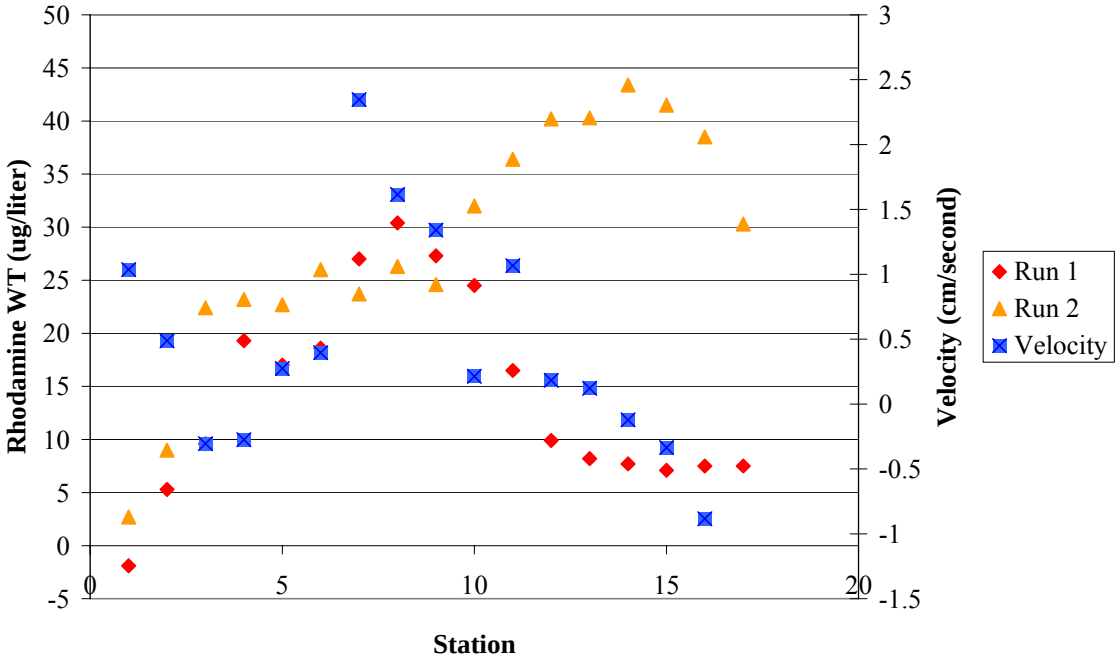

Run 10 7/28/2006

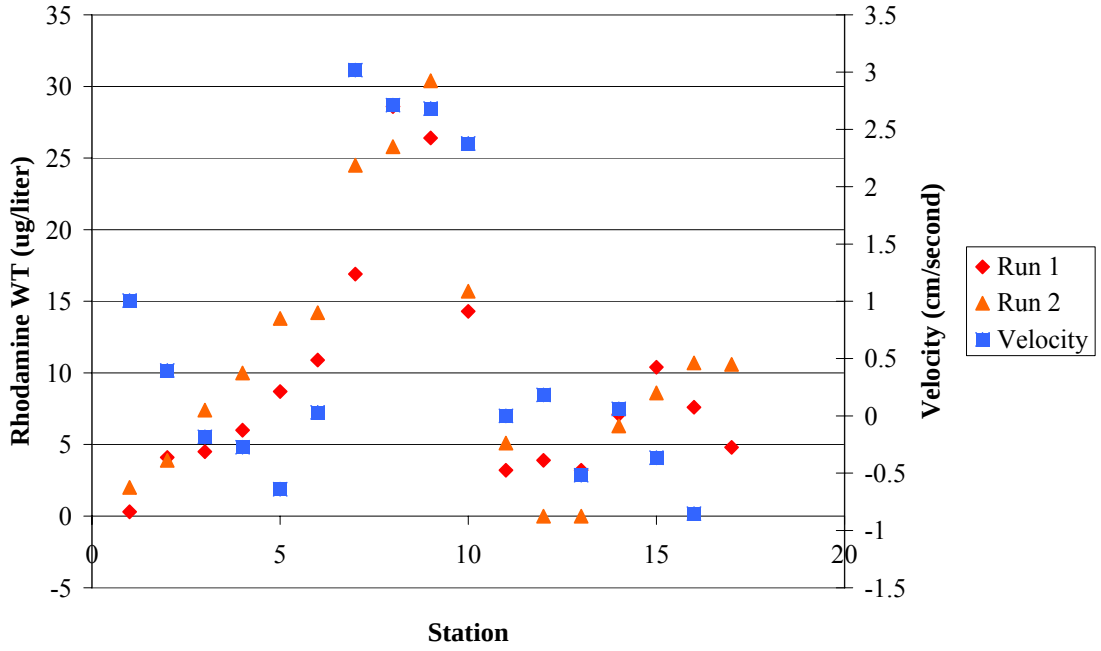

.

Run 11 7/31/2006